Advances in the Development of Photonic Crystal Hydrogels as Versatile Biomolecular Sensors

by

Sarah Ann Goda

B.S., Chemistry, University of New Haven, 2018

B.S., Forensic Science, University of New Haven, 2018

Submitted to the Graduate Faculty of the

Dietrich School of Arts and Sciences in partial fulfillment

of the requirements for the degree of

Doctor of Philosophy

University of Pittsburgh

2023

UNIVERSITY OF PITTSBURGH

DIETRICH SCHOOL OF ARTS AND SCIENCES

This dissertation was presented

by

Sarah Ann Goda

It was defended on

October 16, 2023

and approved by

Dr. Jennifer Laaser, Assistant Professor, Department of Chemistry, University of Pittsburgh

Dr. Sunil Saxena, Professor, Department of Chemistry, University of Pittsburgh

Dr. Sachin Velankar, Professor, Mechanical Engineering and Material Science, University of Pittsburgh

Dissertation Director: Dr. Sanford A. Asher, Distinguished Professor of Chemistry, Department of Chemistry, University of Pittsburgh

Advances in the Development of Photonic Crystal Hydrogels as Versatile Biomolecular Sensors

Sarah A. Goda, PhD

University of Pittsburgh, 2023

We expanded the understandings of photonic crystal hydrogel fabrication and swelling behavior pertaining to their use as sensing materials. Our hydrogels are comprised of a polymer network containing a recognition group and a photonic crystal array embedded within the hydrogel network. The molecular recognition groups within the hydrogel allow us to make these sensors highly selective to target analytes. Hydrogel changes from analyte binding result in a volume phase transition (VPT). Hydrogel VPTs alter the distance between particles that make up the photonic crystal array, leading to changes in diffracted light according to the Bragg condition. Studies reported herein demonstrate the use of photonic crystal hydrogel sensors as sensing platforms that are easily adaptable.

We investigated the use of oxyamine functionalized hydrogels to monitor lactate dehydrogenase's enzymatic conversion of lactate to pyruvate. Pyruvate's covalent attachment to the hydrogel enables a swelling response which corresponds to lactate concentrations in solution. We detected < 0.5 mM lactate in buffer solutions within an hour with detection limits < 4 mM lactate in serum solutions. This work is the first to demonstrate indirect detection of analytes by coupling enzymatic reactions with photonic crystal hydrogel sensors.

DNA aptamers are small biomolecules that are highly selective in their binding and are stable under a variety of conditions. We incorporated hybridized DNA aptamers into 2DPC hydrogels forming crosslinks. These DNA crosslinks break due to analyte-DNA binding which

enables hydrogel swelling. We demonstrated this aptamer sensing motif is easily modified from detecting the small molecule adenosine to the large protein thrombin.

Poly (N-isopropylacrylamide) (pNIPAM) hydrogels are thermoresponsive, undergoing large VPTs at temperatures above their lower critical solution temperature (LCST). pNIPAM's LCST is shifted due to changes in the hydrophobicity of pNIPAM's environment from disruptions to pNIPAM's solvation shell. This enables detection of hydrophobic analytes that can typically require complex detection methods. We are the first to investigate using shifts in pNIPAM's LCST for detection of hydrophobic analytes such as Xe. We spectroscopically investigated Xe-protein binding to monitor favorable Xe binding environments and increase pNIPAM's sensitivity to the presence of Xe.

Table of Contents

List of Tables

List of Figures

Preface

I would like to thank those who have supported me on this journey, without them I would not be where I am. Thank you to my research advisor, Dr. Sanford Asher, whose support and mentorship over the years have helped me to become the scientist I am today. I would like to thank my committee members, Dr. Jennifer Laaser, Dr. Sunil Saxena, and Dr. Sachin Velankar for their time and guidance.

Thank you to the members of the Asher group, both past and present, who I have had the pleasure of working with over the years, Sergei Bykov, Andrew Coukouma, Tom Deering, Kyle Hufziger, Daniel Mainshein, Ryan Roppel, and Dipak Rout. I thank Dr. Ryan Jakubek and Dr. Stephen White for helping me get acclimated to the group and being good collaborators. I am grateful for Dr. Ivan Pallares, Dr. Natasha Smith, and Dr. Kyeongwoo Jang whose guidance and mentorship have made me a better scientist. I would also like to thank Dr. James Westbay for all the great discussions both as coworkers and friends. I would like to give a big thank you to Sharon Mansfield for always going above and beyond, seeing her smiling face always made the day better.

Finally, I would like to thank my friends and family who have been with me through it all. I am especially thankful for Megan Clark, without her friendship and support I would not have been able to achieve what I have. I would like to show my appreciation for my mother Debbie and sister Amanda who have always supported and encouraged me. I would like to thank Jaccob for everything he has done for me over the years. Finally, I would like to thank my nieces Ashley and Ellie for reminding me that science is fun even when it is frustrating.

1.0 Introduction

1.1 Motivation

Biomolecular sensors are useful devices for monitoring both one's health and environment.[1-3] As the field of biomolecular sensors has expanded, so has the development of portable devices that are usable to the public, also called point-of-care devices.[4] Some of the most recognized portable sensors are glucose meters which have been in use since the 1980's.[5] While the first glucose meters were developed 50 years ago, development of new glucose sensing methods are still ongoing demonstrating the constant drive to increase their sensitivity, accuracy, and usability.[6-7]

The ability to quickly and easily fabricate sensors for new and emerging health risks would enable extensive monitoring, treatment, and mitigation of their spread. While these developmental endeavors are underway, finding a sensing motif with results that are easily determined by the public while maintaining high accuracy and sensitivity can be difficult.[8-9] Taking these established platforms and adapting them for the detection of more than one analyte can lead to even larger challenges.

While point-of-care testing should not be used as a replacement for laboratory diagnostics, early detection and monitoring of health and environmental risks can decrease the time needed to diagnose and receive treatment, enabling more favorable outcomes.[10] Development of inexpensive sensors that are easily transported allows faster and more accessible testing in areas with low population density that typically have little access to healthcare.[11-13]

A platform for the development of smart materials called photonic crystal hydrogels has been previously developed by the Asher group.[14-15] Our photonic crystal hydrogels are inexpensive, transportable, and give optical readouts that are easily monitored by the public, making them ideal for point-of-care sensing. Investigations into photonic crystal sensor fabrication and behavior will allow quick and easy sensor modification to be used for a variety of targets.

1.2 Hydrogels and Volume Phase Transitions

Hydrogels are made of an interconnected polymer network with an aqueous mobile phase. The amount of mobile phase within the hydrogel network is dependent on the hydrogel system and environment. Stimuli such as pH/temperature changes[16-17], light[18-19], or analyte binding[20-21] modulate the hydrogel's environment creating a hydrogel volume phase transition (VPT). During the VPT, the polymer network either takes in more solvent and swells or expels solvent and shrinks. Hydrogels are very sensitive to their environment leading to large volume changes from small changes in solution conditions. An example of this is poly(N-isopropylacrylamide) (pNIPAM) which has a lower critical solution temperature (LCST) of 32.5 °C. Above the LCST the polymer undergoes a coil-to-globule transition expelling large amounts of solvent.[22-23]

VPTs derive from changes in the hydrogel's Gibbs free energy (ΔG_{tot}) as explained by Flory and Tanaka polymer theory.[24-25] When the Gibbs free energy of the hydrogel is altered, there is a generation of osmotic pressure (Π) that shifts the hydrogel's volume, either by intaking or expelling solvent, until a new equilibrium is reached (Equation 1.1).

$$\Pi = -\frac{\partial \Delta G_{tot}}{\partial V} = -\frac{\partial \Delta G_{mix}}{\partial V} - \frac{\partial \Delta G_{el}}{\partial V} - \frac{\partial \Delta G_{ion}}{\partial V} = 0$$

Equation 1.1

Gibbs free energy changes can be divided into three contributing factors, the free energy of mixing (ΔG_{mix}), the elastic free energy (ΔG_{el}), and the ionic free energy (ΔG_{ion}). Since the osmotic pressure modulates hydrogel volume based on free energy changes caused by stimuli, the hydrogel volume changes are related to the amount of stimuli.

1.2.1 Free Energy of Mixing (G_{mix})

The free energy of mixing describes interactions between the solvent and polymer network. Essentially, it is the polymer network's solubility in the mobile phase. The polymer-solvent interactions have both entropic and enthalpic contributions and can be described using the Flory-Huggins interaction parameter, χ.[24, 26] A small χ indicates good solubility of the polymer network through polymer-solvent interactions, and a large χ indicates low polymer network solubility. Changes to the hydrogel network through the addition or removal of the analyte along with polymer conformational changes can alter the free energy of mixing by increasing or decreasing the polymer solubility.

Free energy of mixing changes can be modeled using Equation 1.2 where R is the ideal gas constant, T is temperature, V_s is the molar volume of the solvent, V_o is the volume of the dry polymer, V is the volume of the swollen hydrogel, and χ is the interaction parameter.

$$-\frac{\partial \Delta G_{mix}}{\partial V} = -\frac{RT}{V_s}\left[ln\left[1 - \frac{V_o}{V}\right] + \frac{V_o}{V} + \chi\left(\frac{V_o}{V}\right)^2\right]$$

Equation 1.2

One example of a hydrogel VPT based on a change in the free energy of mixing is a pNIPAM hydrogel in water. At T < 32.5˚C pNIPAM-water interactions are favorable due to the highly ordered states of the water around the polymer. As the temperature increases to T > 32.5 ˚C the ordering of the water is no longer favorable. The p-NIPAM expels the water from within the hydrogel network, forming more polymer-polymer interactions instead.[27-29]

1.2.2 Elastic Free Energy (G_{el})

Hydrogel networks are created using crosslinks to hold the polymer strands together. These crosslinks also act as a restoring force during hydrogel swelling. The presence of the crosslinks imparts finite swelling of the hydrogel. The more crosslinks present within the hydrogel the less the hydrogel can swell.

A hydrogel's crosslink density can be changed due to the addition or breaking of crosslinks. Adding crosslinks adds rigidity to the hydrogel actuating a shrinking response while the removal of crosslinks gives the hydrogel access to a wider range of movement actuating a swelling response. If there are two hydrogels that have the same composition, except for the crosslink density, they will undergo different swelling responses to the same stimuli. The hydrogel with the higher crosslink density will be more rigid and will undergo a smaller swelling response compared to the hydrogel with the lower crosslink density.

The hydrogel's swelling response due to changes in the elastic free energy can be modeled using Equation 1.3 where R is the ideal gas constant, T is temperature, n_{cr} is the effective number of crosslinks in moles, V_r is the initial volume of the hydrogel, and V is the hydrogel volume in the swollen/shrunken state.

$$-\frac{\partial \Delta G_{el}}{\partial V} = -\frac{RT \cdot n_{cr}}{V_r}\left[\left(\frac{V_r}{V}\right)^{\frac{1}{3}} - \frac{1}{2}\left(\frac{V_r}{V}\right)\right]$$

Equation 1.3

1.2.3 Ionic Free Energy (G_{ion})

Changes in ionic free energy are caused by the addition of charged species within the hydrogel network.[30] Hydrogel charges can be ionizable groups initially polymerized within the hydrogel network or charged species that become bound to the hydrogel network. These charges within the hydrogel form an electrochemical gradient known as a Donnan potential, which creates osmotic pressure between the hydrogel and the bulk mobile phase. Osmotic pressure is relieved through the inward flow of the mobile phase which brings in counter ions resulting in hydrogel swelling. The more charges within the hydrogel network, the more the mobile phase partitions into the hydrogel.

The degree of the hydrogel swelling response from ΔG_{ion} is dependent on the ionic strength of the solution. High ionic strength solutions inhibit significant hydrogel swelling responses from ionic free energy changes. The large number of available charges in high ionic strength solutions screens the electrochemical potential between the charge density within the hydrogel network and the charge density within the mobile phase.[31] Swelling responses due to ionic mechanisms can be described by Equation 1.4 where R is the ideal gas constant, and c_i is the concentration of mobile ions with c_i being the concentration within the hydrogel and c_i^* the concentration outside the hydrogel.[31]

$$\frac{\partial \Delta G_{ion}}{\partial V} = -RT \sum_{i} (c_i - c_i^*)$$

Equation 1.4

1.3 Photonic Crystals

Photonic crystals (PCs), sometimes known as colloidal crystals, are nanostructures that control the propagation of light based on their periodicity and refractive indices.[32-33] PCs occur in nature and can be seen in the vibrant colors some animal species have for reproduction/predator warnings such as peacock feathers and the Brazilian diamond weevil's scales.[34]

The ability to alter light propagation has made photonic crystals invaluable in various applications such as optics[35-36], sensors[2, 37], and inks[38]. Insights into photonic crystal behavior and fabrication are instrumental in the widespread applications of PCs and to optimize PC performance. This work will focus on periodicities in two- or three-dimensions (2D or 3D) PCs, although one-dimension PCs exist as well.

1.3.1 Photonic Crystal Self-Assembly

Charged nanoparticles interact with each other through a mixture of electrostatic interactions, Van der Waals forces, and Brownian motion that lead from an initially disordered state into a highly ordered crystal array.[39] Placing monodisperse nanoparticles with highly charged surfaces into low ionic strength solutions allows the electrostatic repulsion from the negatively charged surface to create non close packed structures.

This assembly process is believed to be entropic in nature[40] and can lead to the development of structures such as face-centered cubic (FCC) or body-centered cubic (BCC) (Figure 1.1). The structure formed is based on the particle density.[41-43] Both BCC and FCC structures contain a sphere in each corner of the unit cell (cubic structure) while BCCs also have a sphere in the center of the cube and FCCs have spheres centered on each face of the unit cell.

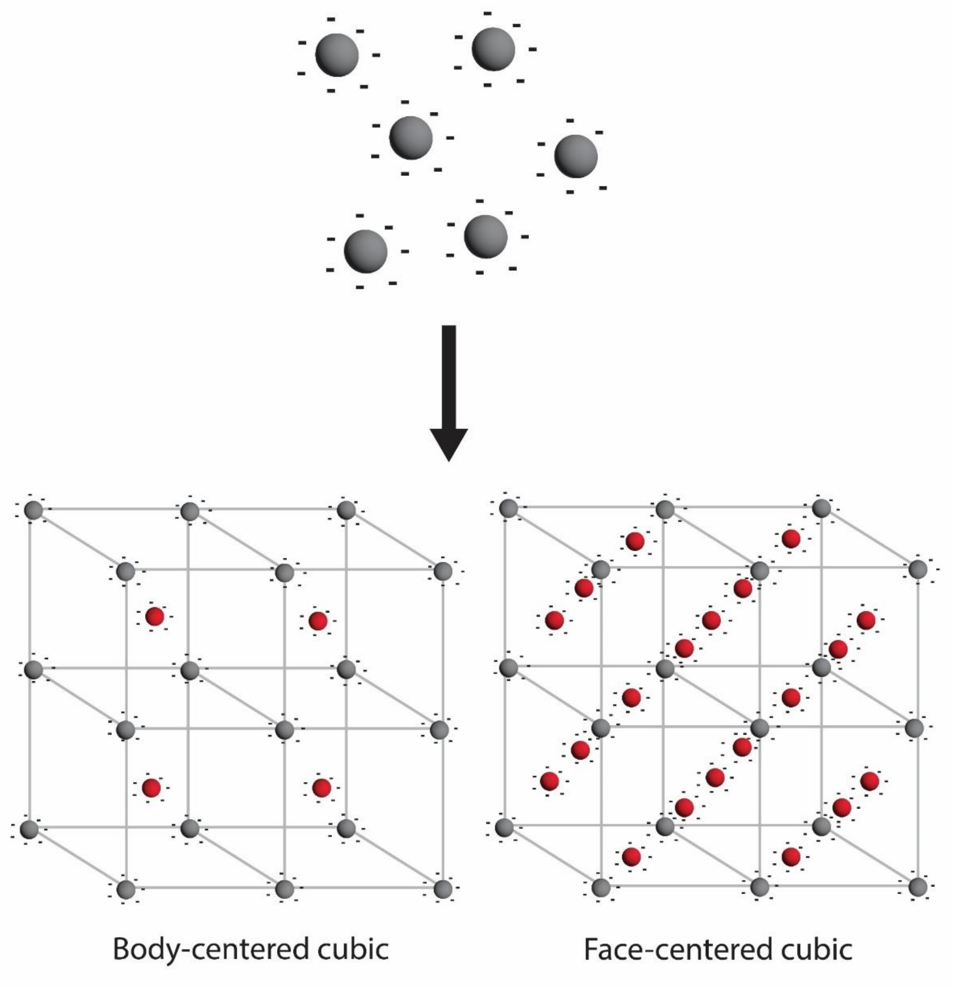

Figure 1.1 Body centered cubic (BCC) and face centered cubic (FCC) lattice structures when undergoing self assembly. Both structures contain nanoparticles in the corner of each unit cell (grey) while BCC structures contain one nanoparticle (red) in the center of each unit cell and FCC structures have a nanoparticle (red) centered on each face of the cubic structure.

Monolayers of photonic crystals can also be created on the surface of water.[44] These monolayers are called two-dimensional photonic crystals (2DPC). The water's surface tension allows assembly to occur at the air-water interface while electrostatic interactions create close packed photonic crystals in hexagonal arrays. Removing the water through drying preserves the ordering of the 2DPC array for later use.

1.3.2 Bragg Diffraction

As light propagates through a suspension of nanoparticles, the light is scattered based on the angle of the incident light and the photonic crystal's physical structure. This work will focus on physical structure changes relating to the particle size and the distance between particles. As the incident light travels through the crystal, it interacts with the array and can undergo constructive or destructive interference. When destructive interference occurs, the light is not able to propagate at certain wavelengths. When constructive interference occurs, light of a certain wavelength is able to travel through the crystal.[32-33] Constructive interference of light scattering within the crystal is determined by the Bragg condition (Equation 1.5),

$$m\lambda = 2n_{eff}d\ sin\theta$$

Equation 1.5

where m is the diffraction order, λ is the wavelength of diffracted light, n_{eff} is the effective refractive index of the system, d is the lattice spacing of the diffracting planes, and θ is the glancing angle of the incident light.[45] The effective refractive index is determined using the weighted average of the refractive indices and volume fraction (f) for each material within the photonic crystal (Equation 1.6).[46] By changing the physical characteristics of the photonic crystal, the Bragg condition is altered and light propagation changes through the crystal.

$$n_{eff} = \sqrt{\sum_i n_i^2 f_i}$$

Equation 1.6

1.3.2.1 Three-Dimensional Array Diffraction

Three-dimensional photonic crystal arrays, referred to herein as crystalline colloidal arrays (CCAs), are multilayered dielectric materials in a three-dimensional alternating pattern. As light travels through the array, it is scattered in all directions due to the change in the dielectric constant.[32] Since CCAs have a large number of particles ordered into a lattice structure, light that meets the Bragg condition (Equation 1.5) will undergo diffraction.

When light is interacting with particles from nearby lattice planes, the light travels dsinθ longer to reach the successive plane than to reach the initial plane (Figure 1.2) .[47] Only distances that are a multiple integer of the wavelength (λ) undergo constructive interference. This typically results in a small number of diffracting wavelengths causing a single color to be seen when diffracting in the visible region. Changes in diffraction in the visible along with other regions of light, such as the ultraviolet or near-infrared regions, can be monitored by sharp diffraction bands measured using a spectrometer.

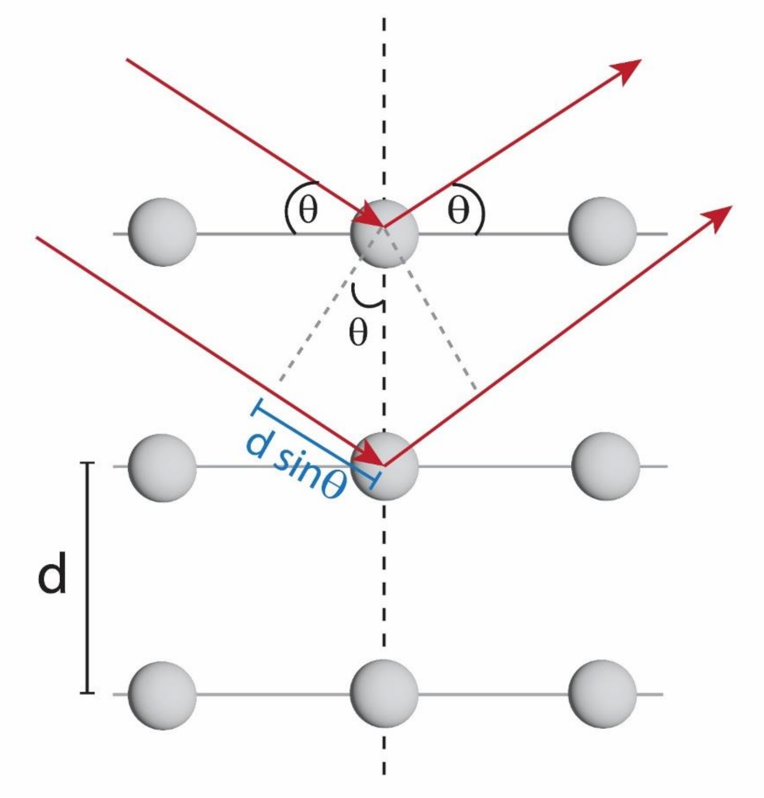

Figure 1.2. Bragg diffraction off an array of particles where the diffracting planes are separated by a distance d. As the light (red arrows) propogates through the crystal at an angle θ and interactts with the particles, the light that fullfills the Bragg condition is diffracted.

1.3.2.2 Two-Dimensional Array Diffraction

Two-dimensional photonic crystal (2DPC) arrays are single layers of alternating dielectric materials that order into hexagonal lattices with a distance, a, between particles (Figure 1.3A). Light that interacts with the 2DPC undergoes constructive interference when the phase shift of the incident light as it travels is equal to the wavelength of light. [44, 48]

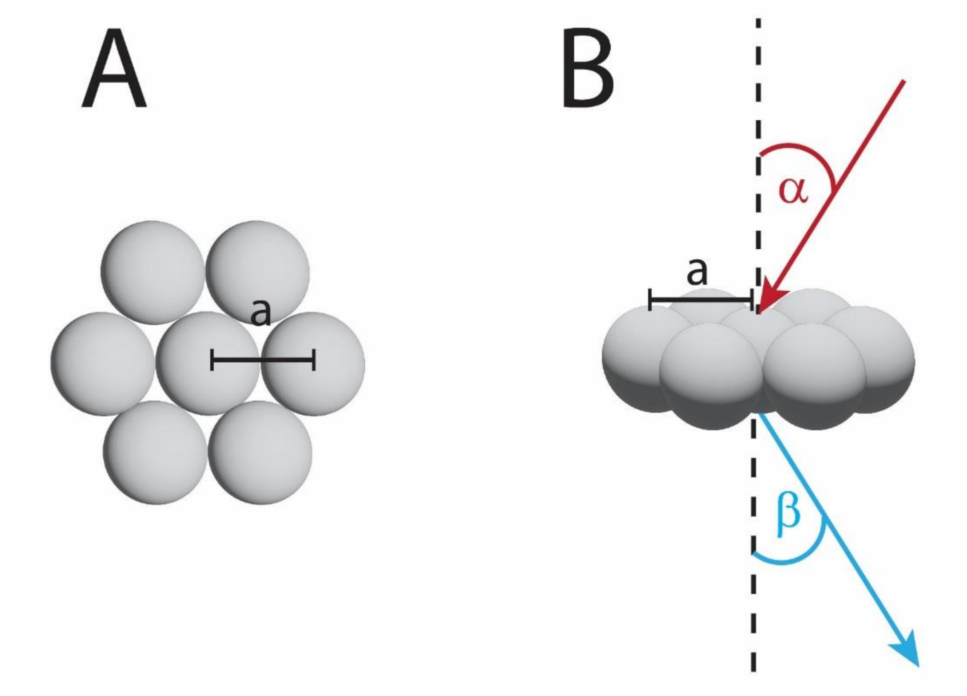

Figure 1.3 (A)Nanoparticles assembled into a hexagonal array (A) where the distance between particles is defined by a. (B) Light introduced at the angle of incidence, α, undergoes Bragg diffraction at angle β when the conditions for constructive inteference occur.

Light that interacts with the 2DPC at an incident angle, α, and meets the Bragg condition is diffracted at an angle β (Figure 1.3B) creating an angle dependence (Equation 1.7).

$$m\lambda = \frac{\sqrt{3}}{2} a(\sin(\alpha) + \sin(\beta))$$

Equation 1.7

In an ordered 2DPC, changes in the 2DPC particle spacing are monitored using the forward scattered light as diffraction off the 2DPC is scattered more strongly in the forward direction.[48] The light is diffracted onto a screen parallel to the 2DPC array into six spots that correspond to the reciprocal lattice vectors of the hexagonal array. Disordering of the array changes the six discrete spots into a continuous ring known as a Debye ring. By measuring the diameter of the Debye ring

(D) and the distance between the 2DPC and the screen (h) we can calculate the diffraction angle using Equation 1.8.

$$\beta = \tan^{-1}\frac{D}{2h}$$

Equation 1.8

If the incident light is normal to the 2DPC, the Bragg diffraction dependence on α becomes zero. Substituting Equation 1.8 into Equation 1.7 for β, forms Equation 1.9. The wavelength of light is known, and the height and diameter are easily measured allowing the particle spacing to be calculated.

$$m\lambda = \frac{\sqrt{3}}{2} a \sin\left(\tan^{-1}\frac{D}{2h}\right)$$

Equation 1.9

1.4 Photonic Crystal Hydrogel Sensors

Photonic crystal hydrogel sensors are developed by polymerizing a hydrogel network around a photonic crystal array. The photonic crystal can be two- or three-dimensional (2DPC or 3DPC) and made up of a variety of materials such as polystyrene or silica.[49-50] The hydrogel network is designed to selectively respond to stimuli by undergoing a volume change through swelling or shrinking. As the hydrogel volume changes so does the spacing between particles, shifting the Bragg diffraction (Figure 1.4). Small changes in the hydrogel's environment can lead to large volume changes making changes in light diffraction highly sensitive to analyte binding.

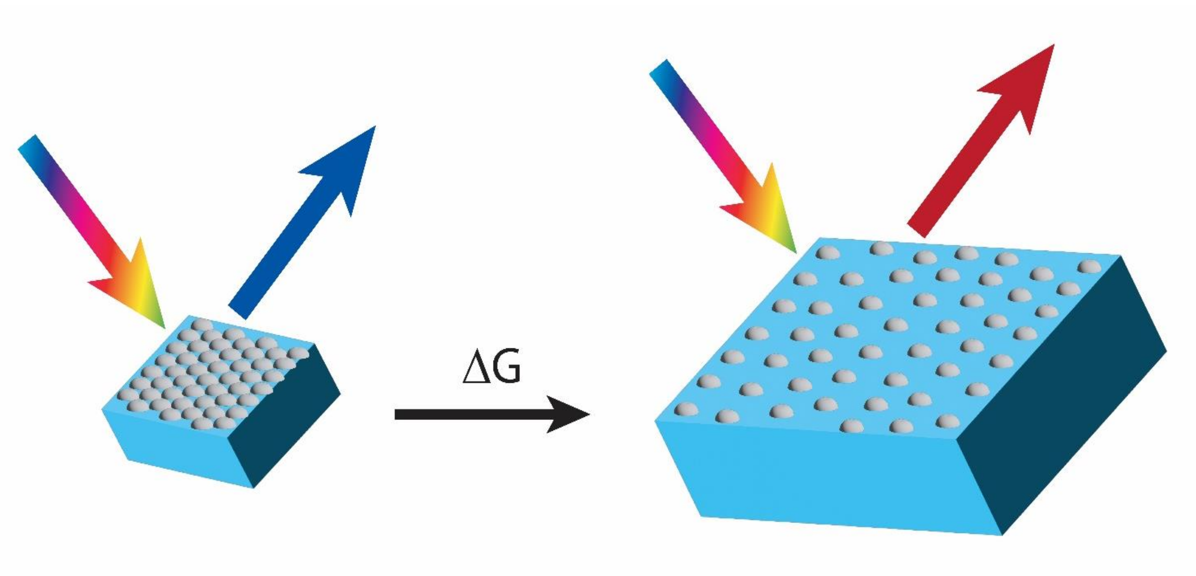

Figure 1.4 Changes in the diffracted light of a 2DPC hydrogel from changes in the hydrogel's Gibbs free energy caused by external stimuli

The Asher group has led the development of photonic crystal hydrogel sensors through the creation of polymerized crystalline colloidal arrays (pCCAs).[14] The development of pCCAs enable the monitoring of a variety of changes visually through changes in light diffraction leading to a color change (Figure 1.5A). While 2DPC hydrogels do produce visible color changes, their swelling responses can also be easily monitored using a laser pointer and ruler (Figure 1.5B).

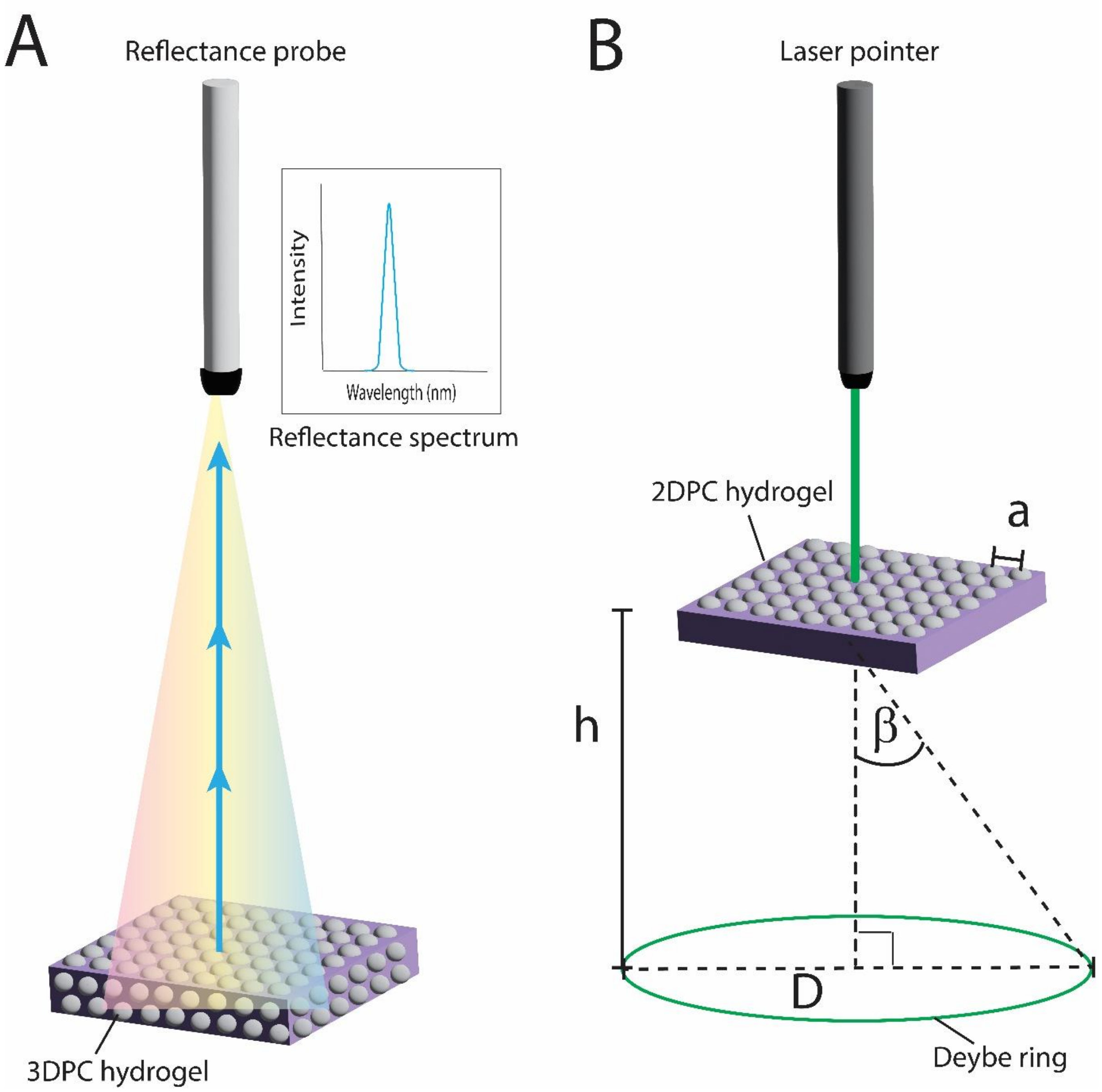

Figure 1.5 Particle spacing measurements for (A) 3DPC hydrogels and (B) 2DPC hydrogels. 3DPC hydrogel measurements use a reflectance probe that sends off a broad range of visible light. When light that meets the Bragg criteria is diffraced back, it is collected by the probe and a reflectance spectrum is created based on the wavelength detected. For 2DPC hydrogels, a laser pointer is used to send a single wavelength of light at the 2DPC. As the forward light is diffracted onto a screen, a Debye ring is visible which can be measured to calculate the particle spacing

Photonic crystal hydrogels are fabricated by creating a crystalline array and embedding it within a polymer network. Nanoparticles that make up the photonic crystal have charged surfaces which create arrays through self-assembly by electrostatic interactions. For 3DPC hydrogels, a colloidal suspension of nanoparticles is added to a monomeric solution. The nanoparticles become ordered within the monomer solution. When initiated, polymerization occurs around the nanoparticles immobilizing the array within the polymer network.

For 2DPC hydrogels, the nanoparticles are injected at the air-water interfaces enabling the formation of a monolayer of nanoparticles into a hexagonal close packed array on the water surface. The array is then picked up and dried on a substrate such as a glass slide. Deposition of a monomer solution on the dried 2DPC array polymerizes the photonic crystal around the hydrogel network.

Using both 2D- and 3D- photonic crystals enables the development of a wider range of sensors for different environments. The obvious color change of a 3DPC sensor is better suited for public use while a 2DPC sensor enables use of high ionic strength monomer solutions without array disordering as the photonic crystal is dried prior to polymerization. By studying photonic crystal hydrogel fabrication and behavior, we can more easily develop and adapt them for portable sensing and widespread monitoring of one’s health and environment.

1.5 Overview of Research Program

In the subsequent chapters we report investigations into the development and adaptations of biomolecular photonic crystal hydrogel sensors for the detection of molecules as small as lactate, to large targets such as the protein thrombin. We used biomolecules to selectively monitor the presence of our target with the sensitivity of the hydrogels' VPTs to monitor analyte concentration. In Chapter 2, we investigate the use of 2DPC hydrogels containing oxyamine functional groups for the detection of lactate and how they can be adapted from sensing phenylpyruvate. The use of enzymes such as lactate dehydrogenase allows wider detection of biomolecules through enzymatic conversion for indirect analyte monitoring. In Chapter 3, we look at how the incorporation of DNA aptamers as recognition groups within 2DPC hydrogel sensors can be used to detect the protein thrombin while being useful as a generalizable sensing motif through adaptation from sensing the small molecule adenosine. In Chapter 4, we investigated the development of polymerized crystalline colloidal array hydrogels for the detection of hydrophobic analytes that may otherwise be difficult to detect. Results from these studies will be used to develop adaptable sensors that can be used for sensitive analyte detection outside a laboratory environment.

2.0 Enzyme Coupled Photonic Crystal Hydrogel Sensors: Detection of Lactate Using Lactate Dehydrogenase

This chapter was authored by Goda, S.A., Jang, K., and Asher, S.A.

Author Contribution: S.A.G. and K.J designed the experiments. S.A.G. fabricated samples, and collected and analyzed data with assistance from K.J. This chapter was prepared by S.A.G with assistance from K.J. and S.A.A

The presence of biomolecules in the body is important in the ability to monitor one's health, but detecting them can require considerable time and effort if not done in a laboratory environment. The development of sensing materials that are accessible and easily used by the general population will allow wider detection of biomolecules. Faster detection methods will enable better monitoring in resource limited settings. We have investigated the use of one such material for the detection of lactate, which can be indicative of health issues and infection, such as sepsis. Below we report the use of two-dimensional photonic crystal (2DPC) hydrogels as sensing materials for the presence of lactate.

2DPC hydrogel sensors contain a photonic crystal array embedded within a stimuli-responsive hydrogel network. The hydrogel undergoes a volume phase transition (VPT) upon analyte binding through alterations in the hydrogel's osmotic pressure. We monitored the presence of lactate through the enzymatic conversion of lactate to pyruvate using lactate dehydrogenase (LDH). The pyruvate is covalently attached to the hydrogel network using oxime ligation resulting in the hydrogel's swelling response. Hydrogel swelling alters the particle spacing of the photonic crystal array shifting the light diffracted from the crystal array. Our sensor can detect 0.24 mM lactate in buffer solutions and < 4 mM lactate in solutions containing protein removed fetal bovine serum.

2.1 Introduction

Lactate and lactic acid are small molecules used in many industries including the food industry[51], cosmetics[52-53], and biopolymer development[54-55]. Lactate levels in the body are also used to monitor patient health such as infection[56], pulmonary function[57], and hepatic and renal function[58-59]. Common lactate detection methods include colorimetric assays[60], fluorimetry[61], gas[62] and liquid[63-64] chromatography, and capillary electrophoresis[65]. These methods can require bulky instrumentation that need large amounts of power and highly trained personnel. In recent years a variety of different lactate sensing motifs have been developed [66-67], however few have the adaptability to be used as hand held devices[68] and many still have sensing limitations.[63-64] There is also discrepancy on the correlation, if any, between lactate levels in different body fluids such as blood and sweat.[69-72] The ability to easily and accurately monitor lactate outside laboratory environments would enable wider surveillance of health risks associated with elevated lactate levels.

Sepsis and septic shock are serious conditions that affect millions of people each year and lead to death for more than one in four people who have them.[73-74] Quick detection and treatment can lead to decreased severity and lower 28-day mortality rates in patients diagnosed with sepsis.[75-76] Combined monitoring of hypertension and elevated lactate levels (> 2 mM)[77-78] have been suggested for use in gauging severity and treatment plans in patients[75], with increased recovery rates for every hour of early lactate monitoring[79-80]. While lactate monitoring is readily available in hospital settings, at home monitoring can allow earlier detection and treatment of elevated lactate levels.

Two-dimensional photonic crystal (2DPC) hydrogel sensors are composed of a stimuli-responsive polymer network with an embedded photonic crystal array. They are small and robust while being inexpensive to fabricate, making them ideal platforms for portable sensing. The hydrogel network undergoes volume phase transitions (VPTs) actuate by chemical stimuli that alter the particle spacing of the embedded photonic crystal array. Alterations in the array's spacing lead to shifts in the light diffracted from the crystal. As changes in the hydrogel's volume are proportional to the concentration of chemical stimuli present, shifts in light diffraction can be used to quantify the target analyte.

The Asher group has previously fabricated 2DPC hydrogels with a variety of different recognition groups, exploring the potential of 2DPC hydrogels to be used as biomolecular sensors.[81-83] One of these 2DPC hydrogels contains an oxyamine recognition group to selectively monitor phenylpyruvate in serum for the development of a phenylketonuria sensor.[84] Phenylpyruvate (PhPy) was covalently attached to the hydrogel's oxyamine group through the pyruvate's ketone functional group with a detection limit in serum solutions of 19 μM PhPy within 30 min.

We are further investigating the behavior of this sensor by showing we can couple the enzymatic production of compounds containing pyruvate moieties with oxime-pyruvate attachment. We used lactate dehydrogenase (LDH), a well-studied enzyme[54-55], for this proof-of-concept study. LDH is an oxidoreductase enzyme that reversibly converts pyruvate to lactate using oxidation/reduction of its cofactor nicotinamide adenine dinucleotide (NADH/NAD^+). The reversibility of this pyruvate-lactate conversion is vital to cellular respiration.[85] The enzymatic production of pyruvate will allow a wider use of our 2DPC hydrogel sensing motif by indirect sensing of compounds like lactate. It will also demonstrate generalizability of our 2DPC hydrogel sensor using oxyamine functional groups. We are the first to look at coupling an enzymatic reaction with photonic crystal hydrogel sensors for indirect analyte detection.

2.2 Experimental Section

2.2.1 Materials

Acrylamide (AAm), N,N'-methylenebisacrylamide (MBAAm), acrylic acid (AAc), 2-hydroxy-4'-(2-hydroxyethoxy)-2 metylpropiophenone (Irgacure 2959), propylene glycol, dimethylsulfoxide (DMSO), 1-propanol, *p*-phenylenediamine (*p*-PDA), L-lactate, L-pyruvate, nicotinamide adenine dinucleotide (NAD), bovine serum albumin (BSA), trizma base, alanine, and lactate dehydrogenase (LDH)-human recombinant expressed in E.coli were purchased from Sigma-Aldrich. Propionic acid and hydrochloric acid (HCl) were purchased from J.T. Baker and Thermo Fisher respectively. Fetal bovine serum (FBS) was purchased from Corning. AAc stabilizers were removed by passing it through a column of aluminum oxide. Unless otherwise stated, all chemicals were used as received.

Tert-butyl(2-acrylamidoethoxy)-carbamate (TAC) was synthesized using the three step sequence published by Jang et al.[84] Polystyrene particles were fabricated using dispersion polymerization as described by Zhang et al.[86] All solution were made using water from a MilliQ Reference A+ system (resistivity 18.2 MΩ·cm, TOC <5 ppb).

2.2.2 2DPC Hydrogel Fabrication

Preparation of the 2DPC hydrogels used for lactate detection is shown in Figure 2.1 and has been described in detail elsewhere.[84] Briefly, a 2D photonic crystal was fabricated by mixing negatively charged polystyrene nanoparticles (~1.2 μm diameter, 16 % w/w in water) with 1-propanol at a 3:1 ratio. The solution was injected at the air-water interface of a crystallization dish of ultrapure water using the needle-tip flow method.[87] The nanoparticles self-assembled into a close packed hexagonal array which was transferred to a glass slide and air dried for 24-48 hrs.

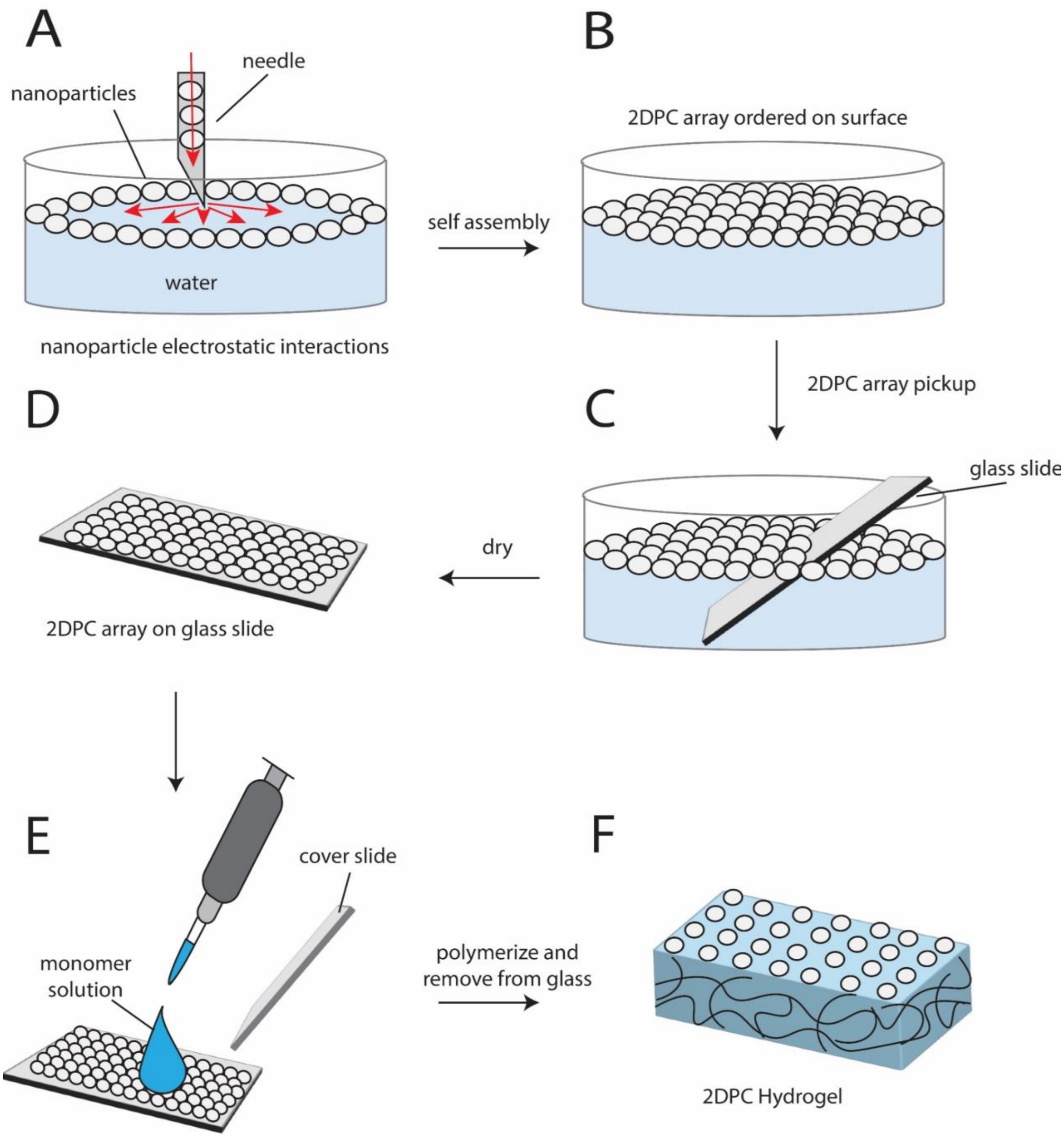

Figure 2.1 2DPC hydrogel fabrication using the needle-tip flow method. Polystyrene nanoparticles are injected at the air-water surface (A) where they self-assemble into an ordered 2DPC array (B). A glass slide is used to pick up the array from the water surface (C) and left to dry (D). A monomer solution is deposited onto the slide with the dried 2DPC and a cover slide is placed on top (E). After polymerization the slides are placed in buffer for 10 min and the hydrogel is removed from the glass slides for use (F).

A monomer solution containing AAm, TAC, MBAAm, AAc, propylene glycol, and water was prepared in accordance with Table and degassed using a vacuum desiccator for 15 min. Irgacure 2959 initiator (33 % w/v in DMSO) was added to the monomer solution at 2 µL initiator for every 100 µL monomer solution. The solution was quickly mixed by pipetting up and down for 15 sec. A 96 µL aliquot of the solution was deposited on the glass slide containing the dried 2DPC and a cover slide was gently placed on top spreading the solution into a thin film for polymerization. Polymerization was initiated with 365 nm light using a UVP UVGL-55 handheld lamp and occurred for 15 min at room temperature. Upon completion, the glass slides were placed in 100 mM phosphate buffered saline solution (PBS, pH 7.2) for 10 min until the hydrogel was able to be gently peeled from the glass substrates. The poly(TAC-*co*-AAm-*co*-AAc) hydrogel was thoroughly washed in PBS and stored in the fridge until deprotection.

Table 2.1 Compostition of precursor solution for lactate sensing 2DPC hydrogels

Component	**Mass (mg)**	**Weight % (w/w)**
AAm	16	8
TAC	20	10
MBAAm	1	0.5
AAc	4	2
Propylene Glycol	90	45
Water	69	34.5
Total	200	100

The TAC monomers contain a *tert*-butyloxycarbonyl (BOC) group for oxyamine protection during polymerization. Acidic conditions were used to remove the BOC group through a stepwise solvent exchange of acid and water within the hydrogel mobile phase. The hydrogel was left in each solution for 10 min before the next addition. The hydrogel was first placed in 1 M HCl increasing the HCl concentration to 3 M and 5 M before decreasing it back to 1 M as described in Table . Following deprotection, the hydrogels were washed with 100 mM tris buffer (pH 7) overnight. Hydrogels were then cut into 0.5 cm x 0.5 cm pieces and stored in 100 mM tris buffer (pH7) in the fridge (4°C) until use.

Table 2.2 Stepwise addition of HCl and water for BOC deprotection of hydrogel

Step	12 M HCl Added (mL)	Water Added (mL)	Total Volume (mL)	Approximate Concentration HCl (M)
1	1	11	12	1.2
2	3	-	15	3
3	5	-	20	5
4	-	16	36	3
5	-	72	109	1

2.2.3 Particle Spacing Measurements

Hydrogel volume was monitored using the 2DPC's particle spacing by measuring the 2DPC's Debye ring diameter (Figure 2.2). Ordered 2DPCs diffract light parallel to the 2D array as six spots otherwise known as a Debye ring. The array diffracts light according to the Bragg condition (Equation 2.1) where m is the diffraction order, λ is the wavelength of incident light, a is the distance between particles in the photonic crystal array, and α and β are the angles of incident and diffracted light respectively.

$$m\lambda = \frac{\sqrt{3}}{2}a(\sin\alpha + \sin\beta)$$

Equation 2.1

By setting the light source normal to the array, the contribution of $\sin\alpha$ becomes zero. Using a monochromatic light source, such as our 532 nm laser pointer, the wavelength of incident light and diffraction order (m=1) are known, giving Equation 2.2.

$$532\ nm = \frac{\sqrt{3}}{2}a(\sin\beta)$$

Equation 2.2

The Debye ring is measured using the forward scattered light at angle β. Based on the height of the 2DPC array and the diameter of the Debye ring, β can be calculated by

$$\beta = tan^{-1}(\frac{D}{2h})$$

Equation 2.3

making Equation 2.4.

$$a = \frac{2(532\ nm)}{\sqrt{3}\sin\left(\ tan^{-1}(\frac{D}{2h})\right)}$$

Equation 2.4

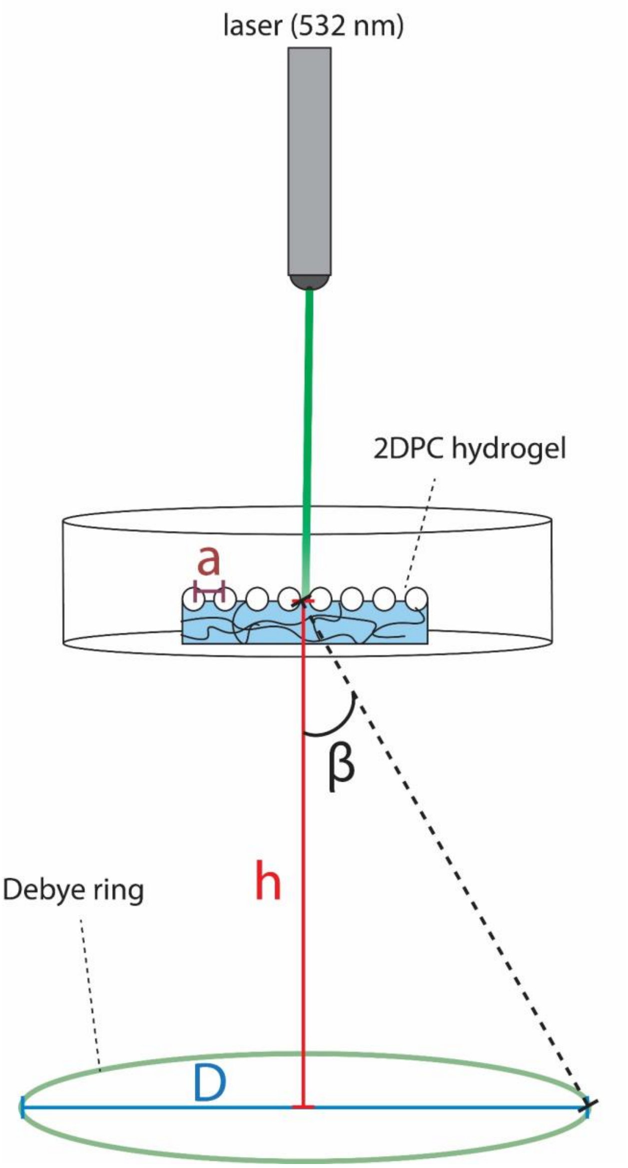

Figure 2.2 Experimental setup for 2DPC hydrogel particle spacing measreuements.

2.2.4 LDH Assays

LDH activity was monitored using LDH's conversion of lactate to pyruvate at room temperature through the formation of the NADH absorbance band centered at 340 nm. Stock solutions were made in 100 mM tris buffer pH 7-9 and contained 5.36 mM NAD^+ or 1.5 M sodium lactate. An LDH/BSA solution was made by adding 8 U LDH to 1.5 mL of 1% (w/v) BSA in 100 mM tris buffer (pH 7-9). Assay solutions were measured in a 1cm pathlength absorbance cuvette and contained 2.8 mL of the NAD^+ stock solution and 0.1 mL of the lactate solution with a micro stir bar. 0.1 mL of the LDH/BSA solution was injected into the cuvette. The absorbance was monitored using Cary WinUV software for a Cary 5000 UV-Vis-NIR spectrophotometer (Agilent) collecting every 0.1 s. The absorbance was monitored at 360 nm to reduce interference from samples containing *p*-PDA.

2.2.5 Lactate Detection Using 2DPC Hydrogels in Buffer Solutions

Each solution for LDH's conversion of lactate to pyruvate was 500 µL in volume. The solutions contained 100 mM tris buffer (pH 9) along with 10 mM NAD^+, 80 U lactate dehydrogenase, 1% BSA protein to stabilize the LDH, and 0, 0.25, 0.5 1, 5, 25, or 50 mM sodium lactate. All concentrations reported are based on the sample volume of 1 mL during hydrogel attachment. The solutions were mixed on a vortex mixer for 30 min at 750 rpm. A 100 µL aliquot of 1.2 M HCl was added to the solution and mixed for 5 min to denature the LDH, stopping the reversible conversion of pyruvate to lactate as the solution pH is adjusted.

A 400 μL aliquot of 350 mM *p*-PDA in 100 mM bis-tris (pH 6) was added to the solution and adjusted to pH 6. A 0.5 cm x 0.5 cm piece of 2DPC hydrogel was equilibrated in 5 mL buffer (100 mM tris, pH 7) and the initial particle spacing was measured. The 0.5 cm x 0.5 cm hydrogel was added to the solution and placed back on the vortex mixer for 30 min for pyruvate attachment. An example of the solution conditions for 5 mM lactate is shown in Table .

The hydrogel was removed from the solution and washed in 5 mL aliquots of 100 mM tris buffer (pH 7) for 15 min changing the buffer every ~ 3- 5 min. The hydrogel's particle spacing was measured and the difference between the final and initial particle spacing was calculated and reported as the particle spacing change (PSC).

A control hydrogel was also fabricated without the TAC recognition group to monitor any hydrogel volume changes from the pH adjustments and adjustments to the solution during sensing. The precursor solution for the control hydrogel contained the same masses for each component as listed in Table apart from TAC which was not added.

Table 2.3 Hydrogel solution conditions for detection of 5 mM lactate. Final concentrations were calculated based on 1 mL solution volume during attachment to the hydrogel.

Step	Component	Stock	Volume Added (µL)	Final Concentration (1000 µL)
1.) Lactate to pyruvate conversion (100 mM tris, pH 9)	Lactate	100 mM	50	5 mM
	NAD^+	50 mM	100	5 mM
	BSA	2 % (w/v)	250	0.5 % (w/v)
	LDH	2000 U/mL	40	80 U
	100 mM Tris pH 9	-	60	-
2.) LDH denaturation	HCl	1.2 M	100	0.12
3.) Enzyme produced pyruvate quantification	*p*-PDA (in 100 mM bis-tris pH 6)	350 mM	400	140
	2DPC Hydrogel	-	-	0.5 cm x 0.5 cm

2.2.6 Determination of 2DPC Hydrogel Swelling Response to NAD$^+$/NADH

Solutions of 0, 1, 2, 5, and 10 mM NAD$^+$ or NADH were used to determine the hydrogel swelling response caused by the enzymatic cofactor. NAD$^+$/NADH concentrations are based on the 1 mL final sample volume for hydrogel attachment. NAD$^+$/NADH solutions did not contain other assay components (lactate, LDH) or BSA, but were made initially using 100 mM tris (pH 9) and vortexed for 30 min followed by pH adjustments using HCl and the addition of *p*-PDA. Once the hydrogels (0.5 cm x 0.5 cm) were added to the 1 mL sample solution, the solution was vortexed, and the hydrogel attachment proceeded for 30 min. Hydrogels were removed from the solution and washed using 100 mM tris buffer (pH 7) before their final particle spacing was measured.

2.2.7 Determination of NAD$^+$ Interference in Pyruvate Detection

Final concentrations of pyruvate solutions were 0, 0.15, 0.25, 0.5, 2, or 5 mM pyruvate during hydrogel attachment. 5 mM NAD$^+$ was added to solutions containing both pyruvate and NAD$^+$. Solutions were made using 100 mM tris buffer (pH 9) at volumes of 500 µL and vortexed for 30 min at 750 rpm. 100 µL 1.2 M HCl was added, and the solution was mixed for 5 min. *p*-PDA was added (400 µL of 350 mM in 100 mM bis-tris, pH 6) and the solution pH was adjusted to 6. Hydrogel pieces (0.5 cm x 0.5 cm) were placed in the solutions and vortexed for 750 rpm for 30 min. The hydrogels were removed from the solution and washed in 100 mM tris buffer (pH 7) for 15 min.

2.2.8 Hydrogel Characterization Using UV-Vis Absorbance Spectroscopy

Attachment of NAD^+/NADH and pyruvate to the hydrogel network were confirmed using UV-vis absorbance measurements. Hydrogels were fabricated as described in Section 2.2.2, however no 2DPC array was attached. Once fabricated and deprotected, hydrogels were cut into ~1 cm x 3 cm pieces. Solutions were initially 5 mL in volume and contained 10 mM pyruvate, NAD^+, or NADH (100 mM tris, pH 9) and vortexed for 30 min. HCl (1 mL, 1.2 M) was added to each solution to decrease the pH to < 2. Solutions were mixed for 5 min followed by the addition of *p*-PDA (4 mL 350 mM in 100 mM bis tris, pH 6) and adjusted to pH 6. A hydrogel was placed in each solution and vortexed for 30 min. Hydrogels were removed from the solutions and washed with buffer (100 mM tris, pH 7) overnight. Samples were placed on a 1 cm x 5 cm quartz slide and UV-Vis spectra were collected on a Varian Cary 5000 UV-vis-NIR spectrometer. The jump of absorbance at 350 nm is due to a changeover of the spectrometer lamp.

2.2.9 Lactate Detection in Fetal Bovine Serum (FBS) Solutions

Two compositions of fetal bovine serum (FBS) solutions were tested. First, solutions containing protein removed FBS (PRFBS) were created by centrifuging FBS in 10 kDa centrifugal filters (as following the instructions of the manufacturer) to remove proteins. 100 mM trizma base was dissolved in the protein removed FBS and the pH was adjusted to pH 9. The PRFBS was used to create all solutions for the enzymatic conversion of lactate to pyruvate. To stabilize the LDH during the conversion, BSA was added back in. The LDH solution was developed the same as in step 1 in Table 2.3 with the PRFBS solution and allowed to proceed the same as in buffer solutions (section 2.2.5) using 1, 2, 3, 25, or 50 mM lactate. Due to the low solubility of *p*-PDA in high ionic strength solutions like FBS, *p*-PDA was not dissolved in FBS instead being left in 100 mM bis-tris buffer. FBS was also not used to create HCl solutions giving a final concentration of 50 % PRFBS.

FBS solutions containing serum proteins were created by adding 100 μL FBS to the enzyme solutions giving a final concentration of 10% FBS. To keep sensing conditions consistent, FBS was used to dissolve 100 mM tris and adjusted to pH 9 before addition. BSA proteins make up a significant portion of the total proteins in FBS so BSA protein was not added into solutions containing 10% FBS.

2.3 Results and Discussion

2.3.1 Lactate Sensing Mechanism

Our sensor relies on the conversion of lactate to pyruvate by LDH through reduction of the NAD^+ cofactor to NADH. While LDH is active from pH 7-11, the conversion of pyruvate to lactate is the more favored reaction around neutral pH with lactate to pyruvate conversion favored at alkaline pHs.[88] Using pH 9 we can more favorably convert lactate to pyruvate. Inhibition of the pyruvate to lactate conversion is achieved through denaturation of the LDH using HCl. Pyruvate attachment to the hydrogel network is catalyzed using *p*-PDA. While *p*-PDA has demonstrated usefulness as a catalyst for bioconjugation, its contribution to oxime ligation is significantly slowed above pH 6 with attachment being ~5x's faster at pH 6 than pH 7.[89] Separating LDH's conversion of lactate to pyruvate from pyruvate's attachment to the hydrogel enables working at conditions that are optimal for each step (Figure 2.3).

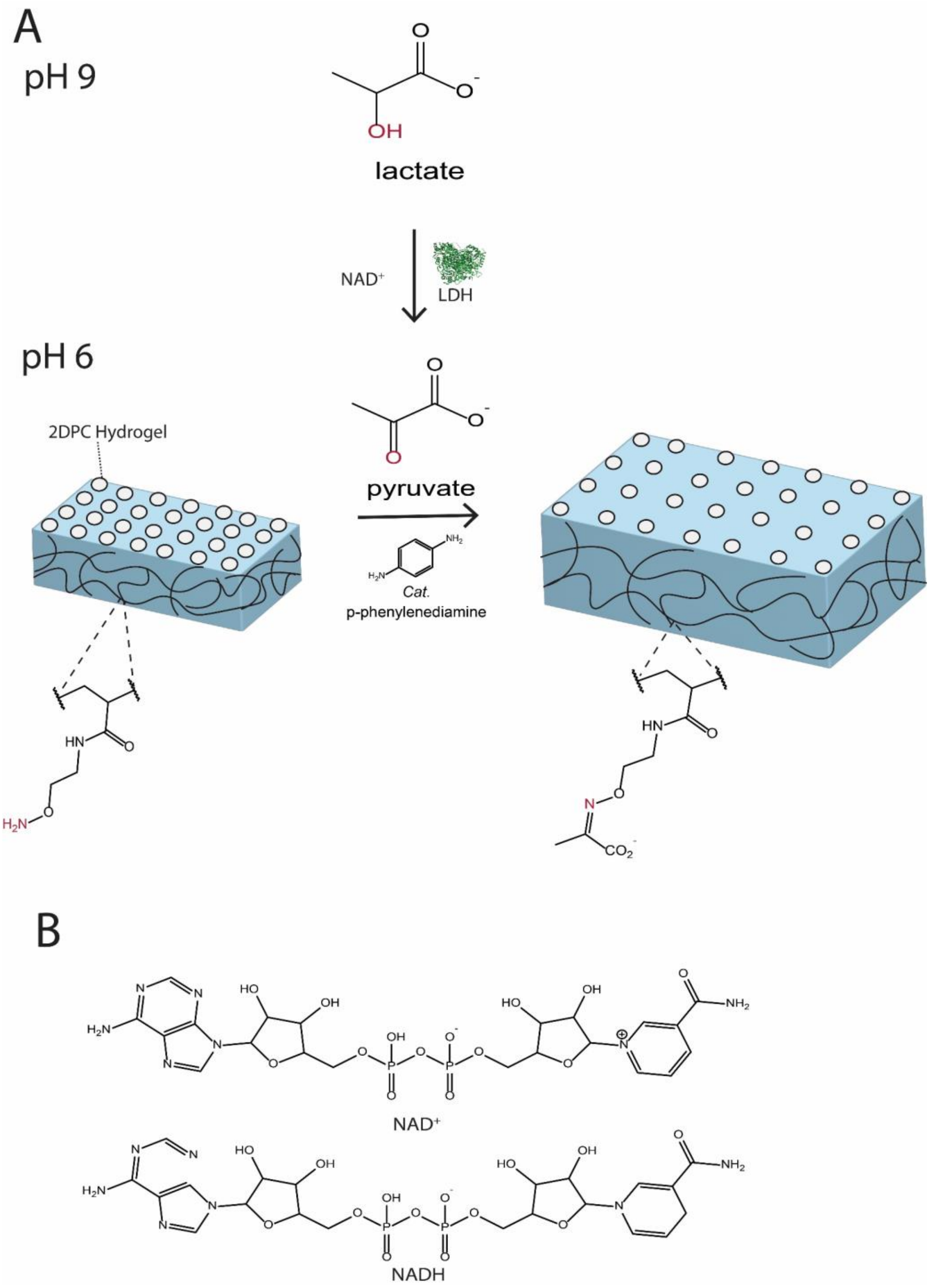

Figure 2.3 (A) Schematic of the 2DPC hydogel’s detection of lactate using enzymatic converison of lactate to pyruvate. LDH is used to covert lactate to pyruvate which is attached to the hydrogel network using catalyzed oximine ligation. Addition of pyruvate to the hydrogel network leads to a hydrogel swelling response proportaional to the concentration of pyruvate attached. Functional groups involved in the sensing reaction are in red. (B) Structures of NAD^+ and NADH.

TAC-*co*-AAm-*co*-AAc hydrogels contain free oxyamine groups that undergo oxime ligation with the ketone on pyruvate. Covalent attachment of the pyruvate to the hydrogel causes a change in the free energy of the hydrogel generating osmotic pressure. The hydrogel relieves this pressure by taking in solvent leading to hydrogel swelling. The hydrogel swelling response increases the particle spacing of the embedded 2DPC as measured by a change in diffraction. Conversion of lactate to pyruvate occurs at a 1:1 ratio creating a correlation between the hydrogel's VPT and lactate concentration.

2.3.2 Lactate Detection in Buffer Solutions

Due to LDH's ability to convert pyruvate back to lactate at neutral pHs, we utilized an alkaline buffer (pH 9) to produce lactate. HCl was then added to denature the LDH stopping the conversion of pyruvate back to lactate. The addition of the bis-tris buffer with *p*-PDA prevented fluctuations outside the buffer range when changing from pH 9 to 6 during the optimized attachment of pyruvate to the hydrogel. The hydrogels were washed in 100 mM tris buffer before particle spacing measurements to remove the additional ionic strength of the solution from the *p*-PDA.

LDH assay times of 30 min were chosen based on UV-Vis absorbance data showing a decrease in NADH production after 30 min. We chose 30 min for the attachment reaction of pyruvate based on earlier investigations of the hydrogel's response to phenylpyruvate[84] which showed a plateau in the hydrogel's swelling response to 5 mM phenylpyruvate after 30 min. Combining the enzymatic production of pyruvate with hydrogel attachment, we are able to detect the presence of lactate in ~1 h while our use of 0.5 cm x 0.5 cm hydrogel pieces enabled use of small sample volumes (1 mL) during detection.

We tested hydrogels before and after reacting with solutions containing 0-50 mM lactate. Initial particle spacing of each hydrogel was measured after incubation in 5 mL of 100 mM tris buffer (pH 7). Assay reactions occurred in a 4 mL dram vial to ensure homogeneity of the solution while mixing and allow full immersion of the hydrogel piece. After the enzymatic production of pyruvate, LDH was denatured using HCl (100 µL, 1.2 M) for 5 min followed by addition of *p*-PDA (400 µL of 350 mM in 100 mM bis-tris buffer pH 6) for a final solution volume of 1 mL. Adjustments to the solution were made using 1.2 M HCl to a final pH of 6. All additions of HCl to each sample were < 15 µL adding < 2 % to the total solution volume during the pH adjustment.

Hydrogels were added to the solution after the addition of p-PDA and pH adjustments. After 30 min the hydrogels were washed with 100 mM tris buffer (pH 7) and the final particle spacing was measured. Each measurement was performed in triplicate using a new hydrogel piece and solution.

The PSC was determined by subtracting the initial particle spacing from the final particle spacing for each hydrogel piece. The average swelling response and standard deviation of the measurements reported were calculated and adjusted by subtracting the average swelling response of the blank from the PSC of each lactate solution and propagating error. The adjusted PSCs are reported in Figure 2.4. The limit of detection (LoD) was calculated using the adjusted blank and lowest two concentrations. The LoD was calculated using Equation 2.5 and determined to be 0.24 mM lactate.

$$LoD = \frac{3 * (stdev\ blank)}{slope\ of\ linear\ fit}$$

Equation 2.5

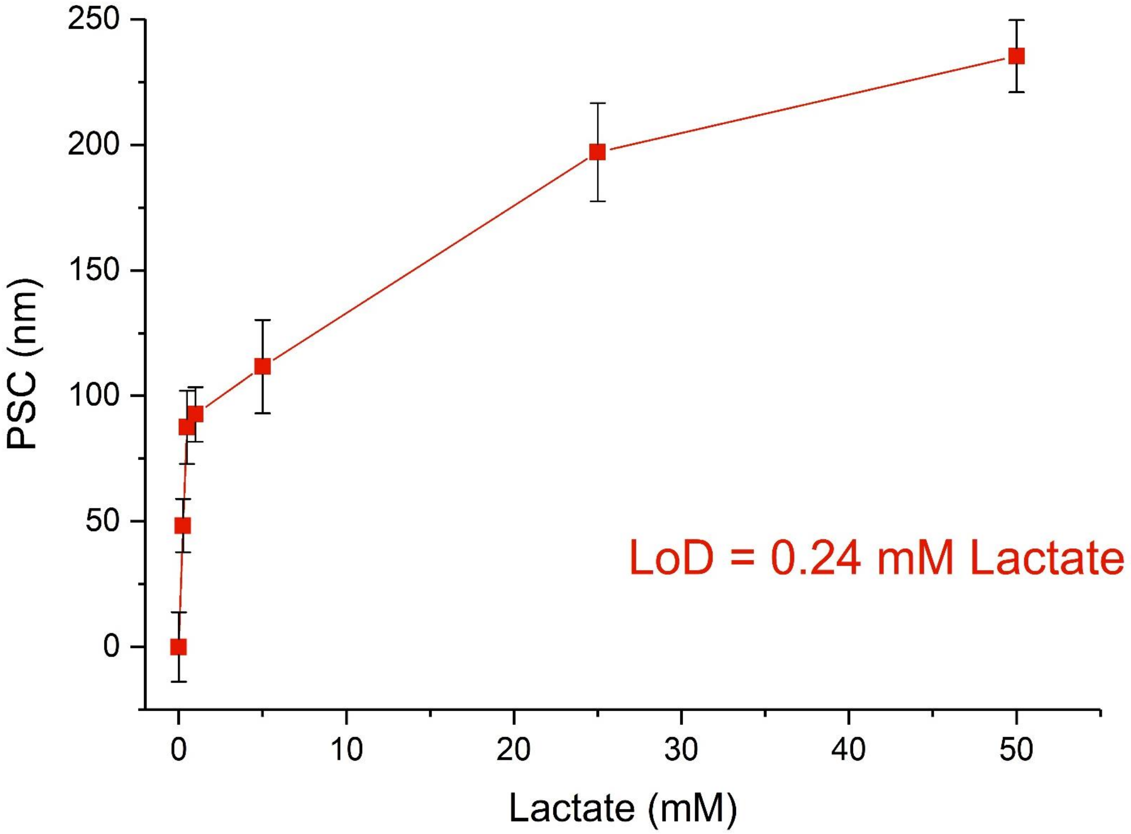

Figure 2.4. Monitoring of 2DPC hydrogel sening response to LDH enzymatic assays containing varying concnetratons of lactate in buffer solutions. Error bars indicate standard deviations (n=3).

Healthy blood lactate levels range from 0.5-2 mM lactate with 2-4 mM lactate considered hyperlactatemia and > 4 mM considered lactic acidosis.[90] Our sensors are able to detect lactate concentrations in buffer solutions that are lower than normal physiological levels in human serum. While the additional components in serum can cause interferences in measurements, elevated lactate levels are over an order of magnitude larger than our calculated LoD in buffer solutions.

2.3.3 2DPC Hydrogel Swelling Response to the Presence of NAD^+/NADH

The response of our control measurements in buffer did not contain lactate but still gave a significant swelling response of 134 nm ± 10 nm. Vigorous hydrogel washing did not reverse the swelling response leading to the hypothesis that a compound other than pyruvate was also being attached to the hydrogel. We investigated further by adding *p*-PDA to solutions containing only individual assay components of 5 mM lactate, 80 U LDH, 1 % BSA or 5 mM NAD^+. All but the solution of NAD^+/*p*-PDA did not swell while the NAD^+/*p*-PDA solution gave a swelling response similar to the blank. The hydrogel's swelling response to the NAD^+ solution was slightly larger than that of the hydrogel's swelling response from the LDH solutions that did not contain any lactate. We hypothesize this is caused by interactions between NAD^+ and BSA/LDH proteins in the LDH solution decreasing the amount of free NAD^+ in solution for hydrogel attachment.

NAD+ and NADH are important biomolecules for their role in metabolism and respiration.[91-93] Due to their widespread use in biochemical reactions, their presence in biological matrices is anticipated. Characterization of NAD's behavior in our system will allow us to better adapt our sensing motif for other enzymatic products.

In our sensors, attachment of pyruvate to the hydrogel occurs via oxime ligation, a process that has become popular as a click-reaction for bioconjugation[94] particularly those catalyzed by *p*-PDA[89]. One such click reaction is for the conjugation of ADP-ribose through the distal ribose ring.[95] NAD^+ and ADP-ribose differ in structure by one nicotinamide group and conversion between NAD^+ and ADP-ribose is used as a posttranslational modification.[96] We hypothesize some of the NAD^+ in our solution is attached to the hydrogel by *p*-PDA through oxime ligation using one of the ribose rings of the NAD.

We investigated the hydrogel's swelling response caused by attachment of NAD^+ and NADH. The hydrogel's swelling response increased with increasing concentration of both NAD^+ and NADH (Figure 2.5). During production of pyruvate by LDH, NAD^+ is also converted to NADH in a 1:1 ratio with the production of pyruvate. While swelling due to NADH gradually increases with concentration, swelling from NAD^+ increases significantly with concentration. There is not complete conversion of lactate to pyruvate creating a combination of NAD^+/NADH in solution.

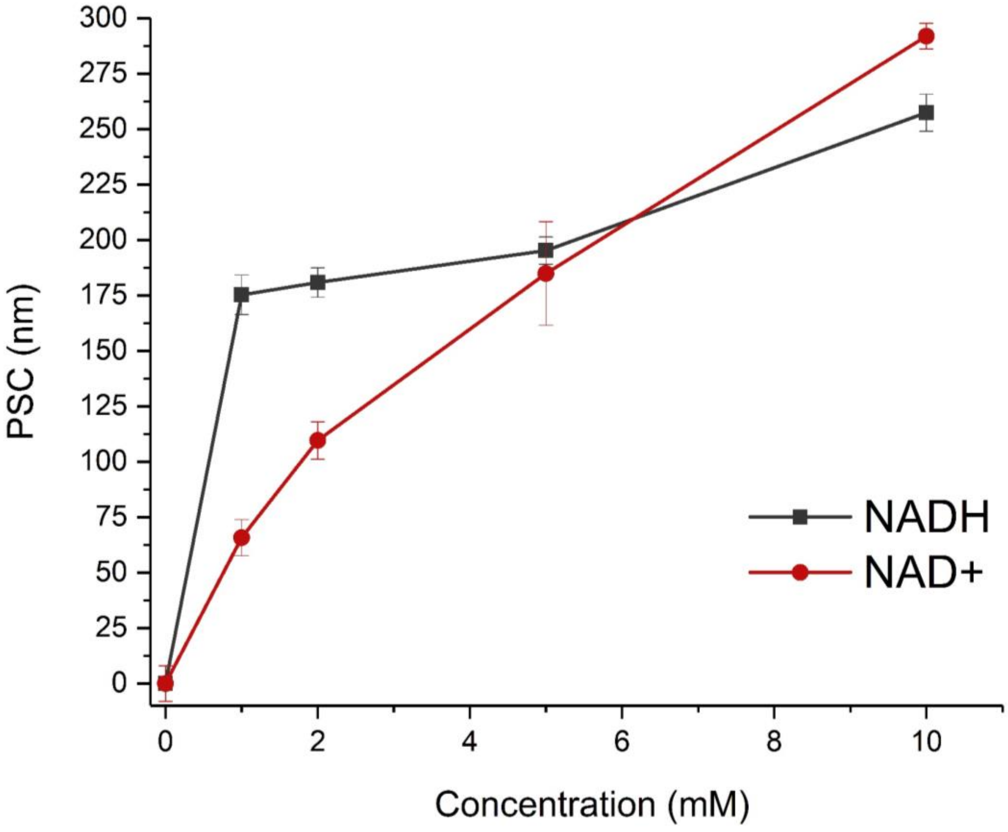

Figure 2.5. 2DPC hydrogel swelling reponse to the presence of NADH (black) and NAD^+ (red) after 30 min of attachment using p-PDA. Solutions of NAD^+/NADH were adjusted to pH 6 for incubation with the hydogel followed by washing with 100 mM tris buffer (pH 7). Error bars indicate standard deviations (n=3).

2.3.4 Impact of the Presence of NAD$^+$ on Sensor Detection Limits

We studied how the presence of NAD$^+$ during attachment impacts our sensor's LoD for lactate/pyruvate. Pyruvate was used as lactate does not attach to the hydrogel. Two sets of solutions were created, one set contained 0-5 mM pyruvate the other set contained 0-5 mM pyruvate with 5 mM NAD$^+$ (100 mM tris, pH 9). Solutions were treated the same, with 30 min vortexing and the addition of HCl (1.2 M). Attachment was performed using *p*-PDA (100 mM bis-tris, pH 6) for 30 min followed by washing the hydrogel in buffer (100 mM tris, pH 7).

Pyruvate and pyruvate with NAD$^+$ samples gave similar swelling responses when looking at the unadjusted particle spacing change (Figure 2.6A). When accounting for the swelling of the blank, the blank for the pyruvate only samples gave a negligible swelling response while the blank from pyruvate with NAD$^+$ swelled by 118 nm ± 34 nm. After subtracting the contribution of the blank from each set of samples, the LoD was determined to be 7.2 μM pyruvate when there is no NAD$^+$ present and 1462 μM in the presence of 5 mM NAD$^+$ (Figure 2.6B).

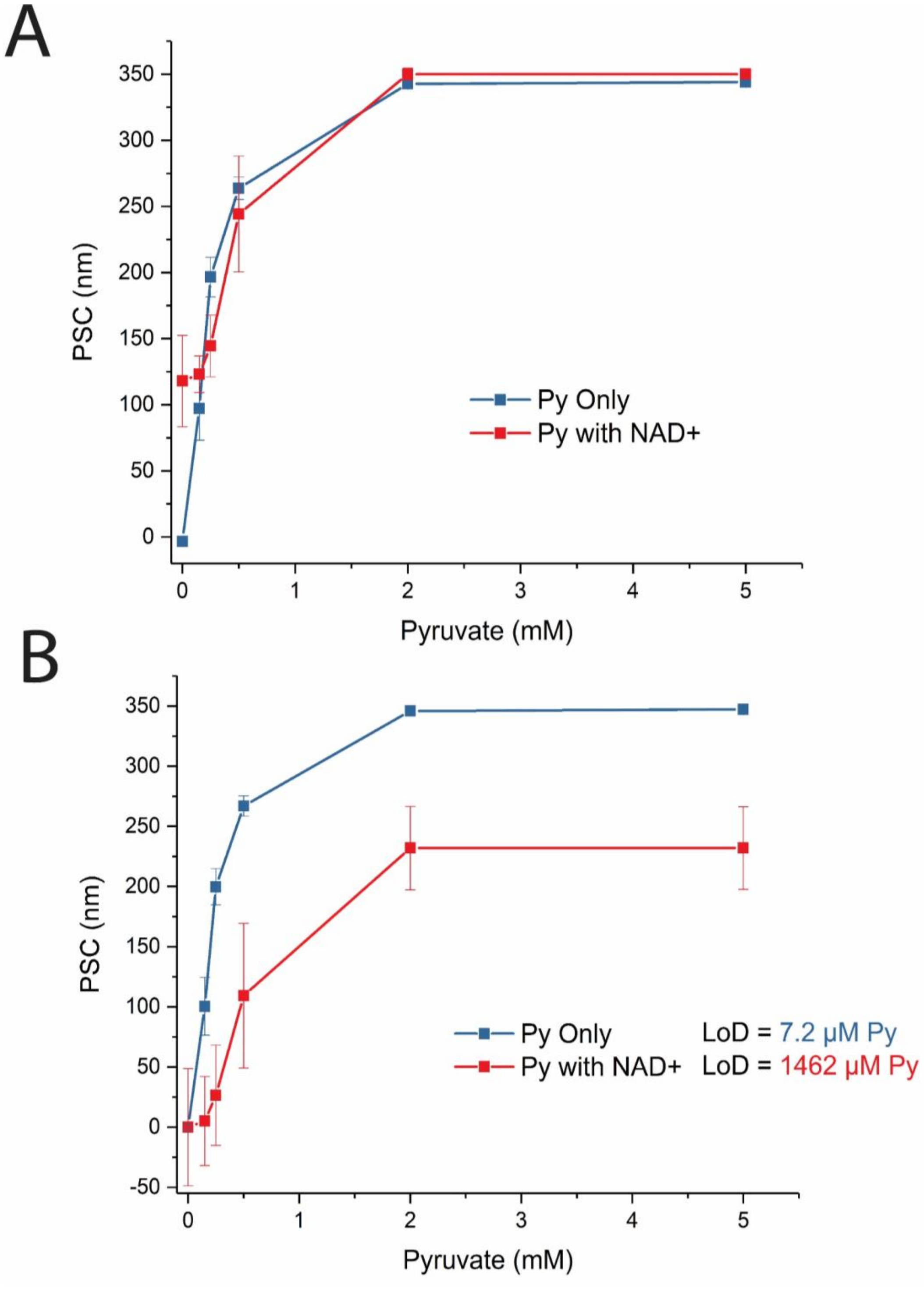

Figure 2.6 2DPC hydrogel swellig response to the presence of varying concentrations of pyruvate (blue) or pyruvate with 5 mM NAD$^+$ (red). PS changes were calculated by subtracting initial particle spacing from the final particle spacing (A). PS changes of solutions containing pyruvate were adjusted by subtracting the PSC of each blank (B).

Deviations in the PSC of samples with NAD$^+$ were also larger than those that only contained pyruvate. If NAD$^+$ undergoes oxime ligation in a similar way as ADP-ribose ligation, it occurs at the ribose ring after the sugar ring opens.[95, 97] We hypothesize that variations in the amount of NAD ring opening contribute to the large deviations in the measurements. The attachment mechanism also becomes more complicated when looking at the stability of NAD$^+$ and NADH based on pH. NAD$^+$ is more likely to decompose at alkaline pHs while NADH is more likely to decompose at acidic pHs.[98-100] NAD$^+$ and NADH decompose into a variety of fragments, some of which contain ribose rings and some of which do not.[101] Attachment of different NAD or NAD degradation fragments would also lead to deviations in the swelling response.

NAD$^+$/NADH attachment to the hydrogel was confirmed using UV-Vis absorbance spectra of hydrogels without 2DPC arrays. Each hydrogel was placed in a solution with a final concentration of 5 mM pyruvate, 5 mM NAD$^+$, or 5 mM NADH. The solutions were made at pH 9 and vortexed for 30 min followed by addition of HCl and *p*-PDA. A hydrogel was added to each solution and vortexed for 30 min. The hydrogels were vortexed overnight in 100 mM tris buffer (pH 7) to remove unreacted analyte.

Spectra showed attachment of all three analytes tested (Figure 2.7). Hydrogels reacted with NAD$^+$ and NADH showed absorbance at ~260 nm which can be attributed to both the adenosine and nicotinamide moieties while NADH also showed a band at 340 nm from the additional electrons within the nicotinamide ring. It is unclear from the absorbance at 260 nm if the adenosine fragment of NAD is attached to the hydrogel as the oxime ligation of ADP-ribose attaches at the place where the nicotinamide portion of NAD is attached. The additional band at 340 nm for NADH confirms incorporation of nicotinamide within the hydrogel.

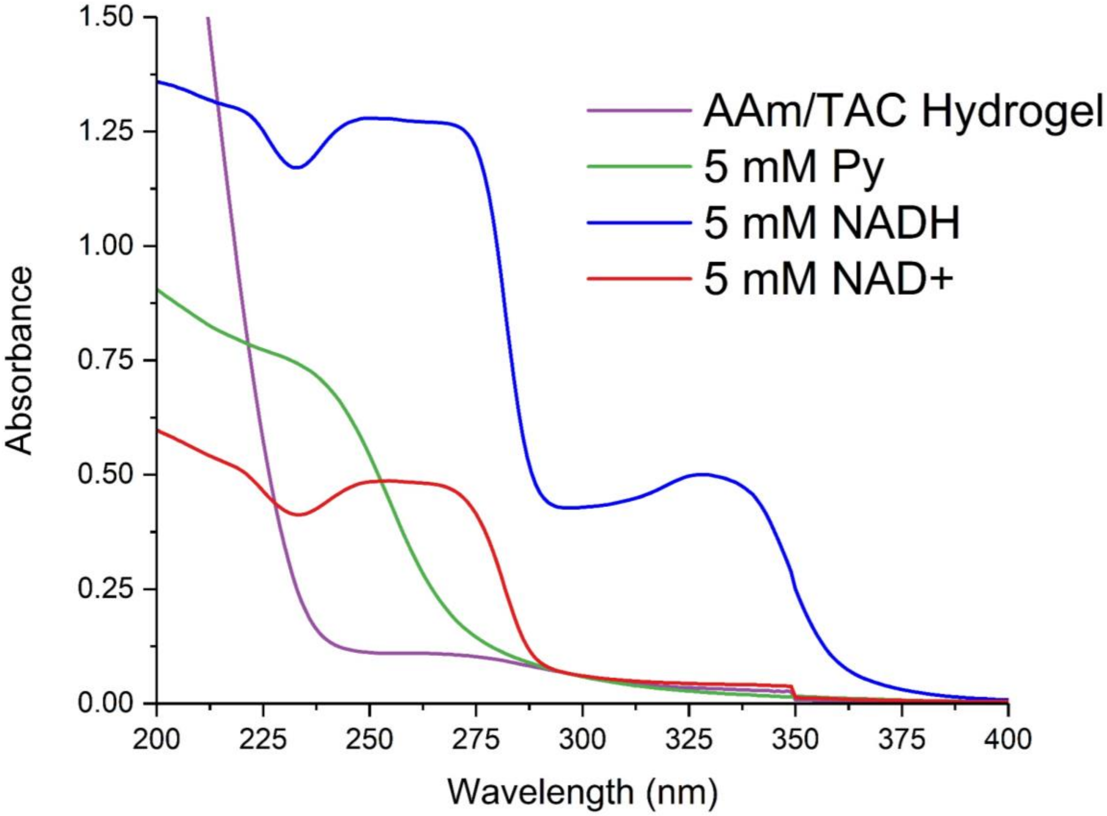

Figure 2.7. UV-Vis absorbance spectra of hydrogels in solutions containing 5 mM pyruvate (green), 5 mM NADH (blue), 5 mM NAD$^+$ (red), or buffer only (purple). Hydrogels were thoroughly washed and placed on a quartz slide for spectral collections.

While we can detect the binding of pyruvate in solutions with NAD$^+$/NADH, their presence leads to a swelling response that increased the measured LoD by ~200 xs. While biologically relevant lactate levels fall within LoDs of our sensor, we need to reduce contributions from NAD$^+$/NADH to look at analytes with lower concentrations. This may be possible through fabrication of an NAD imprinted polymer network for NAD removal.

Use of modified NAD moieties with covalently attached alginic acid is also possible. The alginic acid alters NAD’s solubility in acidic conditions with the NAD becoming insoluble at a pH below 3 without affecting enzymatic activity.[102-103] As we use acidic conditions to stop the reversibility of our pyruvate production, NAD^+/NADH precipitation could be performed at the same time. Further investigation into the removal of NAD^+/NADH is needed.

2.3.5 Lactate Detection in Fetal Bovine Serum

Our 2DPC hydrogels show good sensitivity to the production of pyruvate in buffer. However, biological matrices have high concentrations of ions and proteins that can cause interferences during detection. We investigated our sensor's response to 50% fetal bovine serum solutions with the proteins removed (PRFBS) spiked with lactate and 10% fetal bovine serum solutions (FBS) spiked with lactate. Serum percentages were determined based on a final solution volume of 1 mL when the hydrogel was added. BSA (0.5% final concentration) was added back into the PRFBS solutions to stabilize the LDH during sensing, additional BSA was not needed in the 10% FBS solutions due to the high concentration of BSA in serum naturally.

PRFBS solutions were 50% FBS as *p*-PDA has low solubility in solutions with high ionic strength and high pH. FBS solutions also contained 100 mM tris buffer (pH 9) to keep the pH stable across solutions. Proteins were removed from the PRFBS using centrifugal filtration with a molecular weight cut off of 10 kDa.

Lactate spiked PRFBS (50%) solutions gave a slightly smaller PSC response than pure buffer solutions. However, the raw PSC in PRFBS was initially larger. The PRFBS blank showed a PSC of 240 ±8 nm which was ~100 nm more than the buffer controls. Once adjusted for the blank, PSCs from pyruvate attachment were smaller in serum solutions. As the hydrogel is washed before measurements to remove any unattached compounds, the blank swelling is attributed to covalent attachment of small molecules in serum such as ATP/ADP and additional NAD moieties.

Our LoD in PRFBS (50%) was determined to be 1.7 mM (Figure 2.8) enabling the detection of elevated lactate in protein removed serum solutions.

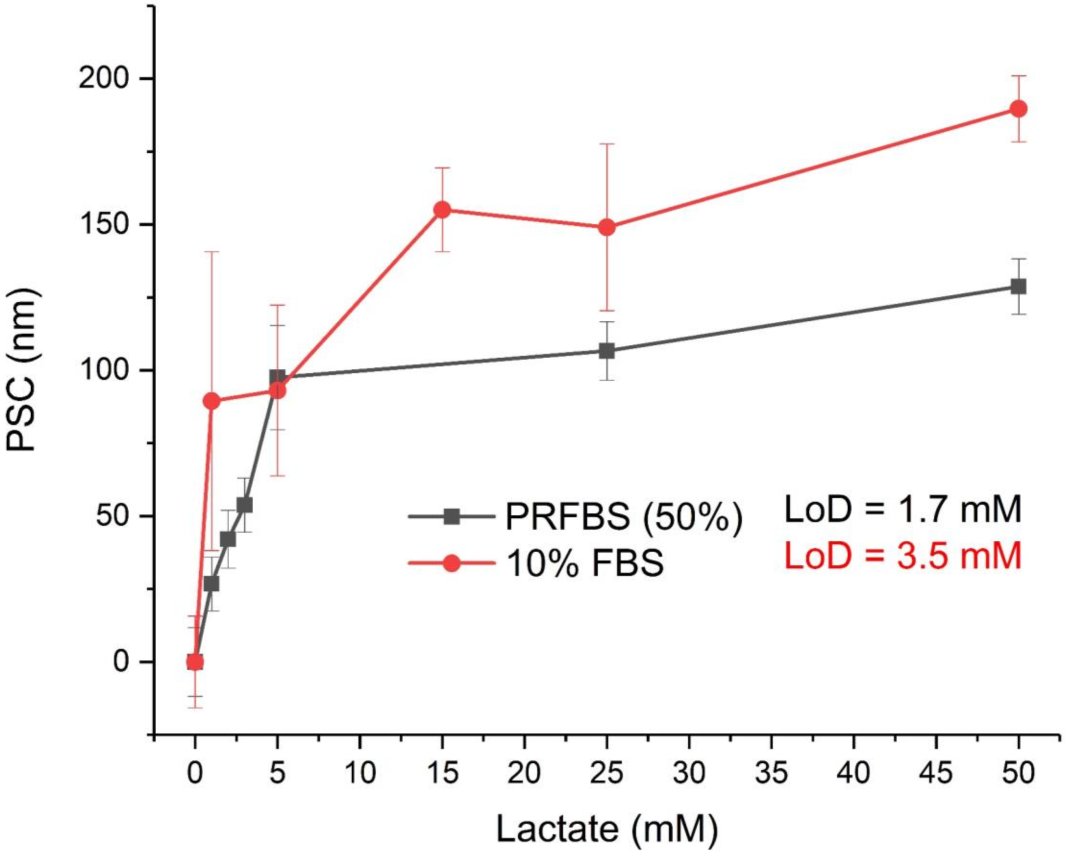

Figure 2.8 Sensing response of 2DPC hydrogels in FBS solutions of protein removed FBS-50% (black) and 10% FBS (red). LDH's conversion of lactate to pyruvate occurred for 30 min followed by 30 min pyruvate attachment using 140 mM *p*-PDA. Error bars indicate standard deviations (n=3).

We also looked at how the presence of low concentrations of serum proteins affected the detection of lactate. LDH's conversion of lactate to pyruvate requires LDH's interaction with both lactate and NAD^+ as they diffuse through the solution. While the presence of low concentrations of BSA increased enzymatic activity by stabilizing LDH, crowded solutions can negatively impact protein diffusion[104] and dynamics[105]. NAD^+ and NADH are also cofactors for other enzymes in blood. Although lactate and pyruvate are small molecules, LDH is a large protein that in its tetrameric form can reach 140 kDa. Other large proteins that impact diffusion in FBS include albumin proteins (~66 kDa) and globulins (~100-150 kDa).

Lactate detection in 10% FBS solutions showed slightly larger swelling responses even after correction for the blank, but the LoD was higher at 3.5 mM lactate (Figure 2.8). The larger swelling response for solutions in 10% FBS only became statistically significant at higher lactate concentrations from the large standard deviations. The increased LoD in 10% FBS is also attributed to the large standard deviations in measurements.

When considering dilution of the 10% FBS during sensing, the 3.5 mM LoD would correspond to a serum lactate level of ~35 mM. Although blood lactate concentrations have been known to be >20 mM in athletes after strenuous activity[106], serum lactate levels that high are not common and are not present in the blood for long periods of time. We hypothesize decreasing hydrogel swelling from the presence of NAD^+ will lower the detection limit in whole serum solutions to more biologically relevant levels.

Covalent attachment of pyruvate allows the 2DPC hydrogels to be washed and any unattached proteins/ions present during sensing to be removed. Removal of the additional proteins and ions gives lower LoDs and allows detection in solutions that may not be usable otherwise. We have demonstrated our 2DPC hydrogel sensor is able to detect lactate in serum solutions.

2.3.6 Comparison of Lactate Sensing Motifs

While we were performing this work, Li et al.[107] published a manuscript on a hydrogel based three-dimensional photonic crystal sensor for lactic acid detection. Although both sensors contain a photonic crystal hydrogel for detection of lactate moieties, they utilize different sensing mechanisms which we believe makes them useful in different ways. Comparing the different sensors can give insights into the adaptability of photonic crystal hydrogels as sensors.

Li et al. used hydrogen bonding interactions between lactic acid and an oxoacetic acid recognition group as the basis of their sensing mechanism. They showed selectivity against compounds similar in structure to lactic and pyruvic acid in water and demonstrated sensor reusability by washing the hydrogel with phosphate buffered saline at pH 9. We believe while sensor reusability can be helpful, the transient nature of the H-bonding interactions may cause difficulties when switching to more complex matrices such as serum. Oxime ligation covalently attaches pyruvate to our sensor allowing it to be washed for use in solutions that contain other complex molecules and have high ionic strength. Our use of LDH’s enzymatic reaction allowed us to indirectly detect lactate while keeping the sensor’s selectivity giving us a platform that is easily adapted to other molecular targets.

Comparison of the sensor developed by Li et al with ours reported here demonstrates the adaptability of the photonic crystal hydrogel as a biomolecular sensing platform. Changing the hydrogel’s recognition group enables different detection methods to be used based on sample conditions and ideal sensing behavior. Investigation into a variety of sensing mechanisms and behavior of photonic crystal hydrogel sensors can lead to easy development of a wider range of photonic crystal hydrogels as platforms for the future development of portable and easy to use sensors.

2.4 Conclusions and Future Directions

We have successfully demonstrated that our 2DPC hydrogel sensor for phenylpyruvate can coupled with enzymatic reactions for indirect detection of analytes. The enzyme LDH converts lactate to pyruvate which undergoes oxime ligation to the hydrogel's TAC recognition group. Incorporation of pyruvate within the hydrogel network alters the hydrogel's free energy which gives rise to a change in the hydrogel's volume. The particle spacing of the hydrogel's embedded 2DPC changes with hydrogel volume allowing quantification of pyruvate, and in turn, the lactate that is present in the solution.

Our sensor has a LoD of 0.24 mM lactate in 100 mM tris buffer. Solutions containing serum gave a LoD of < 3.5 mM lactate in serum using 500 µL serum volumes. Normal blood lactate levels are between 0.5 mM and 2 mM with >4 mM having been connected to hospitalized patients with sepsis and septic shock. Our sensor shows potential as a simple and portable way of detecting elevated lactate levels in blood for monitoring infections such as sepsis.

Although we can detect a wide range of lactate levels in serum solutions, LDH's cofactor NAD^+/NADH is also covalently attached to the hydrogel during sensing. In future work, we plan on inhibiting NAD^+/NADH attachment to the hydrogel through NAD removal before hydrogel attachment with imprinted hydrogels or NAD precipitation through modification with alginic acid. By eliminating the hydrogel's response to NAD^+/NADH, we can use this sensing motif for detection of other analytes that have much lower concentrations in blood.

One such use would be for our continued development of a sensor for phenylalanine using phenylalanine dehydrogenase. The ability to easily quantify phenylalanine in blood would enable sensor fabrication for the metabolic disorder phenylketonuria. Development of cost-effective sensors that do not require large instrumentation for analyte detection, like our 2DPC hydrogels, enables widespread monitoring outside of laboratory environments.

2.5 Acknowledgements

The authors acknowledge the University of Pittsburgh for providing instrumentation and financial support. The authors thank Dr. James Westbay for insightful discussions.

3.0 Aptamer-Actuated Two-Dimensional Photonic Crystal Hydrogel Sensor for Detection of Human Thrombin

This chapter is in preparation for submission to the journal *Analytst*, authored by Westbay, J.H.; Goda, S. A; Jang, K.; and Asher, S. A..

Author Contribution: S.A.G and J.H.W contributed equally to this work. S.A.G, J.H.W., and K.J., designed the experiments. J.H.W. and S.A.G. fabricated samples, and collected and analyzed data with the assistance of K.J. The manuscript was prepared for publication by J.H.W and S.A.G with assistance from K.J., and S.A.A.

There is a need to develop versatile sensing motifs that can be used in resource-limited settings. Ideally, sensors can be easily adapted to detect a wide variety of targets. We recently reported the development of a 2D photonic crystal (2DPC) hydrogel sensor that utilizes aptamer recognition groups to detect a small molecule, adenosine. Here, we extend that sensing motif to detect a protein, human thrombin. Our protein sensor is a 2DPC hydrogel with DNA crosslinks. DNA crosslinks are formed by hybridized DNA strands attached to the hydrogel network. One of the DNA strands contains a thrombin-binding aptamer sequence. On addition of thrombin, competitive aptamer-thrombin binding causes crosslinks to break, actuating hydrogel swelling. This, in turn, causes the particle spacing of the attached 2DPC array to increase, shifting PC diffraction. Thus, thrombin concentrations can be monitored by measuring changes in 2DPC diffraction. Our thrombin sensor can detect thrombin in buffer and serum solutions at physiologically relevant concentrations, with calculated detection limits of 191 nM and 488 nM, respectively. These results demonstrate the generalizability of our aptamer-actuated 2DPC

hydrogel sensing motif and suggest that sensors for other targets can be fabricated by simply exchanging the sequences of the attached DNA strands used during detection. We further investigate the physical phenomena that actuate the observed response to better understand the aptamer-actuated sensing mechanism.

3.1 Introduction

There is a need to develop novel sensing technologies that are deliverable to end-users.[108] Recently, there has been significant progress in the development of sensors.[109-114] However, gold-standard technologies still suffer from the need for expensive equipment, trained personnel, and other limitations that inhibit their widespread use.[11, 108] Ideal sensors can be used in resource-limited settings and have wide-ranging utility, including to monitor environmental[115-117], agricultural[118-120], and military[121-122] hazards, and as diagnostic devices[11, 110, 117, 123-124]. Sensing motifs that are generalizable can be easily adapted to detect new targets and enable the rapid development of novel sensors.

Aptamers have emerged as a promising component of sensors. Aptamers are short DNA or RNA strands that have been selected using the systematic evolution of ligands by exponential enrichment (SELEX) process to sensitively and specifically bind a chemical target.[125-126] Aptamers are analogous to antibodies, but tend to be more stable and cheaper to produce, thus enabling them to function as convenient molecular recognition agents.[127] Sensors that incorporate aptamers are categorized as aptasensors. Aptasensors have been incorporated into a variety of colorimetric[128-130], fluorometric[131-133], and electrochemical[134-135] assays.

Photonic crystal (PC) hydrogels are a sensing platform invented by the Asher research group.[14] PC hydrogels consist of a PC array embedded into a stimuli-responsive hydrogel. This couples the PC particle spacing to the hydrogel volume. Changes in the chemical environment that actuate hydrogel volume changes cause the PC particle spacing to change and can be monitored through shifts in PC diffraction. PC hydrogels are inexpensive to fabricate, require minimal to no sample preparation, and have a simple, colorimetric readout, enabling them to be used in resource-limited settings. PC hydrogels have been used to fabricate sensors for a variety of targets, including ions[136-137], small molecules[116, 130], proteins[138], and whole cells[81].

Recently, we reported the development of a novel two-dimensional (2D) PC hydrogel aptasensor for a small molecule, adenosine.[139] In our aptasensor, the hydrogel contains noncovalent crosslinks formed by hybridized DNA. One of the DNA strands contains an adenosine-binding aptamer. On addition of adenosine, competitive aptamer-adenosine binding breaks hydrogel crosslinks. The breaking of crosslinks generates an osmotic pressure, causing the hydrogel to swell. This, in turn, increases the 2DPC particle spacing, shifting PC diffraction. Thus, adenosine concentration can be monitored by measuring changes in PC diffraction. Our sensor can detect adenosine in buffer and serum solutions, with detection limits of 13.9 μM and 26.7 μM, respectively.[139]

Subsequently, the Zhang group reported the development of a 2DPC hydrogel aptasensor to detect a protein target, human thrombin.[140] Thrombin is a serine protease involved in blood coagulation.[141] This aptasensor similarly relies on the breaking of DNA crosslinks actuated by a thrombin-aptamer binding. Despite utilizing a similar sensing motif as our adenosine aptasensor, the Zhang group reports a different fabrication procedure.

Here, we report the development of a novel aptamer-actuated 2DPC hydrogel sensor to detect human thrombin. We fabricated a thrombin aptasensor in the same way as our adenosine aptasensor, save that a thrombin-binding aptamer was used in place of the adenosine-binding aptamer.[142] On addition of thrombin, competitive aptamer-thrombin binding breaks hydrogel crosslinks. As was the case in our adenosine sensor, the breaking of crosslinks generates an osmotic pressure, causing the hydrogel to swell. This actuates changes to the PC particle spacing, shifting PC diffraction. Thus, thrombin concentration can be monitored by measuring changes in PC diffraction. We calculate detection limits of 191 nM thrombin in thrombin-binding buffer, and 488 nM thrombin in protein-removed fetal bovine serum.

Our thrombin sensor is fabricated using the same methodology as our adenosine sensor, and thus demonstrates the generalizability of our aptamer-actuated 2DPC hydrogel sensing motif. Like our adenosine sensor, our thrombin sensor requires minimal sample preparation and equipment to use, ideally positioning it for use in resource-limited settings. This indicates that sensors can be fabricated for other targets by simply exchanging the aptamer molecular recognition group. We further highlight differences between the response of our thrombin sensor and that reported by the Zhang group[140] to better elucidate the mechanisms that actuate the sensing response.

3.2 Experimental

3.2.1 Materials

Acrydite-modified DNA strands (DNA 1: 5’-acrydite-ACT GTG GTT GGT GTG GTT GG-3’, DNA 2: 5’-acrydite-ACC AAC CAC AGT-3’, purified with high performance liquid chromatography) were purchased from Integrated DNA Technologies. Stock solutions of DNA 1, and 2 were prepared separately at 2 mM concentration in TE buffer (10 mM Tris, pH 8.0; 0.1 mM EDTA) and stored at -20 °C. Tris base (≥99.9%), magnesium chloride, HEPES (99%), sodium hydroxide pellets (≥97%), sodium styrene sulfonate (NaSS) (≥90%), 2,2’-Azobisisobutryonitrile (AIBN) (98%), styrene (99%), acrylamide (≥99%), N,N’-methylenebisacrylamide (MBAAm) (99%), ammonium persulfate (98%), tetramethylethylenediamine (TEMED) (99%), bovine serum albumin, and myoglobin was purchased from Sigma-Aldrich. Ethylenediaminetetraacetic acid (EDTA) (99.5%) was purchased from JT Baker. Sodium chloride and thrombin (human plasma, high activity) (see Appendix A for concentration determination) was purchased from EMD Millipore. Hydrochloric acid (36.5-38% w/w), potassium acetate (99%), calcium chloride, methanol (99.8%), and 2-propanol (≥99.5%) were purchased from Thermo Fisher Scientific. Potassium chloride was purchased from Spectrum Chemical. Ethanol (200 proof) was purchased from Decon Labs, Inc. Cover glass (thickness 1, 24 × 60 mm^2) and FBS were purchased from Corning. To remove serum proteins, FBS was filtered using 10 kDa centrifugal filters. Microscope premium frosted glass slides (25 × 75 × 1 mm^3) were purchased from Fisher Scientific. All chemicals were used as received unless otherwise specified. Ultrapure water (18.2 MΩ·cm) obtained from a Milli-Q Reference A+ was used for all experiments.

3.2.2 Hydrogel Fabrication

2DPC hydrogels were fabricated using described procedures, as summarized in Figure 3.1.[139] Briefly, negatively charged polystyrene particles with diameter ~1.20 μm were synthesized by a dispersion polymerization method described by Zhang et al.[143] These particles (~15 %w/w in water) were mixed with 2-propanol in a 3:1 ratio and assembled into a hexagonally close-packed 2DPC array through the needle tip flow method.[144] The 2DPC array was deposited on a glass substrate (24 × 60 mm^2, cover glass, Corning) and dried at room temperature for 48 h. A polymerizable monomer solution was prepared that contained 25 %w/v acrylamide in water, 0.2 %w/v N,N'-methylenebisacrylamide (MBAAm) in water, and annealed DNA. DNA was annealed by heating a solution containing 200 μM of DNA 1 and 2 in duplex buffer (30 mM HEPES, 100 mM potassium acetate; pH 7.5) to 95 °C on a Corning LSE Digital Dry Bath Heater for 5 min and cooling the mixture on a bench top at room temperature for 30 min. The annealed DNA was then dried for ~4.5 h on a Labconco Centrivap Concentrator (78100-00 A). The final concentration of DNA in the monomer solution was 0.8 mM. The monomer solution was then degassed in a vacuum desiccator for 15 min. Two layers of tape were applied to the 2DPC array sectioning off 0.048 cm^2 per 1 μL of monomer solution. After adding initiator solution (0.7 μL of 5% (v/v) TEMED in water and 0.7 μL of 10% (w/v) ammonium persulfate in water), the monomer solution was stirred for 5 seconds and then deposited on the 2DPC array using a micropipette tip. A glass cover (25 × 75 × 1 mm^3, microscope premium frosted glass slides, Fisher Scientific) was placed over the solution, and polymerization proceeded for 30 min in a vacuum desiccator. After polymerization, the glass substrates were placed in thrombin-binding buffer (20 mM Tris, 140 mM NaCl, 4 mM KCl, 1 mM $CaCl_2$, 1 mM $MgCl_2$; pH 7.4) for 10 min. The glass cover was then removed using a razor blade, and the PC hydrogel was gently peeled from the glass substrate. The PC hydrogel was washed in thrombin-binding buffer for 3 min, cut into ~0.25 × 0.25 cm^2 pieces, and refrigerated in a petri dish without buffer for storage. Figure 3.1 summarizes this fabrication process.

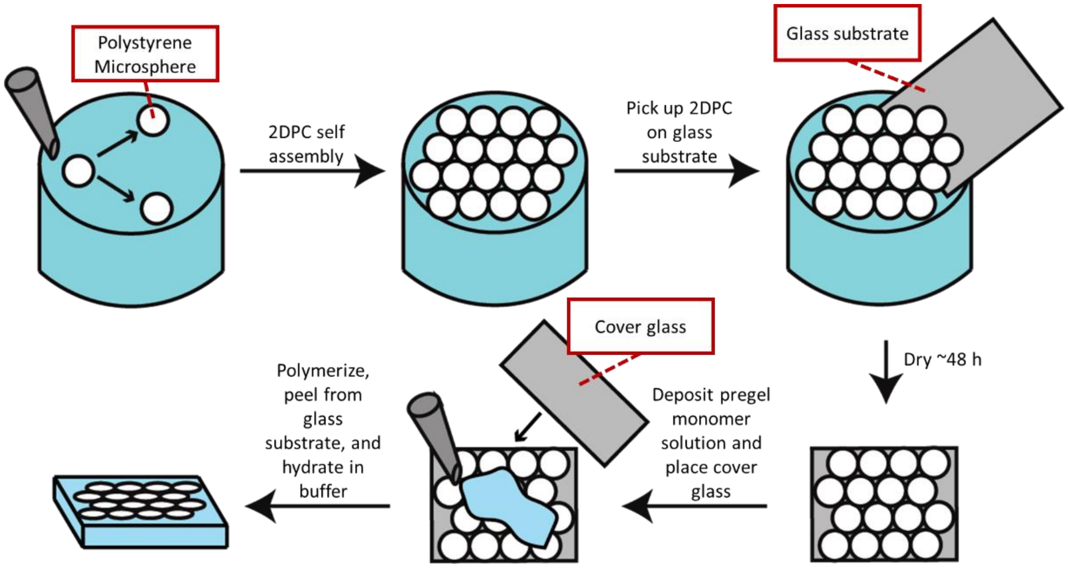

Figure 3.1 2DPC hydrogel fabrication procedure. A 2DPC array is fabricated through a self-assembly process by injecting polystyrene particles onto the surface of water. The array is picked up on a glass substrate and dried. A monomer solution containing acrylamide, methylenebisacrylamide, DNA, and initiator is deposited onto the dried 2DPC array. A glass cover is placed over the monomer solution. After polymerization, the 2DPC hydrogel is peeled from the glass substrate, washed in buffer, and cut into pieces.

3.2.3 Particle Spacing Measurements

2DPC hydrogel particle spacing changes were monitored by measuring changes in Debye ring diameter.[145] Equation 3.1 gives the condition for Bragg diffraction of a 2D hexagonally close-packed PC array, where m is the diffraction order, λ is the wavelength of light, a is the 2DPC lattice spacing, α is the angle of incidence, and β is the angle of diffraction.

$$m\lambda = \frac{\sqrt{3}}{2}a(\sin\alpha + \sin\beta)$$

Equation 3.1

Figure 3.2 shows a schematic of the set up for our Debye ring measurements. Briefly, the PC hydrogel is placed on an elevated stand, and a laser pointer is positioned along its normal ($\sin\ \alpha = 0$). This illuminates a Debye ring. By measuring the height between the Debye ring and the PC hydrogel, h, and the Debye ring diameter, D, the diffraction angle, β, can be determined using Equation 3.2.

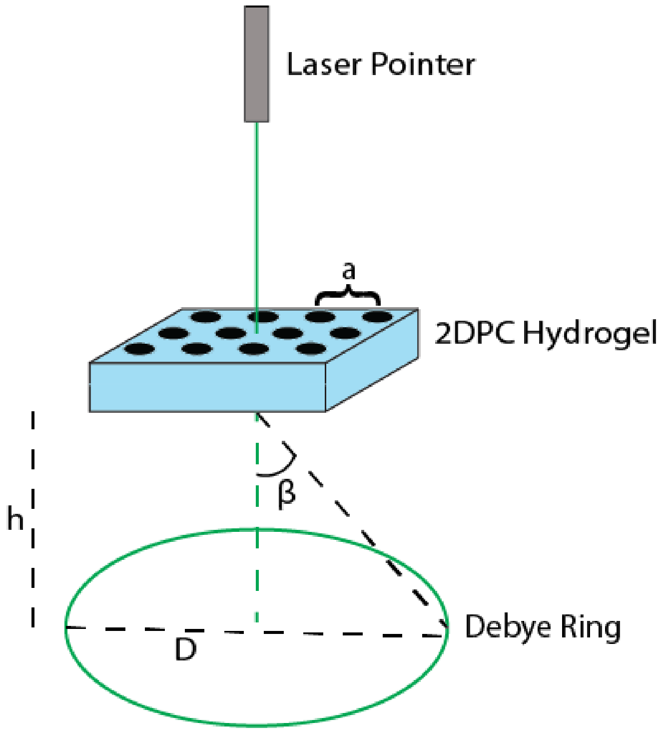

Figure 3.2 2DPC hydrogel particle spacing measurement setup.

$$\beta = \tan^{-1}\left(\frac{D}{2h}\right)$$

Equation 3.2

Equation 3.1 and Equation 3.2 can be combined to give Equation 3.3.

$$a = \frac{2\lambda}{\sqrt{3}\sin\left(\tan^{-1}\left(\frac{D}{2h}\right)\right)}$$

Equation 3.3

Since the wavelength of the light source is known (532 nm), and the height between the PC hydrogel and Debye ring is kept constant (h=15 cm), PC hydrogel particle spacing changes can be monitored by simply measuring the Debye ring diameter, D, with a ruler. To calculate a, we measured and averaged D values at 5 different locations within each PC hydrogel piece.

3.2.4 Thrombin Sensing in Buffer Solution

2DPC hydrogel pieces were brought to room temperature and immersed in 5 mL of thrombin-binding buffer (20 mM Tris, 140 mM NaCl, 4 mM KCl, 1 mM $CaCl_2$, 1 mM $MgCl_2$; pH 7.4). After 10 min, the initial particle spacing change was measured. PC hydrogel pieces were then immersed in 1 mL of thrombin-binding buffer solutions containing 0 (blank), 250, 500, 750, 1000, or 2000 nM thrombin. Particle spacing measurements were taken at time intervals of 30, 60, 90, and 120 min. Each measurement was repeated 3 times using a separate PC hydrogel piece.

3.2.5 Changing the Buffer System

2DPC hydrogel pieces were brought to room temperature and immersed in 5 mL of alternate buffer (20 mM Tris, 150 mM NaCl, 10 mM $MgCl_2$, 1 mM EDTA; pH 7.4). After 10 min, the initial particle spacing change was measured. PC hydrogel pieces were then immersed in 1 mL of alternate buffer solutions containing 0 (blank), 500, 1000, 1500 or 2000 nM thrombin. Particle spacing measurements were taken at time intervals of 30, 60, 90, and 120 min. Each measurement was repeated 3 times using a separate PC hydrogel piece.

3.2.6 DNA Concentration Optimization

2DPC hydrogels were fabricated using procedures described in Section 3.2.2, except that the concentration of DNA in the monomer solution was varied. PC hydrogels were fabricated using 0.1 mM, 0.8 mM, and 1.067 mM DNA.

After polymerization, 2DPC hydrogel pieces were brought to room temperature and immersed in 5 mL of thrombin-binding buffer (20 mM Tris, 140 mM NaCl, 4 mM KCl, 1 mM $CaCl_2$, 1 mM $MgCl_2$; pH 7.4). After 10 min, the initial particle spacing change was measured. PC hydrogel pieces were then immersed in 1 mL of thrombin-binding buffer solutions containing 0 (blank) or 1000 nM thrombin. Particle spacing measurements were taken after incubation for 120 min. Each measurement was repeated 3 times using a separate PC hydrogel piece.

3.2.7 Thrombin Sensing in Fetal Bovine Serum

2DPC hydrogel pieces were brought to room temperature and immersed in 5 mL of thrombin-binding buffer. After 10 min, the initial particle spacing change was measured. Protein-removed fetal bovine serum was diluted 50% using a serum-diluting buffer (40 mM Tris, 210 mM NaCl, 8 mM KCl, 2 mM $CaCl_2$, 2 mM $MgCl_2$; pH 7.4) so that the final concentration of the solution was similar to that of the pure thrombin-binding buffer (20 mM Tris, 140 mM NaCl, 4 mM KCl, 1 mM $CaCl_2$, 1 mM $MgCl_2$; pH 7.4). PC hydrogel pieces were immersed in 1 mL of 50% fetal bovine serum solution spiked with 0 (blank), 500, 750, or 1000 nM thrombin. The particle spacing was measured after incubation for 120 min. Each measurement was repeated 3 times using a separate PC hydrogel piece.

Solutions of 10% FBS containing serum proteins were composed of a 1:4:5 dilution of serum to water to a TMN buffer of 40 mM Tris, 266 mM NaCl, 8 mM KCl, 2 mM $CaCl_2$, 2 mM $MgCL_2$ pH 7.4. This kept the buffer capacity and the concentration of NaCl the same in the 10 % FBS solution as in pure TB buffer (20 mM Tris, 140 mM NaCl). After immersion in 5 mL TB buffer for 10 min, the hydrogel pieces were placed in 1 mL 10% (v/v) FBS solution spiked with either 0 or 750 nM thrombin. After incubation in the 10% FBS solution for 120 min, the particle spacing of each piece was measured. The reported values are an average and deviation of 3 trials using different hydrogel pieces.

3.2.8 Selectivity Measurements

PC hydrogel pieces were brought to room temperature and immersed in 5 mL of thrombin-binding buffer. After 10 min, the initial particle spacing change was measured. PC hydrogel pieces were then immersed in thrombin-binding buffer solutions containing 0 (blank) or 1000 nM thrombin, bovine serum albumin, or myoglobin. Particle spacing was measured after incubation for 120 min. PC hydrogels without DNA were fabricated using procedures described in Chapter 3.2.2, save that no DNA was added to the monomer solution. Each measurement was repeated 3 times using a separate PC hydrogel piece.

3.2.9 Free Energy of Mixing Measurements

PC hydrogels were fabricated using procedures described in Chapter 3.2.2 with minor adjustments. For PC hydrogels with dangling, single-stranded DNA, only DNA 1 was added to the monomer solution. For PC hydrogels with melted DNA crosslinks, after polymerization, PC hydrogel pieces were transferred to centrifuge tubes containing 1 mL of thrombin-binding buffer. These tubes were sealed, heated to 95 °C on a Corning LSE Digital Dry Bath Heater for 5 min, and cooled to room temperature on a lab bench for 30 min. All PC hydrogel pieces were brought to room temperature and immersed in 5 mL of thrombin-binding buffer. After 10 min, the initial particle spacing change was measured. PC hydrogel pieces were then immersed in thrombin-binding buffer solutions containing 0 (blank) or 1000 nM thrombin, and particle spacing was measured after 120 min. Each measurement was repeated 3 times using a separate PC hydrogel piece.

3.3 Results and Discussion

3.3.1 Aptamer-Actuated 2DPC Hydrogel Sensing Motif for Detection of Thrombin

Our sensing motif for detection of thrombin is based on that of our reported adenosine sensor.[139] As summarized in Figure 3.1, hydrogels were copolymerized with acrylamide, MBAAm, and annealed DNA strands. MBAAm formed covalent crosslinks that enhanced the mechanical robustness of the hydrogel and prevented dissolution. Annealed DNA strands were capped with an acrydite group (Figure 3.3). Acrydite is a phosphoramidite that has similar reactivity to an acrylamide monomer.[146] Thus, we were able to incorporate DNA into the hydrogel network with a single-step polymerization.

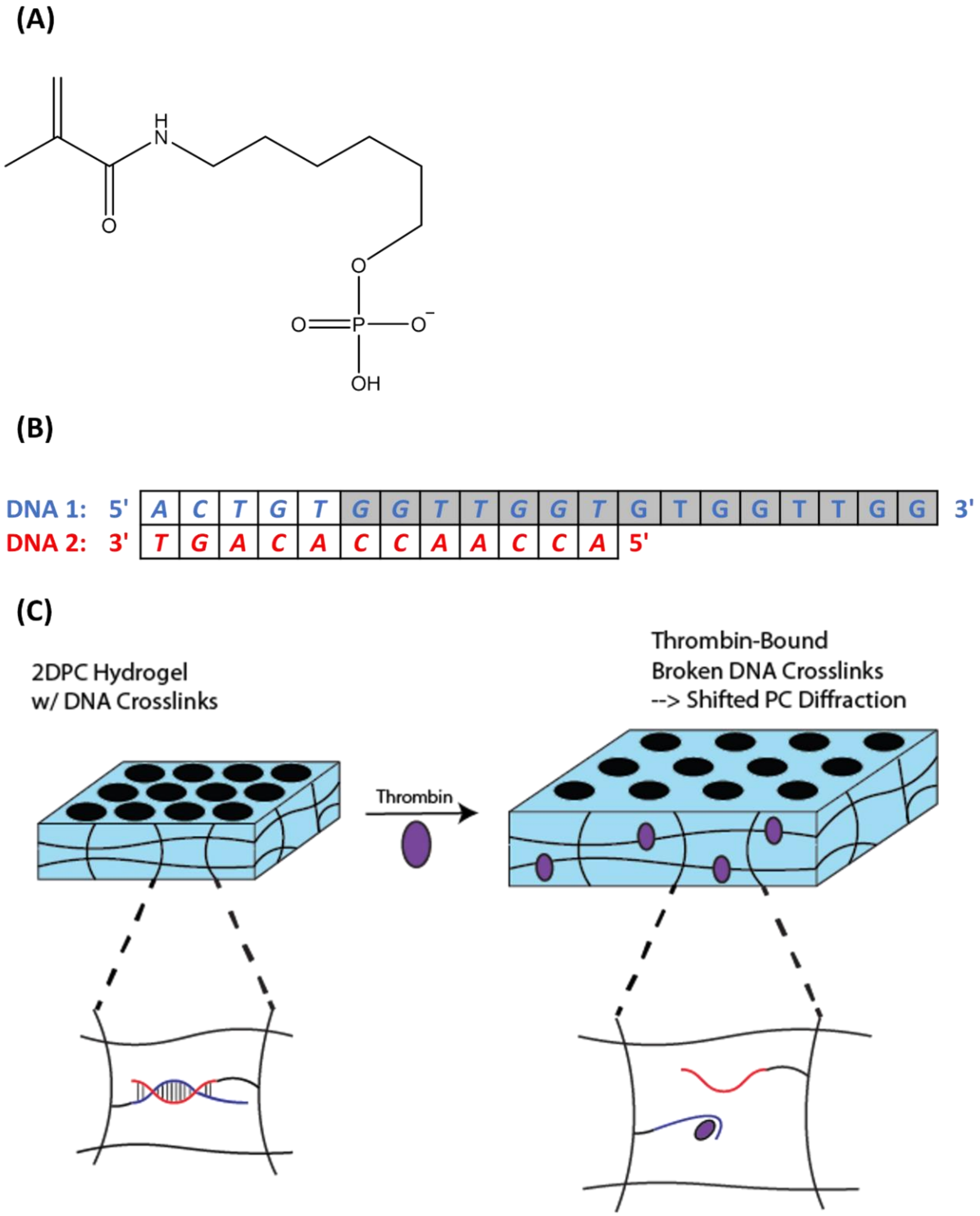

Figure 3.3 (A) Structure of acrdyite. (B) DNA sequences used to fabricate PC hydrogels. Bases that make up the aptamer sequence are shaded. Complementary sequences are aligned and italicized. (C) The thrombin-sensing mechanism using a DNA-crosslinked 2DPC hydrogel. DNA 1 (blue) and 2 (red) are attached to the polyacrylamide hydrogel network, and competitive aptamer-thrombin binding actuates the sensing response.

Within the hydrogel, hybridized DNA forms non-covalent crosslinks. The hybridized DNA consists of a 15-mer thrombin-binding aptamer[142] and a 12-mer strand with bases complementary to the thrombin-binding aptamer. On addition of thrombin, competitive thrombin-aptamer binding breaks hydrogel crosslinks. This alters the elastic free energy of the hydrogel, generating an osmotic pressure.[147] The hydrogel swells to relieve this pressure, in turn increasing the particle spacing of the embedded PC array, shifting PC diffraction. Thrombin concentration was monitored by measuring 2DPC hydrogel Bragg diffraction shifts.

3.3.2 Thrombin Detection in Buffer Solution

The sensing response of our thrombin-binding 2DPC hydrogels was monitored by measuring the 2DPC hydrogel particle spacing change of each 0.25×0.25 cm^2 piece immersed in buffer solutions. 2DPC hydrogels were first immersed in thrombin-binding buffer (20 mM Tris, 140 mM NaCl, 4 mM KCl, 1 mM $CaCl_2$, 1 mM $MgCl_2$; pH 7.4) that was blank and did not contain thrombin. After 10 min, the initial particle spacing was measured. Then, each hydrogel was immersed in a buffer solution containing 0 to 2000 nM thrombin.

Figure 3.4 shows the 2DPC hydrogel particle spacing changes over time in different concentrations of thrombin. Particle spacing change was evaluated by subtracting the initial particle spacing (at time = 0 min) from each subsequent measurement. Over time, hydrogels in larger concentrations of thrombin swelled more quickly and to a greater extent.

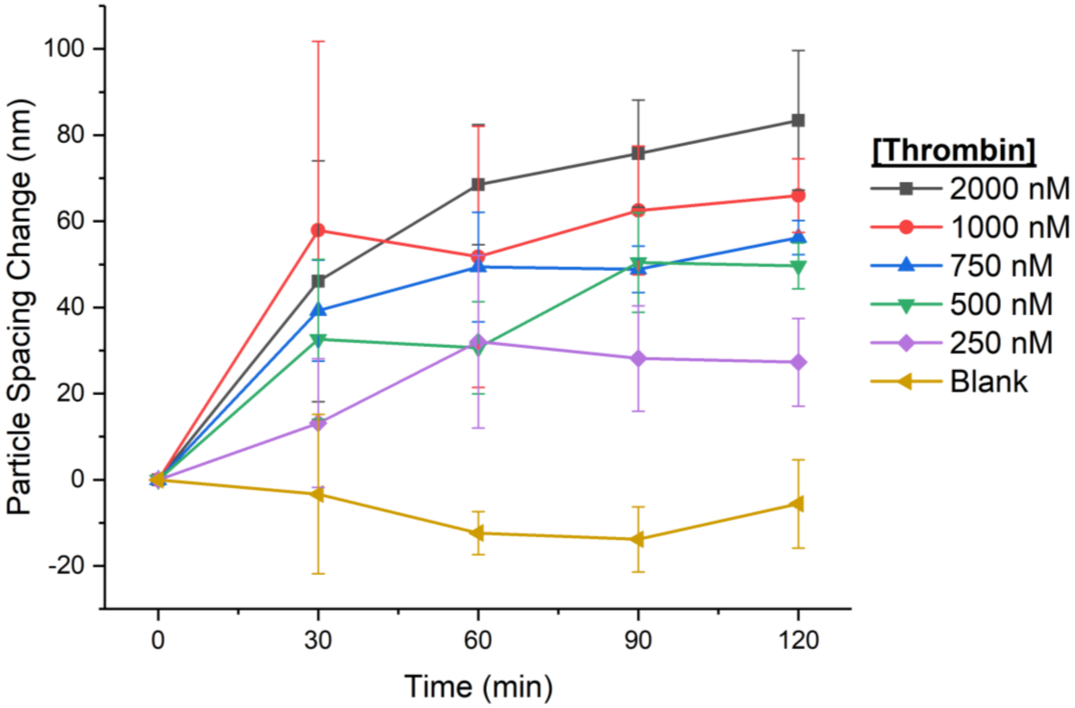

Figure 3.4 2DPC hydrogel particle spacing changes over time in different concentrations of thrombin solution. Error bars indicate standard deviations (n=3).

The 2DPC hydrogel particle spacing changes depend on the concentration of thrombin because, as explained in Chapter 3.3.1, aptamer-thrombin binding actuates the response. Larger amounts of thrombin cause more aptamer-thrombin binding. This breaks a greater amount of DNA crosslinks, generating a larger osmotic pressure that causes more swelling. Since the 2DPC hydrogel particle spacing is proportional to the hydrogel volume, more swelling causes a larger particle spacing change.

Since the particle spacing change is actuated by aptamer-thrombin binding, particle spacing measurements can be used to estimate the aptamer dissociation constant (K_D) (Appendix A.2). The K_D was estimated to be ~369 nM, which is slightly larger than the reported K_D for the thrombin-binding aptamer in solution (~100 nM)[142]. We hypothesize this slight decrease in binding affinity is caused by competitive binding of the aptamer to its complementary DNA, and by spatial restrictions due to the attachment of the aptamer to the hydrogel polymer network. Interestingly, the estimated K_D of our adenosine-sensing PC hydrogels (68 μM) was also of the same order of magnitude as the reported K_D of the adenosine-binding aptamer (~10 μM).[139] This indicates that the response of our aptamer-actuated sensors is limited by aptamer-target equilibrium binding.

Particle spacing changes after 120 min were used to generate a calibration curve, as shown in Figure 3.5. Prior to 120 min, we observed large variability in particle spacing measurements, as indicated by the large standard deviations in Figure 3.4. We hypothesize that at these early time points, the PC hydrogel had not yet reached an equilibrium volume. After 120 min, we observed that 2DPC hydrogels swelled significantly in blank solutions without thrombin. To make the calibration curve, the average particle spacing change in blank solutions without thrombin was subtracted from that at each concentration of thrombin and plotted against thrombin concentration. A best fit line can be used to estimate thrombin concentration. Using the calibration curve, we calculated a detection limit of 191 nM (S/N=3). This detection limit is below reported physiologic concentrations of free thrombin found in the body during blood coagulation (> 500 nM) and demonstrates real-world viability.[148]

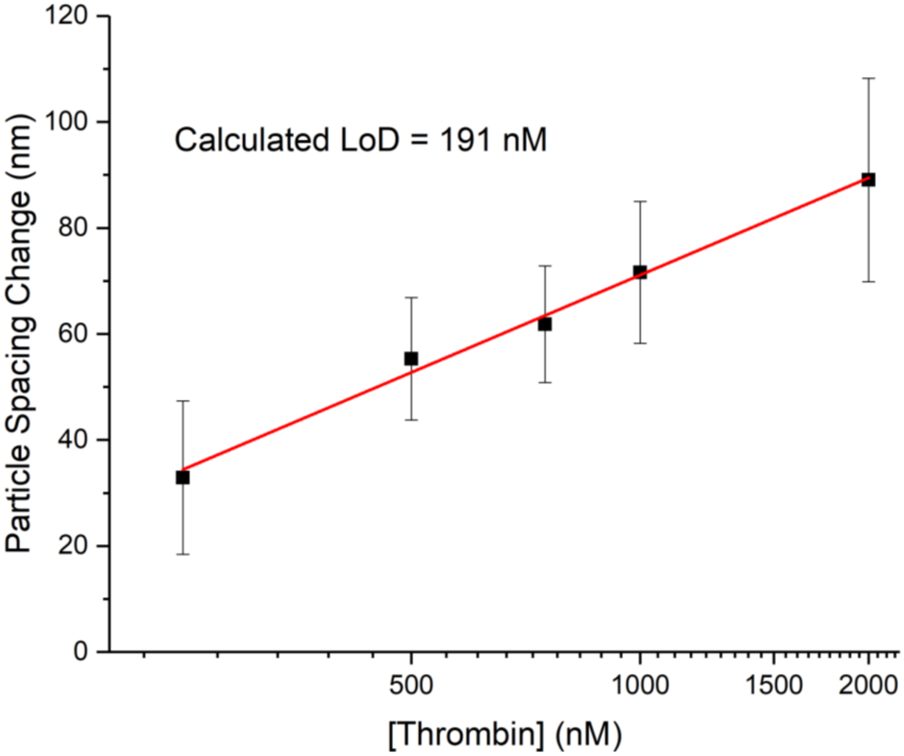

Figure 3.5 Dependence of particle spacing changes on thrombin concentration in buffer solutions at t=120 min. The average particle spacing change in blank solution without thrombin was subtracted from each data point. The red line shows a linear fit (see Supporting Information). Error bars indicate standard deviations (n=3).

3.3.3 Changing the Buffer System

DNA conformation is impacted by buffer conditions in the surrounding environment.[149-150] Thus, buffer conditions can impact aptamer binding and stability. Despite the impact of buffer on aptamer-thrombin binding, several different buffer conditions have been reported in studies that utilize the same thrombin-binding aptamer as our 2DPC hydrogels.[133, 142, 151-152] Researchers rarely comment on why a specific buffer system was utilized.

Ideally, buffer conditions are independently optimized for systems that utilize aptamer-target binding. However, optimization experiments require additional resources that can be prohibitive. When designing our adenosine sensor, we optimized buffer conditions for aptamer-adenosine binding using a fluorescence assay.[133, 139] In contrast to adenosine, thrombin is more expensive and less stable. Thus, we were unable to utilize a fluorescence assay to optimize buffer conditions when designing our thrombin sensor.

In the absence of buffer optimization, it is best practice to utilize the buffer conditions reported during selection of the aptamer.[153] While different systems may have different optimal buffer conditions—for example, the optimal conditions for aptamer-target binding in solution may be different than the optimal conditions for aptamer-target binding in a hydrogel—absent other data, the original selection conditions are more likely to maximize aptamer-target binding than conditions that have not been tested.

For this study, we selected a buffer system similar to that initially reported during selection of the thrombin-binding aptamer.[142] To support this selection, we measured 2DPC hydrogel particle spacing changes in an alternate buffer system. This alternate buffer (20 mM Tris, 150 mM NaCl, 10 mM $MgCl_2$, 1 mM EDTA; pH 7.4) was based on that utilized for our adenosine-sensing PC hydrogels (20 mM Tris, 10 mM $MgCl_2$, 300 mM NaCl; pH 7.5).[139] Compared to the buffer used for our adenosine-sensing system, this alternate buffer contains less NaCl and a slightly lower pH, since these conditions are reported to be favorable for thrombin-aptamer binding.[142] We also included a small amount of EDTA to assist in stability of thrombin during storage. Figure 3.6 shows the particle spacing changes over time for 2DPC hydrogel pieces in this alternate buffer system with varying concentrations of thrombin.Particle spacing changes after 120 min were used to generate a calibration curve, as shown in Figure 3.7.

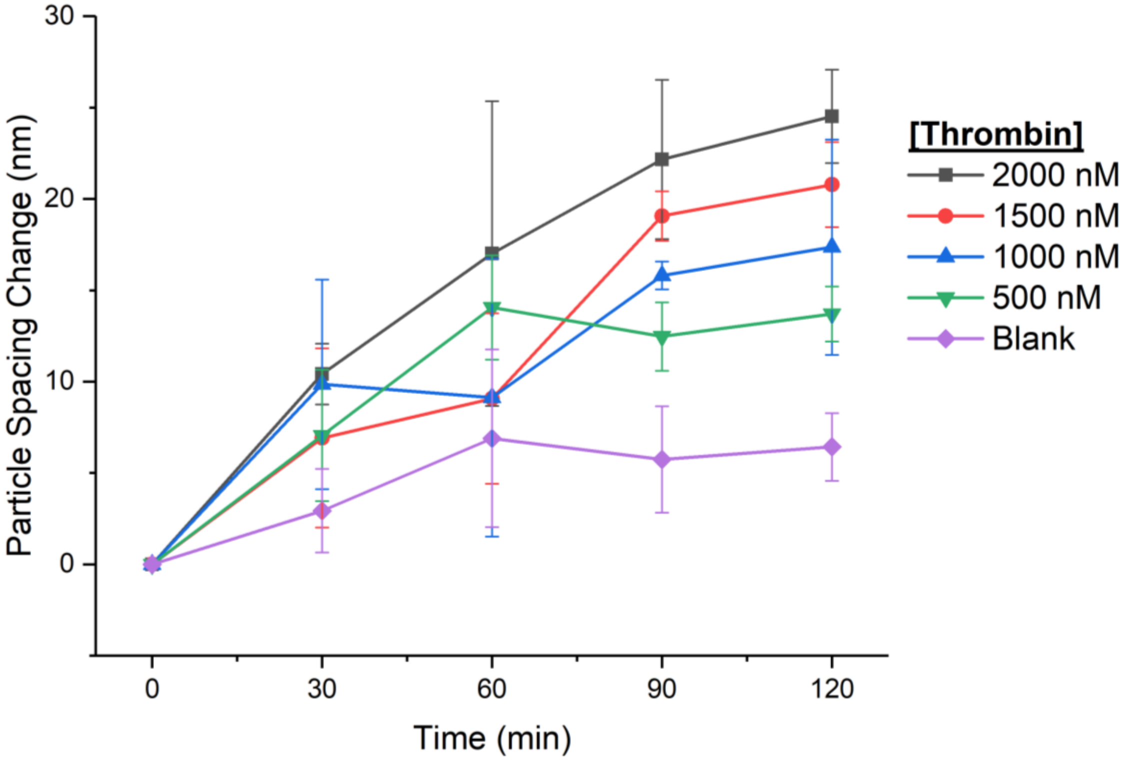

Figure 3.6 2DPC hydrogel particle spacing changes over time in an alternate buffer system with varying concentrations of thrombin. Error bars indicate standard deviations (n=3).

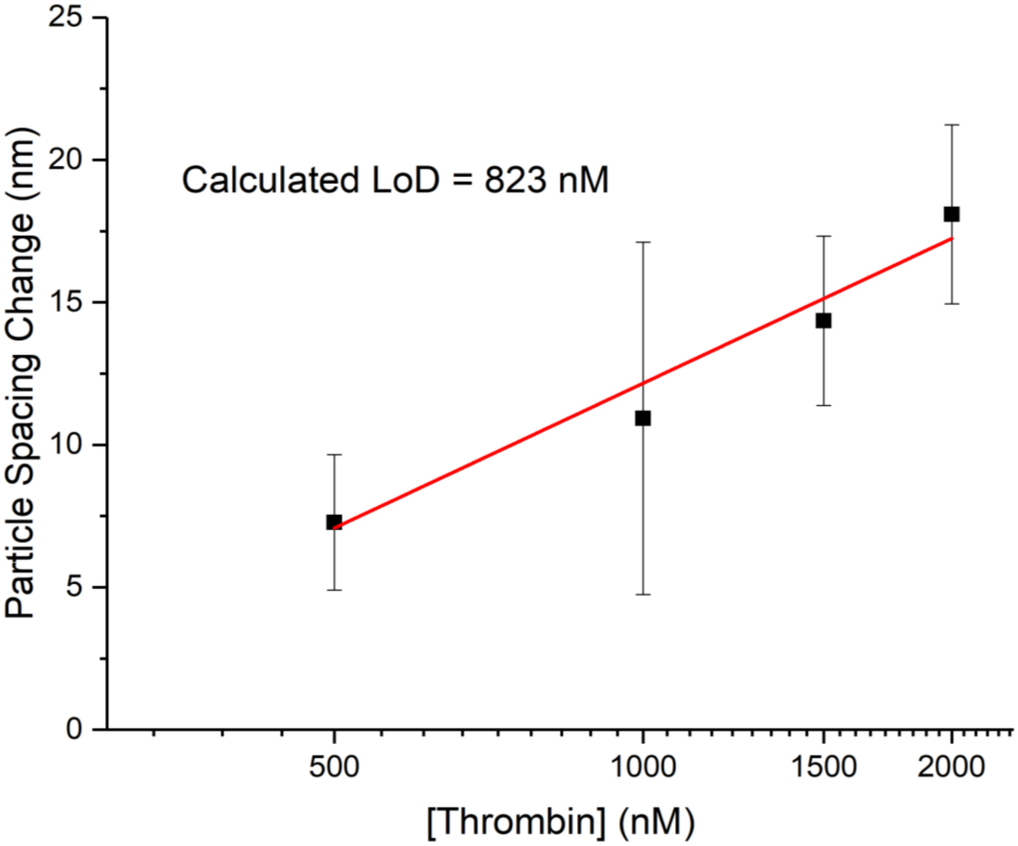

Figure 3.7 Dependence of particle spacing changes on thrombin concentration in an alternate buffer system at t=120 min. The average particle spacing change in blank solution without thrombin was subtracted from each data point. The red line shows a linear fit (see Supporting Information). Error bars indicate standard deviations (n=3).

These results indicate that our 2DPC hydrogels are less responsive in alternate buffer compared to thrombin-binding buffer. For example, after 120 min in solutions with 2000 nM thrombin, the particle spacing change in alternate buffer is ~65 nm smaller than that in the thrombin-binding buffer system. Furthermore, we calculated a detection limit of 823 nM (S/N=3), which is over 4× that calculated in the thrombin-binding buffer system, indicating a significant decrease in sensitivity.

We hypothesize that this decrease in responsivity and sensitivity is caused by a decrease in aptamer-thrombin binding in the alternate buffer system. It is possible that KCl and $CaCl_2$, which are absent in the alternate buffer but present in the thrombin-binding buffer, are necessary for the aptamer to fold into the proper conformation to bind thrombin.[149-150, 154] It is also possible that EDTA, which is present in the alternate buffer but absent in the thrombin-binding buffer, inhibits aptamer-thrombin binding. For example, EDTA complexes with divalent metal ions. If the aptamer must interact with divalent ions to fold into the proper conformation for aptamer-thrombin binding, the EDTA-divalent ion complexes may inhibit interaction of the divalent ions with the aptamer, thus inhibiting aptamer-thrombin binding. Further investigation should be done to determine the impact of each component of the buffer system and optimize conditions for detection of thrombin.

3.3.4 Optimization of DNA Concentration

We investigated the impact of DNA concentration on 2DPC hydrogel particle spacing changes to optimize response to thrombin. Originally, we began studying 2DPC hydrogels with 800 μM DNA.[139] Here, we also fabricated hydrogels using 100 μM and 1067 μM DNA. As summarized in Figure 3.8, PC hydrogels fabricated with different amounts of DNA were immersed in buffer solutions with 1000 nM thrombin, and particle spacing changes were measured after 120 min.

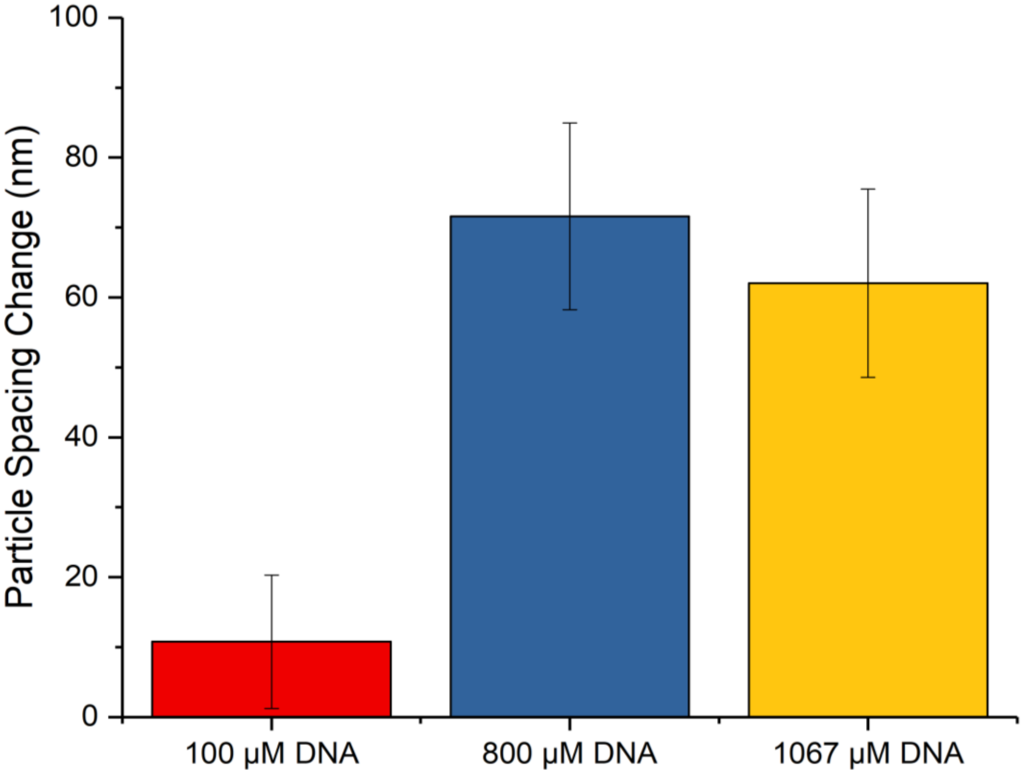

Figure 3.8 Particle spacing changes of 2DPC hydrogels fabricated with different amounts of DNA in buffer solutions with 1000 nM thrombin after 120 min. The average particle spacing change in blank solution without thrombin was subtracted from each data point. Error bars indicate standard deviations (n=3).

The results indicate that 2DPC hydrogel response depends on DNA concentration. In our 2DPC hydrogels, particle spacing changes are actuated by aptamer-thrombin binding. We hypothesized that 2DPC hydrogel response can be increased by increasing the concentration of DNA, since this would increase the amount of aptamer, and thus the amount of aptamer-thrombin binding. The data suggests this is true for DNA concentrations at and below 800 µM. Thus, 2DPC hydrogel responsivity can be tuned by altering the concentration of DNA between 0 and 800 µM.

At concentrations above 800 µM, the observed particle spacing change decreases. We hypothesize this is because increasing the concentration of DNA above 800 µM limits diffusion of thrombin into the hydrogel. In our sensors, DNA is dispersed throughout the hydrogel, and there are aptamer strands both on the hydrogel surface and in the internal polymer network. Initially, thrombin binds to aptamer strands on the hydrogel surface. Over time, thrombin diffuses into the hydrogel, accessing internal aptamer strands that increase the amount of aptamer-thrombin binding and thus the response of the sensor. Increasing the concentration of DNA increases the concentration of aptamer strands on the hydrogel surface. It is possible that at DNA concentrations above 800 μM, the amount of aptamer-thrombin binding on the surface of the hydrogel inhibits further diffusion of thrombin into the hydrogel network, limiting the sensing response.

Our results indicate that the response of our sensor is maximized when hydrogels are fabricated with 800 μM DNA. In contrast, the Zhang group reports an optimal DNA concentration of 100 μM for their thrombin-binding 2DPC hydrogel sensor.[140] They further report that increasing the concentration of DNA in their hydrogel above 100 μM decreases response to thrombin.[140] We hypothesize that this difference in optimal DNA concentration is due to different fabrication chemistries.

We fabricate our sensors with acrydite-capped DNA. As explained in Section 3.3.1, acrydite has similar reactivity to the acrylamide monomer. We thoroughly mix the acrydite-capped DNA into our pre-gel monomer solution and fabricate hydrogels with a single-step polymerization. In contrast, the Zhang group utilizes DNA capped with an amine group. They incorporate amine-capped DNA using EDC coupling after their hydrogels have been polymerized.[140] Since the hydrogel has already been polymerized, it is more difficult to evenly distribute the DNA throughout the hydrogel polymer network, and it is likely that DNA is concentrated on the surface of the hydrogel. Since DNA is concentrated on the surface of the hydrogel, thrombin will bind more at the surface of the hydrogel. The accumulation of thrombin on the hydrogel surface may limit diffusion of thrombin into the hydrogel network and could account for the observed decrease in responsivity when hydrogels are polymerized with more than 100 μM DNA.

We also fabricated PC hydrogels with 100 μM DNA and compared the sensing response to that reported by the Zhang group. Despite using the same concentration of DNA, we observed a smaller response to thrombin. This observation supports the hypothesis that DNA is concentrated on the surface of the hydrogels reported by the Zhang group. In PC hydrogels, when a molecular recognition group is concentrated on the surface of the hydrogel, analyte-recognition group interactions at the surface disproportionately actuate the sensing response.[81] Thus, accumulation of DNA on the surface of the hydrogel could explain why the Zhang group observed a larger response to thrombin despite fabricating hydrogels with the same amount of DNA. While this may be advantageous for larger sensing targets that diffuse slowly into the hydrogel, it may limit the detection of smaller targets, thus diminishing the generalizability of the fabrication methodology reported by the Zhang group.

3.3.5 Thrombin Detection in Fetal Bovine Serum

The response of our 2DPC hydrogels was validated in a complex matrix of first protein-removed fetal bovine serum (FBS) followed by diluted FBS (10 % v/v). Protein was removed from the FBS through centrifugal filtration and diluted with buffer such that the buffer system conditions were similar to those reported in Section 3.3.2. Our detection of thrombin is limited by thrombin diffusion. Protein diffusion is largely impacted by solution conditions such as temperature[155-156] and increased viscosity due to a high concentration of solution components[104-105, 157]. While small molecules in serum such as electrolytes and lipids will affect thrombin diffusion to an extent, we anticipated the greatest impact on thrombin diffusion to be due to the large presence of serum proteins such as albumins and globulins.

We first investigated our sensing capability in a protein removed FBS solution spiked with varying concentrations of thrombin. Figure 3.9 shows the response of our 2DPC hydrogels in protein removed FBS solutions spiked with 0, 250, 500, 750, or 1000 nM of thrombin after incubation for 120 min. The particle spacing changes due to thrombin binding were slightly smaller than those reported in pure TB buffer solution. We hypothesize that this is due to interferants in the serum matrix that inhibit aptamer-thrombin binding. We further calculated a detection limit of 488 nM (S/N=3), ~2.5×'s larger than that reported in pure TB buffer. This decrease in sensitivity is greater than that observed for our adenosine sensor in FBS.[139] We hypothesize this greater decrease is due to the larger size of thrombin compared to adenosine. Larger molecules are more limited by diffusion. Thus, the impact of interferants that inhibit diffusion of analyte into the hydrogel will be more pronounced in the detection of thrombin when compared to adenosine.

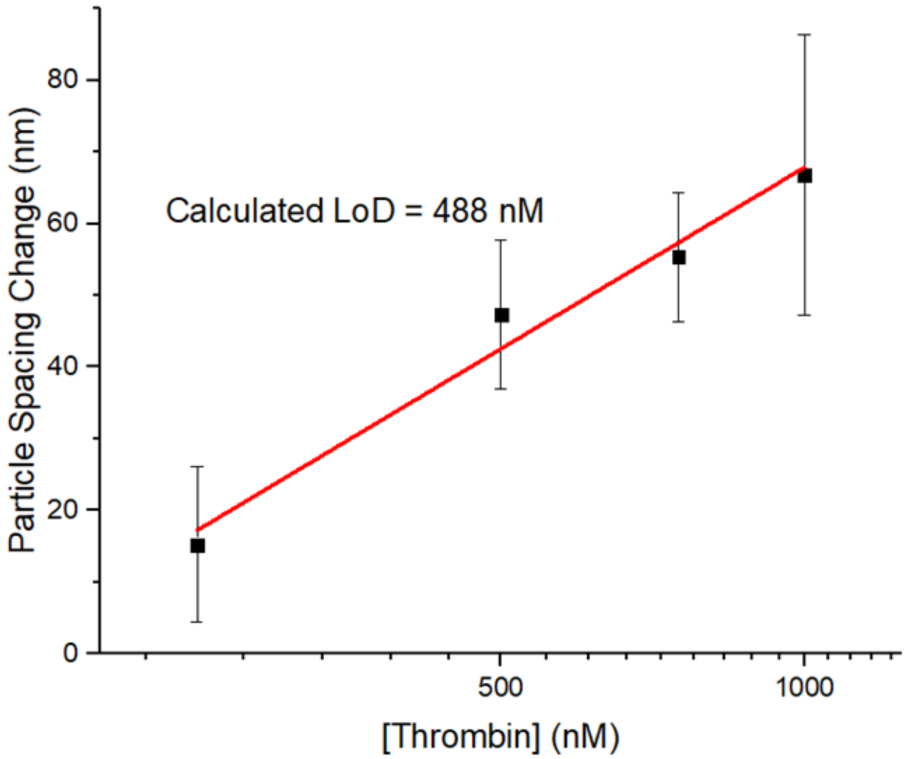

Figure 3.9 Dependence of particle spacing changes on thrombin concentration in protein-removed FBS solutions at t=120 min. The average particle spacing change in blank solution without thrombin was subtracted from each data point. The red line shows a linear fit (see Supporting Information). Error bars indicate standard deviations (n=3).

We also looked at thrombin detection in the presence of other serum proteins using a 10% FBS solution. A 10% FBS solution was spiked with 750 nM thrombin to investigate the impact of other serum proteins on thrombin binding. Based on the FBS certificate of analysis from the manufacturer the 750 nM thrombin made up less than 2% of total protein present in the solution. Over half the proteins present in serum are albumins with a majority of the remaining proteins being globulins.[158] The sensor's swelling response in 10% FBS was further decreased but retained >50% of the response measured in pure TB buffer (Figure 3.10). We have shown that our sensor does not significantly swell in the presence of the serum protein BSA, leading us to believe the decrease in the swelling response between the protein removed serum solution and the 10% FBS solution is due to limitations in thrombin's diffusion from the large presence of other proteins.

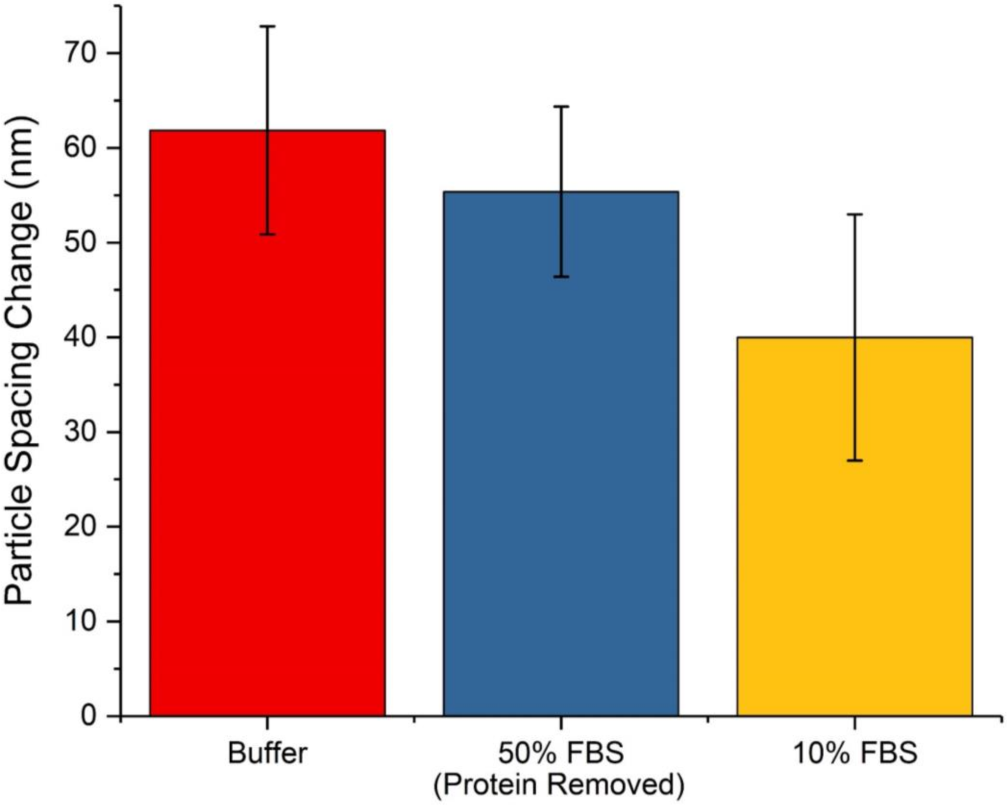

Figure 3.10 Particle spacing changes of 2DPC hydrogels in thrombin binding buffer (red), protein removed 50% fetal bovine serum (blue), and 10% fetal bovine serum (yellow) spiked with 750 nM thrombin. The average particle spacing change of the 2DPC hydrogel in the appropriate solution containing no thrombin was subtracted before reporting the values above.

Despite the decrease in responsivity and sensitivity, this calculated detection limit is of the same order of magnitude as the reported K_D of the thrombin-binding aptamer. This indicates that the sensing response has been largely preserved in FBS and demonstrates real-world viability. We have demonstrated the sensor's ability to retain thrombin detection in complex biological matrices.

3.3.6 Selectivity of Thrombin-Sensing 2DPC Hydrogels

To investigate the selectivity of our thrombin sensor, we measured 2DPC hydrogel particle spacing changes in solutions spiked with proteins that do not bind the thrombin-binding aptamer. As summarized in Figure 3.11, only 2DPC hydrogels in solutions with thrombin swelled significantly after incubation for 120 min. We further measured the response of a 2DPC hydrogel fabricated without DNA, and thus without the thrombin-binding aptamer, in thrombin solution and observed a negligible change. These results confirm that the response of our sensor is actuated by aptamer-thrombin binding.

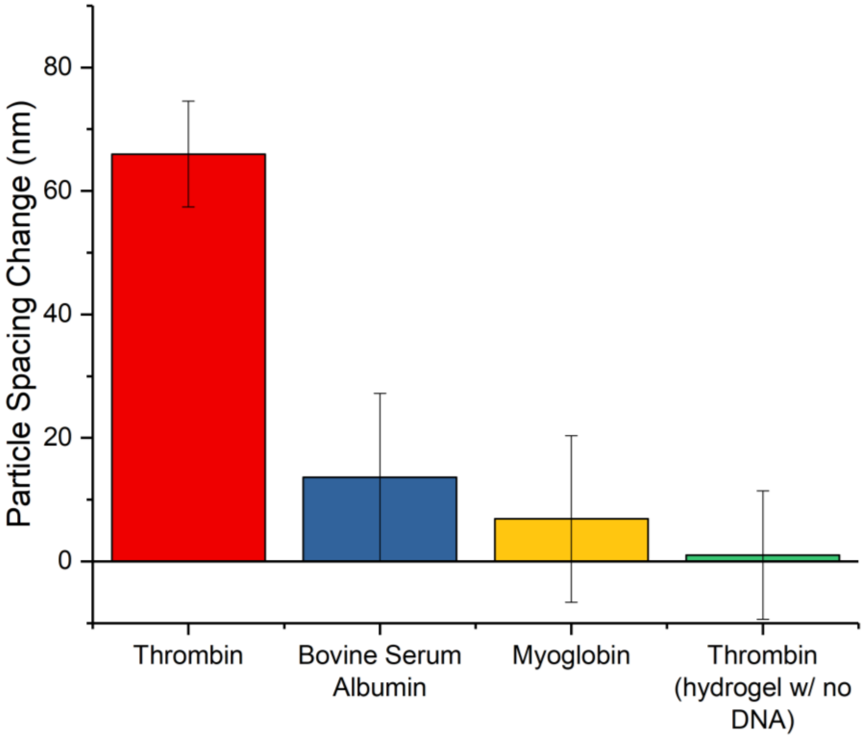

Figure 3.11 Selectivity measurements for thrombin-binding 2DPC hydrogels. Particle spacing change was measured after 120 min in buffer solutions spiked with 0 (blank) or 1000 nM protein. The response of a 2DPC hydrogel without DNA (labeled "hydrogel w/ no DNA") in 1000 nM thrombin was also measured. The average response in a blank solution without protein was subtracted from each data point. Error bars indicate standard deviations (n=3).

3.3.7 Investigation of Free Energy of Mixing Phenomena

In their work, the Zhang group hypothesized that changes in the free energy of mixing contribute to the response of their thrombin sensor.[140] However, they provide no data to specifically confirm this hypothesis. It is possible that aptamer-thrombin binding alters the free energy of mixing of the hydrogel. Free energy of mixing phenomena arise from interactions between the hydrogel polymer network and surrounding mobile phase.[147] Briefly, aptamer-thrombin binding effectively incorporates thrombin into the hydrogel polymer network. If interactions between thrombin and the hydrogel mobile phase are energetically favorable, the hydrogel will take in more mobile phase and swell. Contrarily, if these interactions are energetically unfavorable, the hydrogel will expel mobile phase and shrink. The Zhang group observed a swelling response, thus suggesting that thrombin-mobile phase interactions are energetically favorable.

To investigate the impact of free energy of mixing phenomena on the observed sensing response, we measured particle spacing changes of 2DPC hydrogels without DNA crosslinks. If no DNA crosslinks are present, there will be no changes to the elastic free energy of the hydrogel on addition of thrombin, and thus changes in the hydrogel volume are actuated by changes in the free energy of mixing.[147]

We utilized two strategies to investigate free energy of mixing phenomena. First, as summarized in Figure 3.12, we heated our DNA-crosslinked PC hydrogels, cooled them to room temperature, and then immersed them in solutions containing thrombin. Heating breaks DNA crosslinks. Since the DNA crosslinks are broken, aptamer-thrombin binding will not cause changes to the elastic free energy of the system, and observed volume changes are actuated by free energy of mixing phenomena.

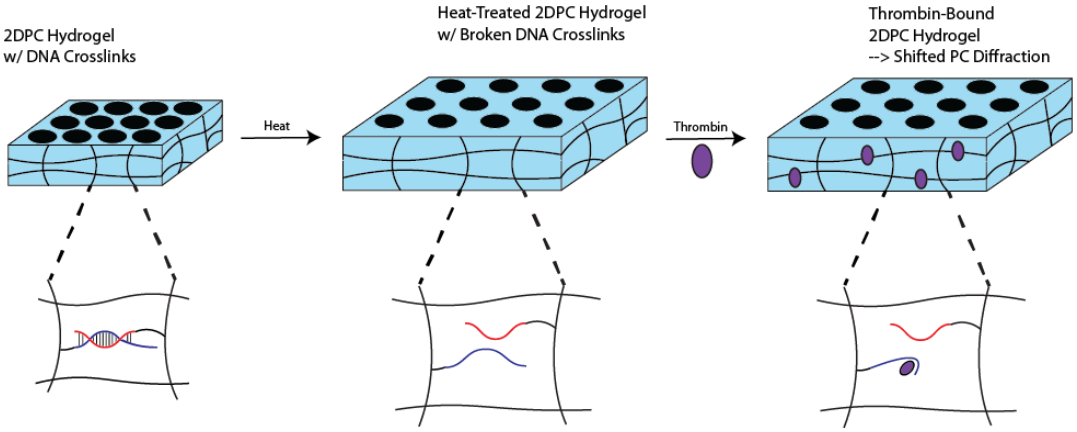

Figure 3.12 Thrombin-sensing mechanism using a 2DPC hydrogel with melted DNA crosslinks to investigate the effect of free energy of mixing phenomena. The PC hydrogels are first heated to break DNA crosslinks, and then immersed in solutions containing thrombin. If aptamer-thrombin binding causes a change in the free energy of mixing of the system, the PC hydrogel will swell or shrink, shifting PC diffraction.

Next, we fabricated 2DPC hydrogels without DNA crosslinks, as summarized in Figure 3.13. These hydrogels contained dangling, single-stranded DNA with the thrombin-binding aptamer sequence. Since there are no DNA crosslinks, aptamer-thrombin binding will not cause changes to the elastic free energy of the system, and observed volume changes are caused by changes to the free energy of mixing.

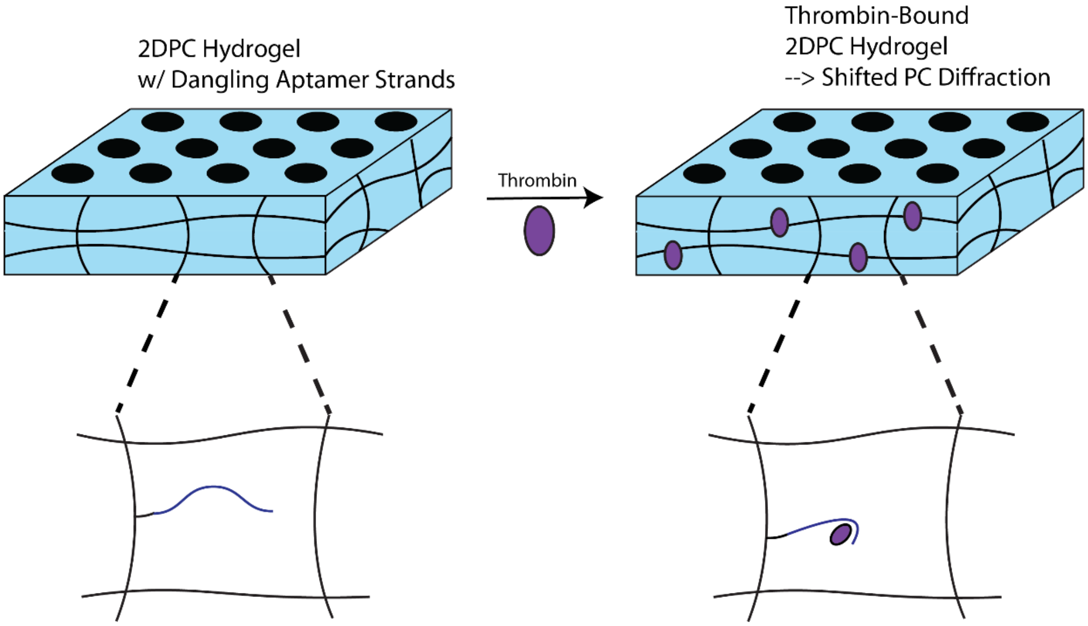

Figure 3.13 Thrombin-sensing mechanism using a 2DPC hydrogel to investigate the effect of free energy of mixing phenomena. The PC hydrogels contain a dangling, single-stranded aptamer instead of hybridized DNA crosslinks. If aptamer-thrombin binding causes a change in the free energy of mixing of the system, the PC hydrogel will swell or shrink, shifting PC diffraction.

2DPC hydrogel pieces fabricated using these strategies were immersed in buffer solutions with 1000 nM thrombin, and the response was compared to those containing DNA crosslinks, as shown in Figure 3.14.

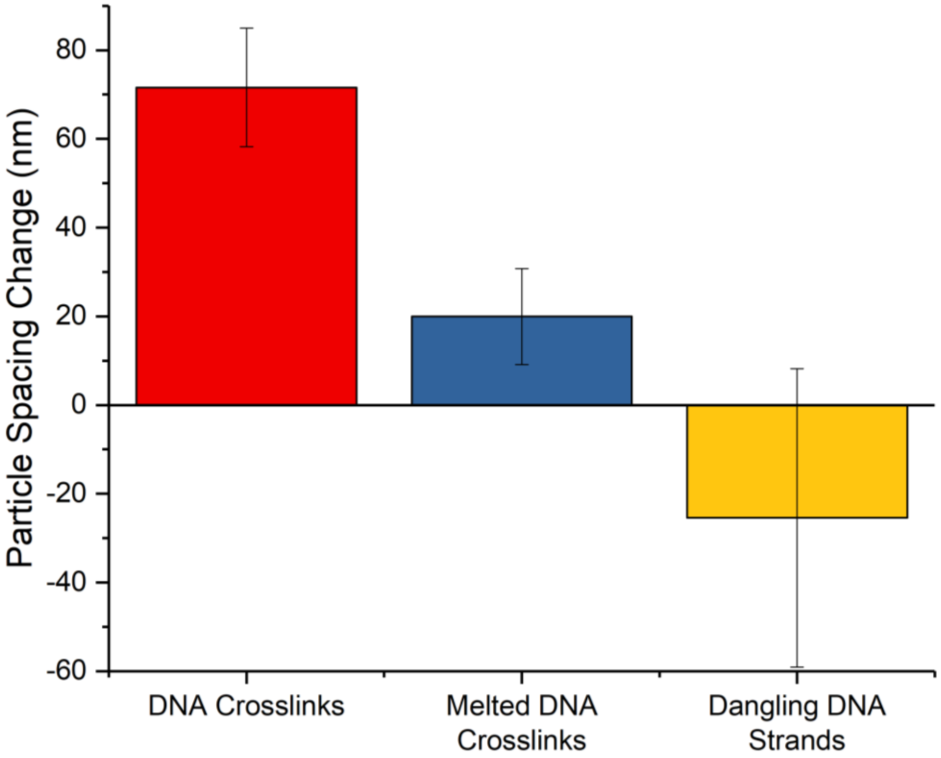

Figure 3.14 Particle spacing changes of 2DPC hydrogels to investigate free energy of mixing phenomena. Particle spacing changes were measured after 120 min incubation in buffer solutions with 1000 nM thrombin. 2DPC hydrogels with DNA crosslinks ("DNA Crosslinks"), crosslinks broken by heating ("Melted DNA Crosslinks"), and dangling, single-stranded aptamer sequences ("Dangling DNA Strands") were analyzed. The average particle spacing change in blank solution without thrombin was subtracted from each data point. Error bars indicate standard deviations (n=3).

2DPC hydrogels with DNA crosslinks swelled significantly more in thrombin solution than those with melted crosslinks and those with dangling single-stranded DNA. This confirms that changes to the elastic free energy are primarily responsible for the observed sensing response. 2DPC hydrogels with melted DNA crosslinks showed a ~20 nm increase in particle spacing after immersion in 1000 nM thrombin. It is possible that this response is actuated by changes to the free energy of mixing of the hydrogel. However, we hypothesize it is more likely this response is due to the breaking of a small number of DNA crosslinks actuated by thrombin-aptamer binding.

Although the hydrogels were heated prior to exposure to thrombin to break DNA crosslinks, it is possible that a small number of crosslinks reformed as the hydrogels were cooled to room temperature. Thus, the breaking of a small number of DNA crosslinks could account for the observed sensing response.

This hypothesis is supported by the response of PC hydrogels fabricated without DNA crosslinks. These hydrogels contained dangling, single-stranded aptamer sequences, and thus the observed response was not actuated by breaking crosslinks. When compared to the response in blank solution without thrombin, these PC hydrogels appeared to shrink. This suggests that incorporation of thrombin into the hydrogel polymer network causes unfavorable changes to the free energy of mixing of the hydrogel. This shrinking response caused by changes to free energy of mixing would counteract swelling caused by changes to the elastic free energy, in contrast to what the Zhang group hypothesized. These results further suggest that the response of our sensor is actuated predominately by changes to the elastic free energy of the hydrogel.

It should be noted that our measurements utilizing PC hydrogels with dangling, single-stranded DNA were highly variable, as indicated by the large standard deviation in Figure 3.14. We hypothesize this variability is due to the smaller number of crosslinks in PC hydrogels with dangling, single-stranded DNA. Prior to immersion in thrombin solution, all PC hydrogels were equilibrated in buffer for 10 min. Samples with DNA crosslinks contained both covalent MBAAm crosslinks and non-covalent DNA crosslinks, totaling to a crosslinker concentration of ~2.1 mM. Samples with dangling, single-stranded DNA did not contain DNA crosslinks, and the total crosslinker concentration was ~1.3 mM. Hydrogels with larger concentrations of crosslinker swell less at equilibrium.[147] We hypothesize that 10 min incubation is enough time for the PC hydrogels with 2.1 mM crosslinker to reach an initial equilibrium volume, but not enough time for PC hydrogels with 1.3 mM crosslinker to reach an initial equilibrium volume. This caused significant variability in the initial particle spacing measurements of PC hydrogels with dangling, single-stranded DNA, thus causing variability in the measured particle spacing changes.

In the future, we plan to fabricate more hydrogels with dangling, single-stranded thrombin-binding aptamers and fully investigate the effect of changes to the free energy of mixing of the hydrogel on measured particle spacing changes.

3.4 Conclusions

We report a novel aptamer-actuated 2DPC hydrogel sensor that detects a protein, human thrombin. Our sensor is user-friendly, requiring only a laser pointer and ruler to operate, specific for thrombin, and sensitive, with calculated detection limits of 191 nM in buffer solution and 488 nM in diluted serum.

The sensing motif described herein is based on that of our reported adenosine-sensing PC hydrogels. The only differences between our thrombin sensor and adenosine sensor are the DNA sequences attached to the hydrogel and the buffer conditions during sensor operation. Thus, these results suggest our motif is generalizable, and sensors for diverse targets can be fabricated by exchanging the attached DNA sequences and buffer system used during detection.

We further investigated the physical phenomena that actuate the response of our sensor. We found that changes to the elastic free energy predominantly cause changes in the PC hydrogel particle spacing rather than changes to the free energy of mixing. In future work, we plan to further investigate the impact of changes to the free energy of mixing.

3.5 Acknowledgements

The authors acknowledge the University of Pittsburgh for providing instrumentation and financial support.

4.0 Investigations into Use of pNIPAM's LCST for Hydrogel Sensor Development

This chapter was prepared in part for the Defense Threat Reduction Agency in reporting for award # HDTRA1-18-1-0017 titled "Xe Sensing via Insights from Noble-Gas Protein Interactions" The adapted work below was authored by Goda, S.A, Pallares, I.G., White S.E., and Asher, S.A.. S.A.G, I.G.P, and S.E.W conceived experiments and collected and analyzed data. This manuscript was prepared by S.A.G with assistance from I.G.P, S.E.W, and S.A.A.

The project depicted was sponsored by the Department of Defense, Defense Threat Reduction Agency. The content of the information does not necessarily reflect the position or the policy of the federal government, and no official endorsement should be inferred.

We investigated the response of photonic crystal hydrogels containing poly(N-isopropylacrylamide) (pNIPAM) to gain insights into how altering the hydrogel composition can be used to create novel sensors. pNIPAM has a lower critical solution temperature (LCST) that is sensitive to changes in the pNIPAM environment. While pNIPAM polymers have been widely used in sensor development, few studies investigate the LCST for sensing applications Our aim is to expand these studies and elucidate how pNIPAM hydrogel fabrication affects the LCST and can be used to detect analytes. Investigations into how the pNIPAM fabrication process and photonic crystal incorporation change the LCST will further development of pNIPAM based sensors in the future.

We studied how pNIPAM hydrogels containing a crystalline colloidal array (CCA) can be adapted to better sense hydrophobic analytes. One such analyte is xenon (Xe) which can be difficult to detect due to its inert nature. Development of adaptable pNIPAM CCA sensors for analytes that are typically difficult to detect, like Xe, would enable more widescale monitoring outside of a laboratory environment.

4.1 Introduction

Crystalline colloidal arrays (CCAs) are three-dimensional photonic crystal materials that control light propagation based on their periodicity and refractive indices.[32-33] Changes in the spacing of the CCA lattice planes alter light propagation through the crystal which can result in changes to the wavelength of diffracted light. CCA diffraction occurs as light travels through the crystal as described by the Bragg condition (Equation 4.1)

$$m\lambda = 2n_{eff}\ d\ sin\theta$$

Equation 4.1

where m is the diffraction order, λ is the diffracted light wavelength, n_{eff} is the effective refractive index, d is the diffracting plane lattice spacing, and θ is the glancing angle of the incident light.[45] The effective refractive index can be calculated by the weighted average of the refractive indices and volume fraction (f) for each material within the system (Equation 4.2).

$$n_{eff} = \sqrt{\sum_i n_i^2 f_i}$$

Equation 4.2

The Asher group invented polymerized crystalline colloidal arrays (pCCAs) by embedding a CCA within a polymer network.[14, 159] A solution of nanoparticles undergoes self-assembly into a CCA within a monomeric solution. By polymerizing the monomer solution around the assembled CCA, the ordered CCA is immobilized within the polymer network. The polymer network can undergo volume changes by taking in or expelling solvent with changes in its environment. As the hydrogel swells the lattice spacing of the CCA increases, resulting in red-shifted diffraction wavelengths. As the hydrogel expels solvent and shrinks, the CCA lattice spacing decreases resulting in blue-shifted diffraction wavelengths.

By embedding a CCA within a stimuli-responsive polymer network, we can develop a sensing platform with a volume that is highly sensitive to a specific target. In these sensors, specific volume changes result in an easily visualized color change. Sensing targets can include changes in pH[16, 160], temperature[161], or the binding of different analytes[162-164].

Poly(N-isopropylacrylamide) (pNIPAM) is a polymer that has been well studied in hydrogels. When polymerized, NIPAM gains thermoresponsive properties.[22-23, 25] At low temperatures, pNIPAM chains contain interactions with the water that makes up its solvation shell. As the solution temperature increases, the water-pNIPAM interactions become less favorable leading to water-pNIPAM bonds breaking and pNIPAM-pNIPAM bonds forming, creating a coil-to-globule transition. The temperature where this transition occurs is called the lower critical solution temperature (LCST).[27-29] The thermoresponsive behavior of pNIPAM has enabled its widespread use in the medical field[165-168], spectroscopic studies[169-171], and sensor development[172-173].

Even though pNIPAM is widely used in the development of sensing materials, little experimentation has been done to investigate changes in the behavior of pNIPAM for development of novel sensors. The research herein is focused on how small changes to the pNIPAM fabrication process alter the behavior of pNIPAM for sensing applications. We then investigate the usefulness of the pNIPAM CCA for monitoring the presence of hydrophobic groups, such as xenon (Xe).

Hydrophobic groups disrupt the ordering of water, lowering LCST. Thus, the presence of hydrophobic analytes can be monitored by measuring shifts in LCST.

Xe is a noble gas that has two radioactive isotopes (^{133}Xe and ^{135}Xe) which are not produced naturally. Radioactive isotopes of Xe are produced through human activity such as nuclear imaging in medical centers, nuclear power plants, and detonation of nuclear weapons.[174-175] While Xe is normally present at low atmospheric levels, the presence of nuclear activity produces increased levels of Xe. Radioactive isotopes of Xe are not easily monitored due to their inert nature and long half-lives.[176-177] Current methods for Xe monitoring are not portable and can take days to weeks to confirm elevated Xe concentrations. Development of a pNIPAM CCA sensor for Xe monitoring would enable portable detection of radioactive Xe isotopes for faster identification.

Although chemically inert, Xe has been shown to alter a variety of biological systems through protein inhibition.[178-181] While Xe's influence on protein activity has previously been studied, the mechanisms behind Xe binding and protein inhibition are still not well known. Insights into the Xe-protein interactions can assist in the development of more optimal Xe binding environments within sensors for better Xe detection.

Typical methods for studying protein-ligand binding in aqueous conditions are difficult to perform in air-tight environments required for reliable Xe monitoring and quantification. ^{129}Xe nuclear magnetic resonance (NMR) spectroscopy has demonstrated utility in reliably monitoring Xe-protein binding in solution.[182-185] Observed Xe chemical shifts are sensitive to Xe's environment both in solution and while interacting with proteins.

Although ^{129}Xe NMR gives useful information on changes in Xe's environment, it does not give information on protein changes from Xe binding. We used resonance Raman spectroscopy to monitor changes in protein structure from the presence of Xe. Resonance Raman utilizes excitation wavelengths that coincide with electronic transitions, enhancing observable changes in molecular structure. Using excitation wavelengths such as 204 nm and 229 nm, we monitored changes in vibrations corresponding to protein secondary structure[138, 159] and aromatic amino acids[186-187] that were anticipated to be altered from the presence of Xe.

Coupling the sensitivity of ^{129}Xe NMR to Xe's environment with the sensitivity of resonance Raman spectroscopy to protein structural changes allows widescale monitoring of Xe-protein binding. We studied these Xe binding interactions in myoglobin and serine proteases, two previously well studied Xe binding systems.[178, 183] The protein systems used did not show measurable structural changes from Xe binding, even with the low limits of detection achieved using resonance Raman. Xe-protein binding was confirmed using ^{129}Xe NMR however, no new information about the relationship between Xe binding and enzymatic activity has been elucidated compared to previous studies.[178, 183, 188] New insights from Xe-protein interactions can be useful in the development of Xe sensors that contain optimal environments for Xe binding. Further experimentation should be performed to observe changes in enzymatic activity from Xe binding.

4.2 Experimental

4.2.1 Materials

N-isopropylacrylamide (NIPAm) (≥ 99%), N,N'-methylenebisacrylamide (MBAm), 2-hydroxy-1-[4-(2-hydroxy-ethoxy)-phenyl]-2-methyl-1-propanone (Irgacure 2959), dimethyl sulfoxide (DMSO) (anhydrous, ≥ 99.9%)), equine heart myoglobin (Mb) and trypsin from porcine pancreas were purchased from Sigma Aldrich. Elastase (porcine pancreas) was purchased from

Alfa Aesar. High purity xenon and nitrogen gas were purchased from Matheson gas. 2,2 azobis [2-methyl-N-(2-hydroxyethyl) propionamide] (VA-086) was purchased from Wako Chemicals. Ethanol (200 proof) was purchased from Decon Labs. N-(3-hydroxyphenyl) acrylamide (HPA) was purchased from Ambeed. Silica nanoparticles (100 nm diameter) were purchased from Superior Silica.

High pressure NMR tubes (10 mm) were purchased from Wilmad lab glass. Gel support films for polyacrylamide and AG-501 ion exchange resin were purchased from Bio-Rad. All glassware was cleaned, and all solutions were made using high purity water (18.2 MΩ·cm) from a Milli-Q Reference A+ system. All chemicals were used as received unless otherwise stated.

4.2.2 Fabrication of pNIPAM Hydrogels and pNIPAM CCAs

Crystalline colloidal arrays were created using solutions of negatively charged monodisperse polystyrene nanoparticles (113 nm diameter) or silica nanoparticles (100 nm diameter) in water. Polystyrene nanoparticles were fabricated by emulsion polymerization using the procedure reported by Reese et al.[31] and modified by Hufziger et al.[189]. Silica nanoparticles were functionalized using 3-(trihydroxysilyl)-1-propanosulfonic acid (THOPS).[190] NIPAM and MBAAm were dissolved in ultrapure water with ion exchange resin, nanoparticles (if embedding a CCA), and Irgacure 2959 (33 % wt in DMSO) according to the formulation in Table 4.1. The solution was wrapped with aluminum foil to avoid interaction with light and gently agitated on a shaker for 30 min to ensure uniform mixing and allow the ion exchange resin to remove ions present that disturb CCA assembly. The solution was placed in a vacuum desiccator for 15 min and was backfilled with argon gas.

Table 4.1 . Composition of monomer solution used to fabricate pNIPAM hydrogels

Component	Reflectance Measurements	Transmission Measurements (no CCA)
NIPAM	20 % (w/v)	20 % (w/v)
MBAAm	0.4 % (w/v)	0.2 % (w/v)
Nanoparticles	2.5 % (w/v) 113 nm PS or 3 % (w/v) 100 nm Si	--
Irgacure (33 % wt in DMSO)	20 μL per mL solution	20 μL per mL solution
Thickness	150 μm	400 μm

The sample cell was comprised of two circular quartz plates with a Teflon spacer (150 μm or 400 μm) and an acrylamide support film between the plates (Figure 4.1A). The plates were held together in a Teflon holder with screws. The top plate had two holes drilled for injection and pressure release syringes during assembly. The quartz plates were cleaned with a piranha solution (70% v/v sulfuric acid, 30% v/v hydrogen peroxide) for fabrication of all pNIPAM hydrogels. The quartz plates were then treated with Sigmacote to make the surfaces hydrophobic for easier hydrogel removal from the plates. All pieces of the cell were washed and rinsed with ethanol and acetone followed by storage in ultrapure water until cell assembly was required. Once assembled, nitrogen gas was flowed through the sample cell until dry.

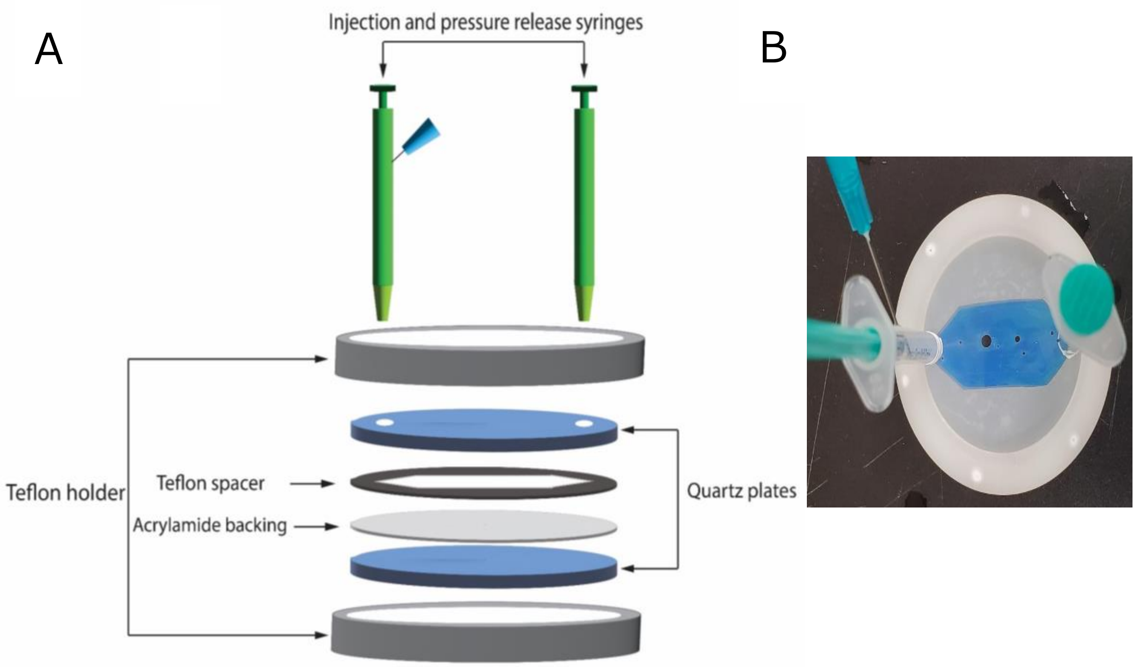

Figure 4.1 Sample cell assembly for injection of the NIPAm/CCA solution for polymerization (A). Photo of an assembled sample holder with an ordered pNIPAM CCA (B).

Injection and pressure release syringes were wrapped with Teflon tape to seal against the quartz plates with a needle placed in the pressure release syringe to allow air flow. The monomer solution was injected into the sample cell and placed in a beaker of cold water for 5-10 min for ordering and equilibration. The beaker was placed in an insulated ice bath to avoid phase separation during polymerization. The strongest CCA diffraction was observed from samples with stable temperatures during polymerization (Figure 4.1B). Samples were polymerized with 1.5 W/cm^2 light using two 365 nm Blak Ray mercury lamps for 3 h. One lamp was positioned above the sample and the other was positioned below for more uniform polymerization.

Following polymerization, samples were refrigerated overnight. After removal from the cell, pNIPAM CCAs were washed with large amounts of water and left to equilibrate in water until use.

4.2.3 Fabrication of pNIPAM-*co*-HPA Hydrogels with V-086 Initiator

HPA was dissolved in water at 1 %, 3%, or 5% w/v and stored in the fridge at ~4 ˚C until use. NIPAM and MBAAm were dissolved using the HPA solutions creating a monomer solution containing 20 % (w/v) NIPAM and 0.2 % (w/v) MBAAm. 20 μL VA-086 initiator (40 mg/mL in water) was added per milliliter of monomer solution and mixed for 30 min. The solution was degassed in a vacuum desiccator for 15 min and backfilled with argon gas. The polymerization process and sample cells used to fabricate the pNIPAM-*co*-HPA hydrogels were the same as previously described in Chapter 4.2.2 for pNIPAM CCAs, however a 415 nm LED was used for polymerization.

4.2.4 CCA Reflectance Measurements

Changes in pNIPAM CCA volume were monitored by measuring changes in light diffraction of the hydrogel’s embedded CCA (Figure 4.2). Reflectance measurements were performed using an Ocean Optics USB2000 spectrometer with an R-series fiber optic reflection probe and a LS-1 Tungsten Halogen light source. The reflectance probe was positioned normal to the face of the cuvette ~2 mm away from the glass wall. Samples were cut to 9 mm in diameter to lay flat against the wall of a screw top quartz cuvette (10 mm) pathlength with 1.75 mL solvent. Sample containing ethanol were equilibrated in the proper mol fraction of ethanol for ~12 h before testing.

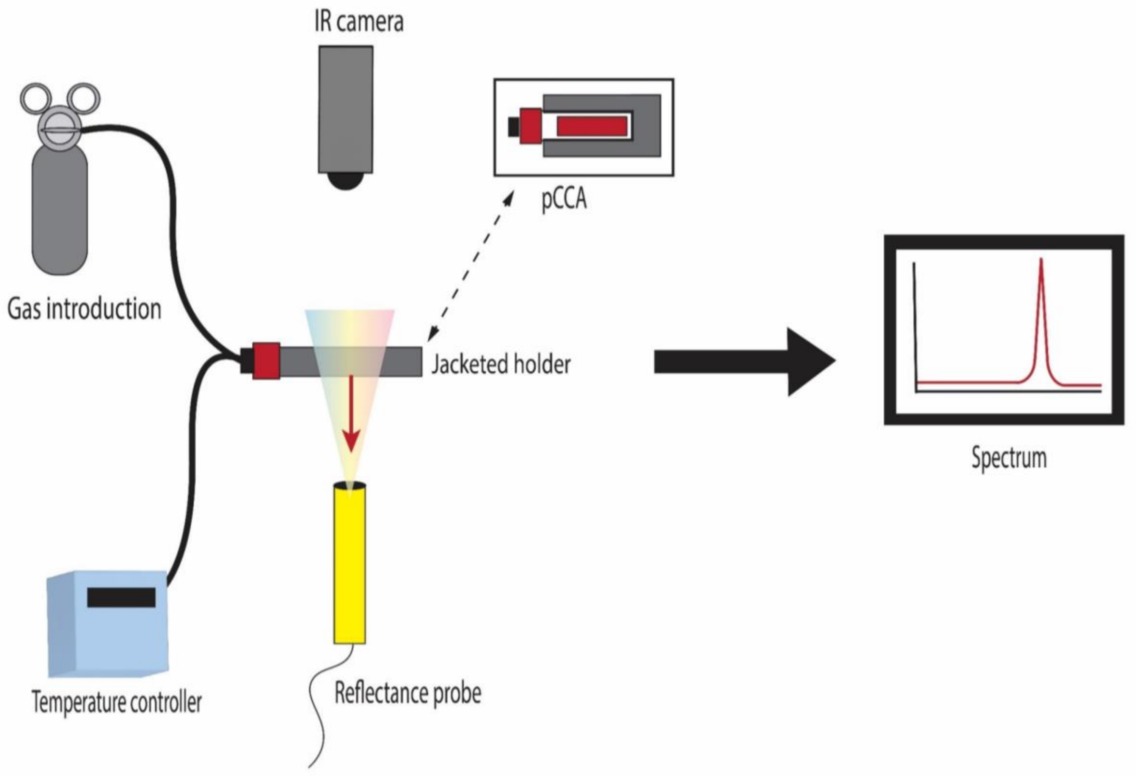

Figure 4.2. Experimental setup for reflectance measurements to monitor pNIPAM CCA LCSTs. CCAs were placed in a cuvette with a jacketed holder for temperature control. A reflectance probe and IR camera were placed normal to the sample to collect spectra and temperature measurements simultaneously.

For samples using Xe or N_2, the cuvette was connected to a gas manifold using an open screw top cap without the septum to degas the sample followed by repressurizing the sample with 40 psi of either N_2 or Xe gas.

A jacketed cuvette holder attached to a programable water circulator was used to cycle the sample temperature between 17-39 °C at a rate of 1 °C every 7 min. The sample temperature was monitored using a FLIR A325sc IR camera. The diffraction was recorded every 30 seconds and the LCST was reported as the temperature at which the pNIPAM hydrogel collapsed to a minimum volume as determined by the diffraction maxima’s wavelength.

4.2.5 LCST Determination Without CCAs

LCST measurements for pNIPAM hydrogels without pCCAs were performed using a Varian Cary 5000 UV-Vis-NIR spectrophotometer (Agilent) equipped with sample temperature control and stirring capabilities. Hydrogel samples were cut into 9 mm wide strips to fit into an open top quartz cuvette with the acrylamide sheet placed flat against the cuvette wall. The sample was held in place using a paper clip and 3 mL of water was added. Water was degassed prior to addition to reduce bubble formation on the sample during heating. A thermometer was placed in the top half of the cuvette to monitor water temperature. The temperature was increased from 31°C to 36 °C with the transmittance collected every 0.1 °C. The LCST was determined through a decrease in the normalized transmittance of 50%.

Caffeine studies were performed by equilibrating pNIPAM hydrogels with and without HPA comonomers in aqueous solutions containing caffeine. LCSTs of each hydrogel piece were first determined in water. Hydrogels were then equilibrated in 4 mL solutions containing 10 mg/mL caffeine for 4 h before LCST measurements were performed. The difference between the initial LCST and the LCST after equilibration in caffeine solutions was determined.

4.2.6 Myoglobin Monitoring- UV-Vis Absorbance

Myoglobin (Mb) solutions were prepared using horse heart Mb. Mb solutions for absorbance experiments were made at concentrations of 0.3-0.5 mg/mL by dissolving lyophilized protein in ultrapure water. Septa sealed fluorescence cuvettes were filled with 3 mL Mb solution and degassed using a vacuum manifold for 15 min followed by repressurizing with 15 psi Xe or

15 psi of N_2 gas. Samples were gently agitated and left on the benchtop to equilibrate for 1 h before spectra were collected. Absorbance spectra were collected from 200 nm to 700 nm using a Cary 5000 UV-Vis-NIR spectrophotometer (Agilent).

4.2.7 Resonance Raman Collection

4.2.7.1 204 nm UV Resonance Raman Measurements

Samples of horse heart myoglobin were prepared at 0.3 mg/mL in high pressure Suprasil quartz NMR tubes (5 mm OD, Wilmad). Samples containing Xe were degassed using a vacuum manifold for 10 min followed by the addition of 15 psi Xe. After Xe addition, samples were gently agitated and left on the benchtop to equilibrate for 1 h.

The instrumental setup is described elsewhere[191]. Briefly, 204 nm light was generated using the third harmonic of an Infinity Nd:YAG laser (Coherent, Inc). The light was shifted using H_2 gas (30 psi) and selected using the fifth anti-Stokes line. A subtractive double monochromator was coupled with a liquid nitrogen cooled CCD camera (Spec10:400B, Princeton Instruments) which were used to collect the ~165° backscattered light. Samples were rotated during collection to avoid the effects of protein photobleaching.

4.2.7.2 229 nm UV Resonance Raman Measurements

Samples were prepared at 0.5 mg/mL Mb with 0.5 M $NaClO_4$ as an internal standard in water. A 3 mL aliquot of the solution was placed in septa sealed fluorescence cuvette (Starna Cells, Inc.) with a microstir bar. Samples were degassed using a vacuum manifold for 10 min followed by the addition of 30 psi N_2 or Xe. After Xe addition, the cuvette cap was covered in parafilm to minimize leaks. The samples were gently agitated and laid on their sides to equilibrate for 1 h. UVRR instrumentation used was an intracavity frequency doubled argon laser (Coherent, Inc.) that produced a 229 nm laser line. The spectrometer and sample orientation were the same as previously described above for 204 nm UVRR measurements (Chapter 4.2.7.1). Samples were stirred during collection to minimize protein photobleaching.

4.2.7.3 405 nm Resonance Raman Measurements

Mb samples were prepared in water using 0.5 mg/mL Mb and 0.5 M $NaClO_4$. A 3 mL aliquot was placed in each septum sealed cuvette with a stir bar and degassed on a gas manifold for ~10 min. Samples were pressurized with 30 psi of N_2 or Xe gas. The cuvette cap was covered in parafilm to minimize leaks. The samples were gently agitated and laid on their sides to equilibrate for 1 h. The effect of the 405 nm light on the sample was monitored using absorbance measurements. Although 405 nm light did not degrade the sample over collection time, samples were stirred during experimentation. Fluorescence was observed in the higher frequency region of the spectra.

The laser is described elsewhere[191] but briefly, 405 nm light was generated using a 5 kHz Ti-sapphire laser continuously tunable between 193-210 nm. The second harmonics generator was used to tune the light to 405 nm. Mirrors were used to separate the 405 nm light from the IR light and to send it outside the laser cavity to the sample. A 405 nm Razor edge Ultrasteep long pass edge filter (Semrock) was placed before the monochromator to reduce the Rayleigh scattered light. A modified Spex single monochromator was used to disperse the Raman scattered light. The light was focused on a nitrogen cooled Pylon CCD camera (Princeton Instruments).

4.2.8 ^{129}Xe NMR

4.2.8.1 Myoglobin

Samples containing Mb were prepared by dissolving protein in 80% H_2O/20% D_2O and were filtered through a 0.45 µm polypropylene syringe filter. UV-vis absorbance measurements were performed to determine final protein concentration. 2.75 mL of the protein solution was added to a 10 mm OD high-pressure glass NMR tube (Wilmad). Phosphate buffer samples (10 mM, pH 7.2) were prepared in 80% H_2O/20% D_2O when performing binding model validation experiments.

All samples containing Xe were degassed for 10 min using a vacuum manifold. High protein concentrations required samples to be degassed slowly to avoid violent bubbling and protein denaturation. Solutions were repressurized with pressures of 15-150 psi Xe gas. The NMR tube was massed while under vacuum and after pressurizing with Xe. The Xe concentration was determined from the difference in the mass of the NMR tube under vacuum and after Xe addition. Samples were gently agitated and left to equilibrate at room temperature for 1 h.

^{129}Xe NMR spectra were collected using a Bruker Avance III 500 MHz spectrometer at a resonance frequency of 138.373 MHz. Mb chemical shift measurements were performed using a 35 µs (90^o) pulse, a 0.5 sec repetition time, and a spectral width of 27,574 Hz. Chemical shift measurements for Xe in water utilized a 35 µs (90^o) pulse and a spectral width of 13,787 Hz. IUPAC standard referencing methods[192-193] were used for all spectra unless otherwise stated. Single scans were collected for spectra of Xe in water. All spectral processing was performed using Bruker TopSpin. The number of scans for protein samples was varied to obtain spectra with a signal-to-noise ratio >10, as determined by TopSpin's SINO function. Sample temperature during collection was controlled at 25.0 ± 0.1 ^{o}C

4.2.8.2 Serine Proteases

Solutions of Xe in water were prepared by adding 2.75 mL of 80% H_2O/20% D_2O to a 10 mm OD high-pressure glass NMR tube. Elastase and trypsin samples were prepared in 80% H_2O/20% D_2O at concentrations of either 25 or 72 µM elastase and 6-8 mM trypsin. Solution concentrations were measured using a Varian Cary 500 UV-Vis-NIR spectrophotometer (elastase ϵ_{280}=45,750 M^{-1} cm^{-1}, trypsin $\epsilon_{280=}$37,600)[194-196]. 2.75 mL of the protein solution was added to a 10 mm OD high-pressure glass NMR tube. Changes to solution pH were made by adding dilute NaOH. Solutions contained 1 mM sodium trimethylsilylpropanesulfonate (DSS) standards unless otherwise stated.

Samples were slowly degassed on a vacuum line for 10 min to avoid protein denaturation. Up to 150 psi of Xe gas was added into the NMR tube, and the samples were equilibrated for 1 h at room temperature. The total Xe gas added to the tube was determined by the difference in the weight of the NMR tube under vacuum and after Xe addition at each pressure.

^{129}Xe NMR spectra were collected using a Bruker Avance III 500 MHz spectrometer at a resonance frequency of 138.373 MHz. Chemical shift measurements for elastase were carried out using a 18 msec pulse with a spectral width of 27,574 Hz. All spectra were referenced to the upfield methyl proton signal of DSS using the IUPAC standard method.[192-193] Temperatures were controlled such that the sample temperature was 25.0 ± 0.1 ˚C. All spectral processing was performed using Bruker TopSpin.

4.3 Results and Discussion

4.3.1 pNIPAM Volume Monitoring

The LCSTs of our pNIPAM CCAs were monitored through the collapse of the hydrogel network as the sample temperature increased. For hydrogels containing CCAs, we monitored volume changes through shifts in the wavelength of the CCA’s diffracted light during the collapse of the pNIPAM network. We fabricated CCAs that diffract at wavelengths that are easily measurable across the visible spectrum as the large changes in pNIPAM volume require monitoring a wide range of wavelengths.

Our NIPAM/Bis formulation was based on that reported by Takeoka et al.[197] who looked at the swelling response of pNIPAM hydrogels with respect to the NIPAM/bis ratio. They reported tunability of the CCA diffraction across the visible region through changes in the crosslinker concentration and temperature. Our concentration of bis crosslinker for pNIPAM CCAs was 0.4% (w/v) giving the hydrogels a [NIPAM]/[bis] ratio of ~60.

pNIPAM’s LCST shifts with small changes in pNIPAM’s environment which include changes to the pNIPAM fabrication process. During our studies, small changes to the concentration of crosslinker used within our pNIPAM hydrogels were needed to create hydrogels robust enough to withstand LCST experiments and to create pCCAs that were able to be monitored within the visible spectrum. While changes in crosslink density can lead to shifts in the hydrogel LCST, the low concentrations of bis crosslinker used in our studies have been shown to not impact pNIPAM’s transition temperature.[197-198]

We used an acrylamide gel support film (BioRad) to restrict hydrogel swelling in the x-y plane, creating a 1-dimensional (1D) hydrogel swelling response instead of a 3-dimensional (3D) response. When the pCCA undergoes 1D swelling, shifts in the CCA diffraction become proportional to the hydrogel's volume ($V \sim \lambda$) instead of the cubed root of the hydrogel volume typical of 3D swelling ($V^{1/3} \sim \lambda$).[163] Restricting hydrogel swelling to 1D created shifts in the diffraction maxima that were larger than would be seen for 3D swelling, increasing measurement sensitivity.

Restricting swelling in the x-y plane also increased reproducibility of the measurements. As the pNIPAM network undergoes 3D collapse, the location of the hydrogel that is within the light path changes. Small inhomogeneities in the sample can lead to drifting in the measured values as the hydrogel collapses, creating discontinuities in the data. The volume change of pNIPAM as it collapses at the LCST is also very large and can result in sample migration out of the beam path during collection.

Our initial photonic crystal diffraction was modeled to be within the visible region based on theoretical analysis from Spry and Kosan.[199] For polystyrene, 113 nm diameter particles were used with a final concentration of 2.5 % w/v within the precursor solution. Hydrogels containing Si CCAs utilized 100 nm Si particles with a final concentration of 3 % w/v. While at room temperature these CCA hydrogels initially give second order diffraction that falls in the blue region of the visible spectrum while the first order diffraction is in the near IR region. As the temperature of the pNIPAM hydrogel increases, the second order diffraction blueshifts and moves into the UV spectrum. The first order diffraction then moves into the visible region until the collapse of the polymer network (Figure 4.3).

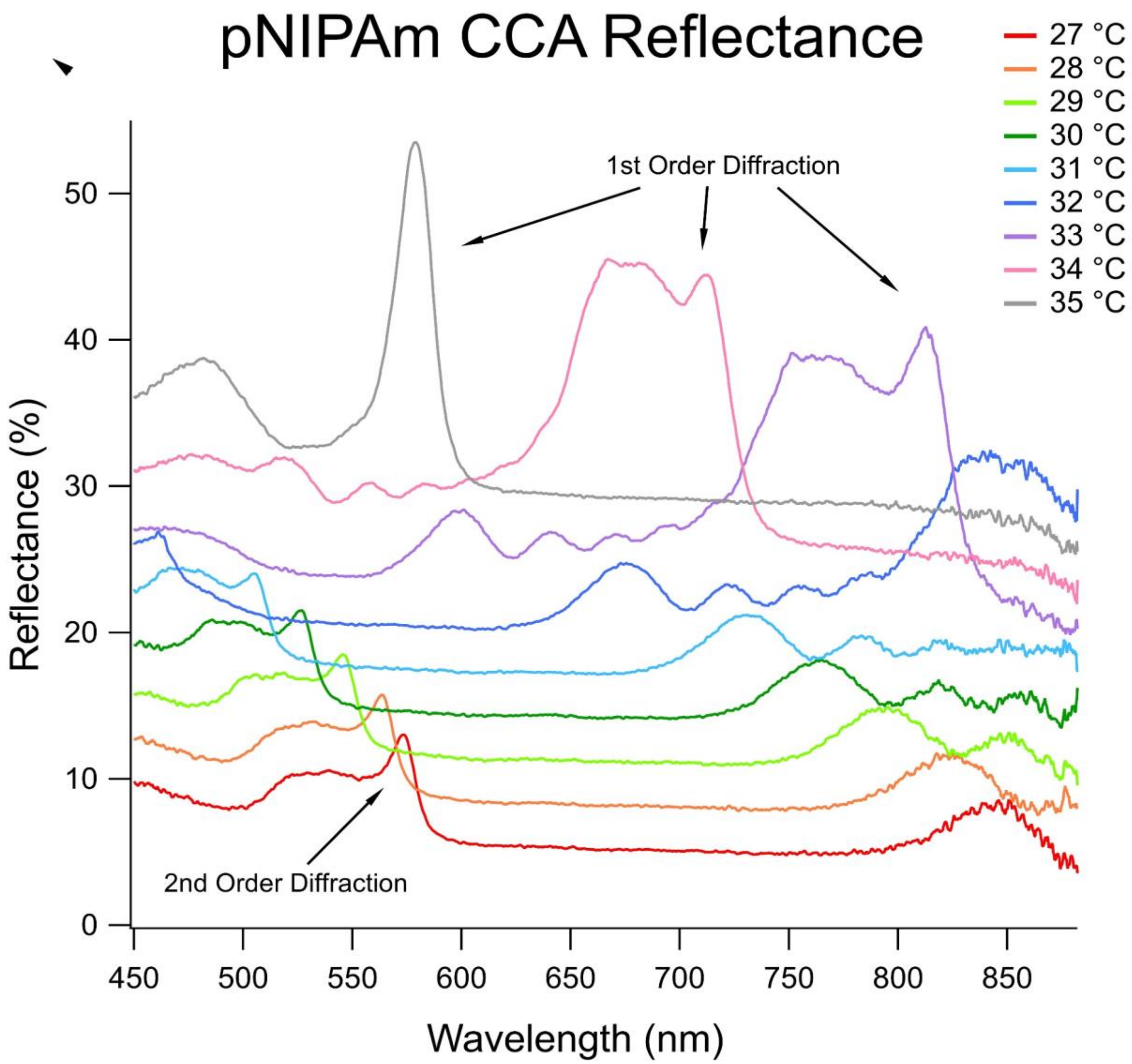

Figure 4.3 Reflectance spectra of pNIPAM CCAs containing PS nanoparticles at different temperatures. Temperatures were determined using thermal imaging data. Each trace is offset vertically from the one collected at a lower temperature by 5% to facilitate comparison of traces. Peak wavelengths and maxima positions of the 1st and 2nd order diffraction bands used to track the gel's volume are highlighted with arrows.

4.3.2 Determination of pNIPAM LCST Using Reflectance Measurements

As the temperature increases towards the LCST, the hydrogel network starts to gradually shrink, blue shifting the measured diffraction. At the LCST, the collapse of the pNIPAM network starts to occur. pNIPAM's volume changes are smaller at temperatures farther from the LCST giving shifts in diffraction that are < 25nm/°C. Volume changes become larger as the temperature approaches the LCST, shifting by as much as 100 nm/°C. More sensitive analyte detection is possible by using the large diffraction shifts that occur from small changes in pNIPAM's environment around the LCST.

As the pNIPAM LCST leads to the expulsion of water, the effective refractive index of the pNIPAM CCA increases from contributions of the larger volume fraction of the nanoparticles and the polymer network. The larger n_{eff} causes a brief increase in diffraction efficiency around the LCST before the loss of diffraction from the collapse of the polymer network. The pNIPAM LCST was determined to be the temperature where the diffraction wavelength reached a minimum.

4.3.3 pNIPAM CCA Adaption for Hydrophobic Sensing

While pNIPAM has been shown to bind compounds with hydrophobic characteristics[200-202], the presence of additional hydrophobic groups disrupts the structure of the water within the polymer network. The coil-to-globule transition of pNIPAM at the LCST disrupts the ordering of the water within the polymer network. The less ordering of the water molecules the less energy it takes to disrupt the water structures leading to a lower observable LCST.[202]

4.3.3.1 Hydroxyphenyl Acrylate Incorporation

We studied the addition of the hydrophobic comonomer hydroxyphenyl acrylate (HPA) to determine if its presence can be used to increase pNIPAM sensitivity to binding of hydrophobic analytes. Hydrophobic comonomers within pNIPAM hydrogels create a more favorable binding environment for hydrophobic analytes, increasing the sensing response.[200] HPA derivatives have been shown to form complexes with a variety of analytes[203-204] including the hydrophobic molecule caffeine[205]. Caffeine is relatively soluble in water up to 20 mg/mL[206] despite its hydrophobicity making it a good hydrophobic analyte for detection using pNIPAM-co-HPA hydrogels.

HPA is very similar in structure to the medication paracetamol and the amino acid tyrosine, both of which undergo photodegradation under UV irradiation.[207-208] Since our pNIPAM hydrogels undergo UV irradiation for 3 h during polymerization, HPA degradation was anticipated to occur during hydrogel fabrication. Hydrogels containing low concentrations of HPA without the addition of a CCA were fabricated using the VA-086 photo initiator. Polymerization occurred by irradiation using a 415 nm LED light. The use of a visible light source during polymerization mitigated UV-photodegradation of HPA.

Samples without CCAs were fabricated with a thickness of 400 μm to increase robustness without the presence of the CCA. Samples of 400 μm and 150 μm thickness showed negligible difference in the transition temperature but the 400 μm thick samples showed more defined changes in transmission allowing better monitoring of shifts in the LCST. The transmittance of 500 nm light through the sample was monitored as the sample temperature was increased from 30 ˚C to 36 ˚C. The LCST temperature was determined to be the temperature at which the amount of light transmitted through the sample was decreased by half (Figure 4.4).

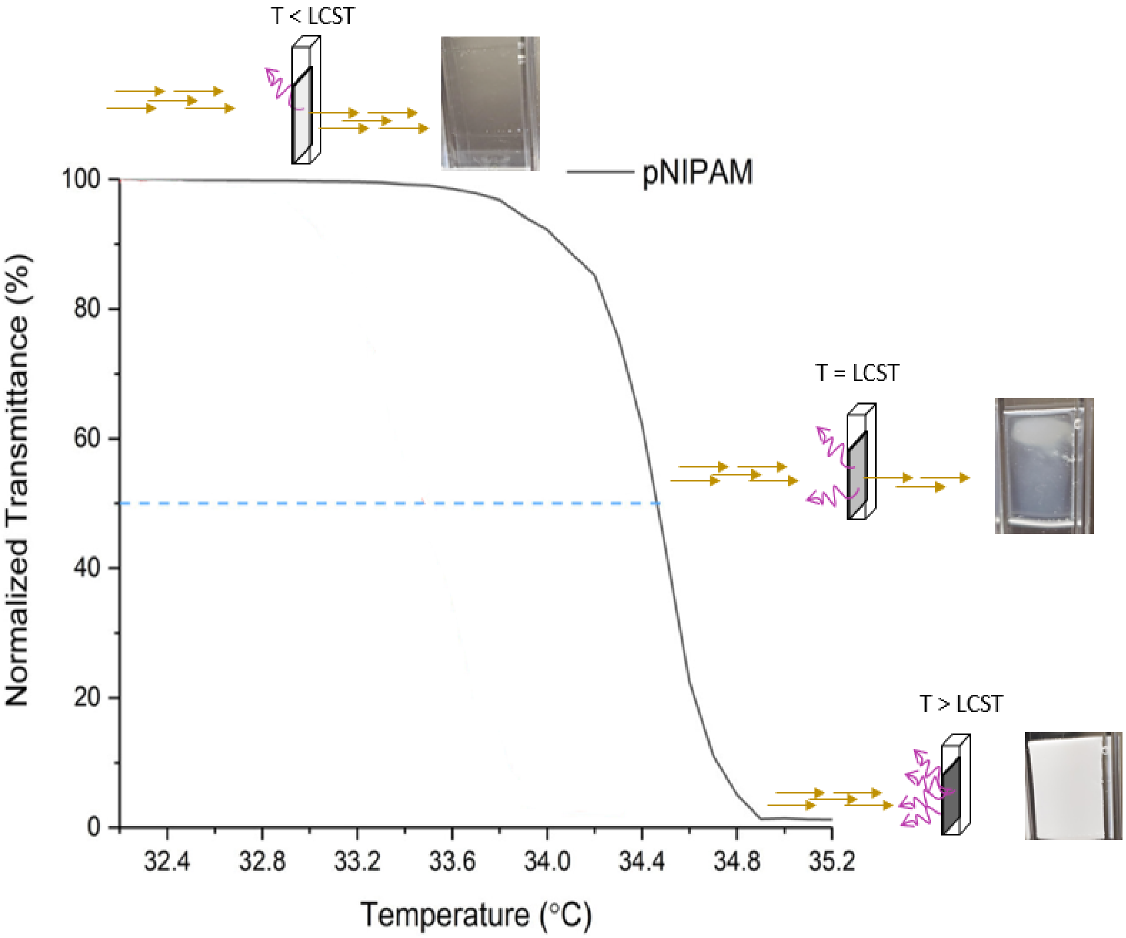

Figure 4.4 LCST determination of a pNIPAM hydrogel (20% NIPAM/0.2 % bis, VA-086 intiator) without CCAs. Transmittance of 500 nm light was measured and the LCST was determined by the temperature where transmission of the light through the sample decreased by half.

pNIPAM-*co*-HPA hydrogels contained 1%, 3%, or 5% w/v HPA. Hydrogels containing HPA showed a ~1°C lower LCST than the control pNIPAM hydrogels at 33.5 ˚C ± 0.2 ˚C and 34.5 ˚C ± 0.2 ˚C respectively. An example of the LCST determination for a pNIPAM hydrogel is shown in Figure 4.5. The decreased LCST shows that we have successfully altered the pNIPAM environment through fabrication of pNIPAM hydrogels with HPA comonomer.

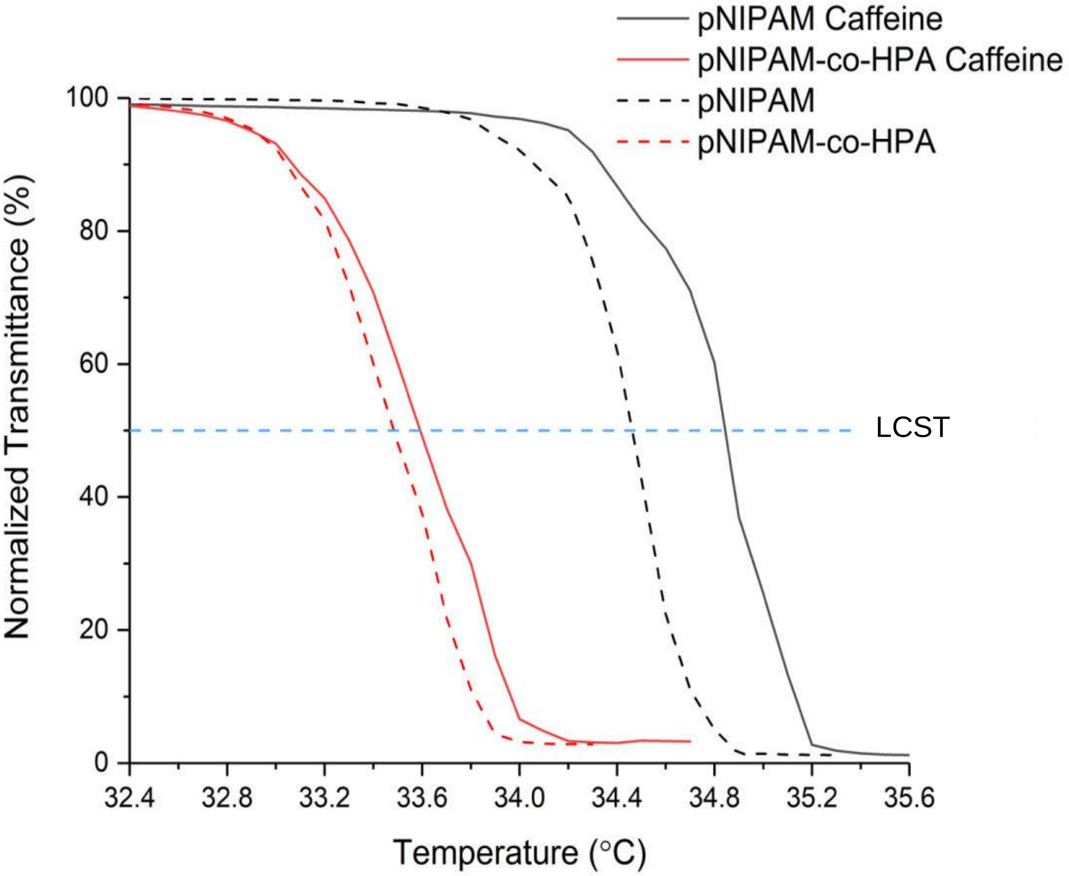

Figure 4.5 LCST determination of hydrogeals containing pNIPAM (black), pNIPAM with 1 % HPA (red), and pNIPAM. The LCST was determined by a 50 % loss of transmittance through the sample. All hydrogels were polymerized on an acrylamide gel support sheet and contained 20% NIPAM/0.2 % MBAAm. Solutions containing caffeine (10 mg/mL) are demonstrated using solid lines

We tested changes to the pNIPAM-*co*-HPA LCST in concentrated caffeine solutions (10 mg/mL). While HPA addition lowered the hydrogel's initial LCST, the presence of caffeine did not cause any significant decreases in the LCST at 33.6 ˚C ± 0.2 ˚C (Figure 4.5). Measured LCSTs of the pNIPAM-*co*-HPA hydrogels also did not show LCST shifts from the HPA concentrations used. It is possible the small concentrations of HPA present are already causing the maximum LCST shift possible for the concentrations of HPA we were able to achieve.

In the presence of caffeine, there is a slight decrease in the LCST of the samples that did not contain HPA, 34.9 ˚C ± 0.1 ˚C in the presence of caffeine compared to 34.5˚C ± 0.2 ˚C initially. The presence of HPA or caffeine individually led to shifts in the LCST, however the presence of HPA does not significantly increase shifts in the LCST in the presence of caffeine. Since pNIPAM's volume is highly sensitive to environmental changes near the LCST, we next investigated the addition of HPA into pNIPAM CCAs in an attempt to elucidate how the binding of caffeine changes the LCST.

4.3.3.2 pNIPAM-co-HPA CCA Development

We first looked at pNIPAM-*co*-HPA CCAs containing polystyrene (PS) nanoparticles as changes in diffraction of visible light are easily observable using PS nanoparticles. As diffraction occurs from modulation in the refractive index, diffraction efficiency increases with changes in the effective refractive index. Polystyrene CCAs have high diffraction efficiency due to the large difference in refractive index between PS (n_{PS}=1.59), and the surrounding medium (n_{air}=1 or n_{water}=1.33).[48, 160] More efficient PS diffraction allows monitoring of small shifts in the diffraction wavelength.

PS's large diffraction efficiency also allows monitoring of the diffraction wavelength even with slight CCA disordering during polymer collapse. The large size of the hydrogel leads to some inhomogeneities during the polymer collapse which can cause disorder within the CCA diffracting planes. Disorder within the CCA can cause broadening of the primary diffraction wavelengths being measured.[209]

The addition of hydrophobic comonomers with PS CCAs was unfavorable and lead to irreversible phase separation during polymerization. While the CCA solution containing NIPAM monomers showed strong diffraction and stability over time, phase separation occurred during polymerization. We attempted to use a cosolvent to increase polymer solubility during fabrication. Low concentrations of cosolvents like propylene glycol did lead to a decrease in phase separation during polymerization. However, slight phase separation still occurred resulting in largely inhomogeneous hydrogel networks. Swelling of the inhomogeneous hydrogels caused CCA disordering, hindering diffraction monitoring. Further increasing the amount of co-solvent present during fabrication stopped CCA self-assembly.

We looked at the use of silica (Si) nanoparticles for CCA fabrication in pNIPAM-*co*-HPA hydrogels in an attempt to eliminate the irreversible phase separation. Like polystyrene, silica nanoparticles have been widely used in photonic crystal development.[48, 210-211] Silica particles used were composed of siloxane (Si-O-Si) networks that were functionalized with silanol (Si-OH) groups on the surface. The silica nanoparticle interactions are also easily tuned through functionalization of the nanoparticle surface giving them wide use in CCA fabrication.[212-215] Phase separation occurring from the pNIPAM-*co*-HPA CCA fabrication was believed to be due to increased hydrophobicity. Thus, we hypothesized the more hydrophilic silica nanoparticles would create a more favorable solution environment for the pNIPAM network during polymerization.

Switching from PS to Si CCAs did eliminate hydrogel phase separation during fabrication, however washing the hydrogel in water resulted in immediate phase separation. Placing the pNIPAM CCA (Si) into a mobile phase of either pure DMSO or EtOH reversed the phase separation that occurred from washing in water and resulted in strong diffraction of the Si CCA. Using high concentrations of organic solvents can lead to polymer co-nonsolvency where pNIPAM does not have an LCST within a reasonable temperature range.[201, 216-217]

Nanoparticles composed of different materials are needed to fabricate pNIPAM CCAs containing hydrophobic comonomers. Our current use of PS- or Si-based CCAs does not allow the incorporation of hydrophobic comonomers within the pNIPAM hydrogel even at low concentrations. pNIPAM hydrogels containing monolayers of nanoparticles ordered into a photonic crystal (2DPC) have been previously fabricated containing hydrophobic comonomers.[200] These 2DPC pNIPAM hydrogels did not show phase separation allowing diffraction monitoring during sensing. However, the use of CCAs within the sensor affords greater sensitivity in monitoring diffraction shifts.

4.3.3.3 Nanoparticle Monitoring for pNIPAM CCA Development

Although photonic crystals have become widely used in the development of sensors, there is little discussion on why the specific material was used to fabricate the photonic crystal. This lack of discussion is easily overlooked when the photonic crystal does not take part in the sensing mechanism but becomes problematic when the mechanism is highly sensitive to sensor composition, as seen in our pNIPAM-*co*-HPA CCAs. While both polystyrene and silica nanoparticles undergo self-assembly into CCAs, polystyrene is primarily hydrophobic while the silica nanoparticles have hydrophilic surfaces. We looked at pNIPAM CCAs that contained polystyrene (PS) nanoparticles or silica (Si) nanoparticles, and pNIPAM hydrogels that did not contain CCAs to elucidate how the CCA composition changes the pNIPAM response.

Hydrogels that did not contain nanoparticles were fabricated to determine pNIPAM's LCST without any additional contribution from the nanoparticle materials. Fabrication of the pNIPAM hydrogels without CCAs resulted in fewer instances of phase separation during polymerization and were more easily removed from the sample holder's quartz plates. We looked at pNIPAM hydrogels that were fabricated using 20% NIPAM/0.2 % bis with Irgacure 2959 used as an initiator (365 nm irradiation). The LCST was determined to be 35.4 ˚C ± 0.2˚C. Previous samples that used VA-086 initiator instead of Irgacure 2959 had an LCST ~1 ˚C lower (34.5 ˚C ± 0.2 ˚C) than that of the hydrogels with Irgacure 2959.

pNIPAM CCAs were also fabricated using Irgacure 2959. The LCST of pNIPAM CCAs containing PS nanoparticles was determined to be 33.4 ˚C ± 0.3 ˚C. The measured LCST was lower than the determined 35.4 ˚C ± 0.2˚C LCST for pNIPAM hydrogels without a CCA for the same fabrication process. We concluded the presence of the PS CCA (113 nm, 2.5 % w/v) decreases the pNIPAM LCST by ~2 ˚C.

CCAs containing silica nanoparticles showed bands with weaker diffraction intensity due to a smaller effective refractive index. Since second order diffraction has a lower intensity than first order diffraction, we were unable to monitor the CCA's second order diffraction and had difficulties measuring the first order diffraction. The LCST of pNIPAM CCAs with Si nanoparticles was estimated to be 35.3 ˚C ± 0.3 ˚C which was similar to that of pNIPAM hydrogels without CCAs.

Our findings support the conclusion that the presence of PS nanoparticles within the CCA can impact pNIPAM's LCST due to their hydrophobic nature. Si nanoparticles are more hydrophilic and do not appear to alter the LCST but when additional hydrophobic moieties are added, such as comonomers, they can lead to phase separation. CCA nanoparticle composition should be taken into consideration when developing pNIPAM CCA sensors.

4.3.3.4 Addition of Ethanol for pNIPAM Sensing

Our goal is to enable sensing outside laboratory settings through the development of portable sensors. While pNIPAM CCAs are portable and color changes are easily perceived, they require heating for LCST monitoring. Ideal pNIPAM sensors would have transition temperatures near ambient conditions to avoid excessive heating and error that may occur from lack temperature stability when heating samples outside a laboratory environment.

One way to decrease pNIPAM's LCST to ambient temperatures is through changes in the mobile phase composition. The amphiphilic nature of pNIPAM makes it soluble in both aqueous and organic solvents. When pNIPAM contains an aqueous mobile phase, the water becomes ordered around the polymer network creating a solvation shell. As the temperature increases, the ordered structure of the water no longer becomes energetically favorable leading to the hydrophobic collapse of the polymer network and expulsion of the water solvent.

When the mobile phase is a combination of water and an organic solvent, ordering of the water in pNIPAM's solvent shell is altered. Decreased ordering of the water caused by the presence of the organic solvent-polymer interactions requires less energy to actuate the polymer's hydrophobic collapse at the LCST. Larger disruptions to pNIPAM's solvation shell, create larger changes in the LCST. Common co-solvents include alcohols[28, 216-219], acetone[220], and dimethyl sulfoxide[169, 221-222].

We looked at pNIPAM's response in solutions that contained 0.18 or 0.20 mol fraction ethanol (EtOH) in water. The use of ethanol lowered the measured LCST to ~24 ˚C ± 0.3 ˚C for 0.18 mol fraction ethanol and to ~21˚C ± 0.3 ˚C for 0.20 mol fraction ethanol. While the presence of ethanol lowered the LCST, it also decreased the measurable diffraction shifts of the CCA. Co-nonsolvency effects from the presence of a second solvent, such as ethanol, can decrease pNIPAM's solubility in the solution mixture compared to the solubility in pure water. Low solubility of the pNIPAM leads to lower intake of solvent resulting in smaller hydrogel swelling responses.

As the amount of ethanol in the solution is increased, pNIPAM's LCST is decreased but so is the measurable swelling response. Solutions of pure water gave diffraction shifts leading up to the LCST of >250 nm for the first order diffraction while solutions containing 0.18 and 0.20 mol fraction EtOH led to shifts of ~80 nm and ~30 nm respectively.

The amount of pNIPAM swelling is not important if the LCST can be easily monitored. Solutions containing 0.20 mol fraction EtOH were highly sensitive to fluctuations in the room conditions and gave only small diffraction shifts making them less ideal for sensing using pNIPAM CCAs. We determined use of 0.18 mol fraction EtOH as a cosolvent lowers the LCST to a more ideal temperature for sensing outside of a lab environment while leading to diffraction shifts that are easily used to monitor changes in the LCST making it a good solvent choice for pNIPAM CCA sensors.

4.3.4 pNIPAM CCA for Detection of Hydrophobic Analytes

Our proposed pNIPAM CCA sensing mechanism utilizes the sensitivity of pNIPAM's LCST for monitoring the pNIPAM environment. Below the LCST our pNIPAM CCAs are swollen. As the analyte binds to the hydrogel, the lattice spacing of the embedded CCA will be altered with changes in the pNIPAM volume. Shifts in the CCA diffraction will occur in proportion to the magnitude of change occurring to the pNIPAM environment.

Analyte binding to the hydrogel network will lead to a more hydrophobic pNIPAM environment causing the polymer network to collapse at temperatures lower than the LCST (Figure 4.6). The increased sensitivity of pNIPAM's volume to environmental changes around the LCST makes it ideal for monitoring analytes that typically do not cause large sensing responses. One such target is xenon (Xe).

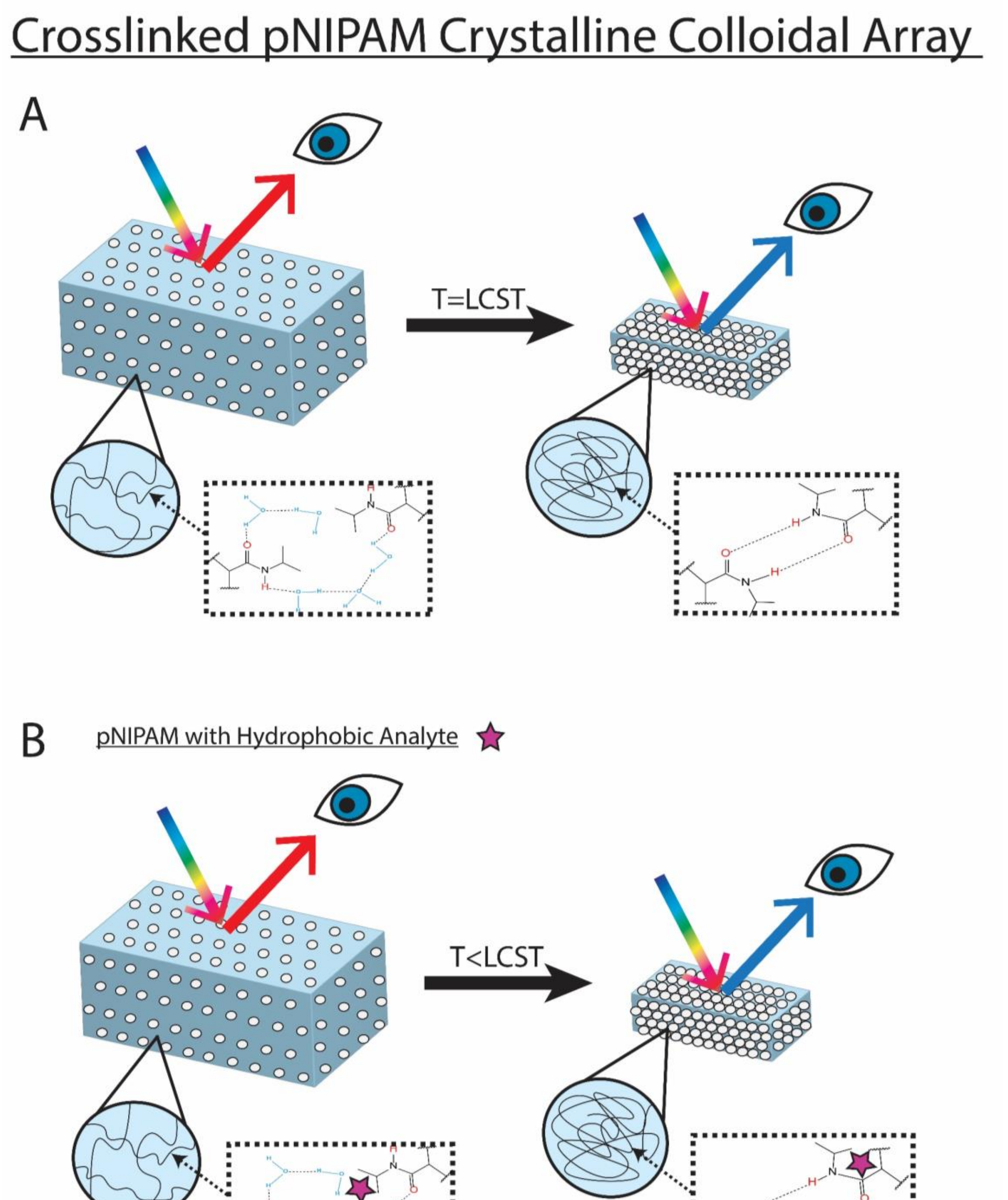

Figure 4.6 Mechanism of pNIPAM CCA detection of hydrophobic analytes. (A) pNIPAM hydrogels are hydrated below their LCST but undergo collapse of the hydrogel network above the LCST. (B) the presence of hydrophobic analytes within the pNIPAM network shifts the LCST to lower temperatures enabling detection of analytes.

pNIPAM's LCST is highly sensitive to changes in pNIPAM's environment such as the addition of hydrophobic groups. We believe our pNIPAM CCAs can be adapted for detection of different hydrophobic analytes showing their use for sensing along with their generalizability for detection of other analytes. This is the first report of pNIPAM's transition temperature being used for analyte recognition in sensing.

4.4 Monitoring Xe Binding

4.4.1 Xe-Protein Interactions

Although Xe-protein interactions are not well known, Xe's binding to the protein myoglobin (Mb) has been well studied.[182-183, 185] Xe binding has also been monitored in serine proteases with the presence of Xe suggested to cause protein inhibition.[178, 180, 223] While there is still a debate on the mechanism behind Xe's effect on proteins, it has been determined that Xe prefers to be located in hydrophobic pockets[223-224] containing aromatic groups such phenylalanine, tyrosine, and tryptophan residues.

Xe is known to associate with hydrophobic functional groups via non-covalent interactions, particularly in proteins.[185] Furthermore, porous organic materials such as metal-organic frameworks (MOFs)[225] and porous covalent organic polymers (COPs)[226-227] have been shown to adsorb Xe with high capacities. We hypothesize that pNIPAM CCAs can be developed for Xe binding. Xe's hydrophobic and inert nature makes it a good candidate for detection using pNIPAM CCAs. Sensors that utilize pNIPAM CCAs are inexpensive to fabricate and robust with analyte detection that is easily visualized through color changes. Fabrication of a pNIPAM CCA whose LCST is modulated from the presence of Xe would enable more widespread monitoring of Xe.

We performed spectroscopic studies of Xe-protein interactions in an attempt to elucidate more information about Xe-protein binding. Our ultimate goal was to develop more favorable Xe binding conditions within the pNIPAM network. We looked for changes in protein structure from the presence of Xe using resonance Raman and ^{129}Xe NMR.

4.4.2 Resonance Raman Spectroscopy

When light is scattered by a molecule it can either be elastically or inelastically scattered. Light that is scattered at the same frequency as the incident light is elastically scattered. This phenomenon is known as Rayleigh scattering when the wavelength of the incident light is much larger than the molecule’s size, and Mie scattering when the incident light is of similar size to the molecule. Raman spectroscopy uses inelastic scattering where the frequency of the scattered light is shifted from the frequency of the initial light. The amount the frequency is shifted is indicative of the molecular vibration being excited. This gives insight into the conformation, identity, and environment of the sample.[228]

Although most of the light is elastically scattered, a small fraction of light is inelastically scattered. The intensity of inelastically scattered light can be increased by using incident light that coincides with one of the sample’s electronic transitions, known as resonance Raman spectroscopy. Through resonance Raman, the intensity of the light that undergoes Raman scattering can be enhanced by up to 10^6.[228] Ultraviolet resonance Raman spectroscopy (UVRR) is useful for protein monitoring due to its sensitivity and selectivity to protein secondary structure, solvent exposure, hydrogen bonding, and aromatic side chain orientation.[159, 191, 229-231]

4.4.2.1 Mb-Xe Interactions Using Resonance Raman

We collected Raman spectra using 204 nm, 229 nm, and 405 nm excitation to monitor changes in Mb from the presence of Xe. A table of the assigned bands used to monitor the presence of Xe can be found in Appendix B.2. Resonance Raman using 204 nm excitation is in resonance with the $\pi \rightarrow \pi^*$ transition that is associated with the amide groups.[231] There are bands in the 204 nm UVRR spectrum that are sensitive to the protein backbone dihedral angles which can be used to monitor protein secondary structure.[229-230, 232] Collected spectra of 0.3 mg/mL Mb were fitted using the bands determined by Cai et al. for bovine serum albumin[138]

Mb spectra showed amide III_3 ($AmIII_3$) bands with a frequency of 1252 cm^{-1} and a broad fitting of the band (Figure 4.7A). This correlates to a Ψ angle distribution centered at ~-40 ° which is indicative of an α-helical conformation. Our data agrees with published crystal structures of Mb showing a primarily α-helical secondary structure with some turn and coil-like regions interspersed within the protein network. $AmIII_3$ bands did not show a significant shift from the presence of Xe that would indicate a change in protein secondary structure.

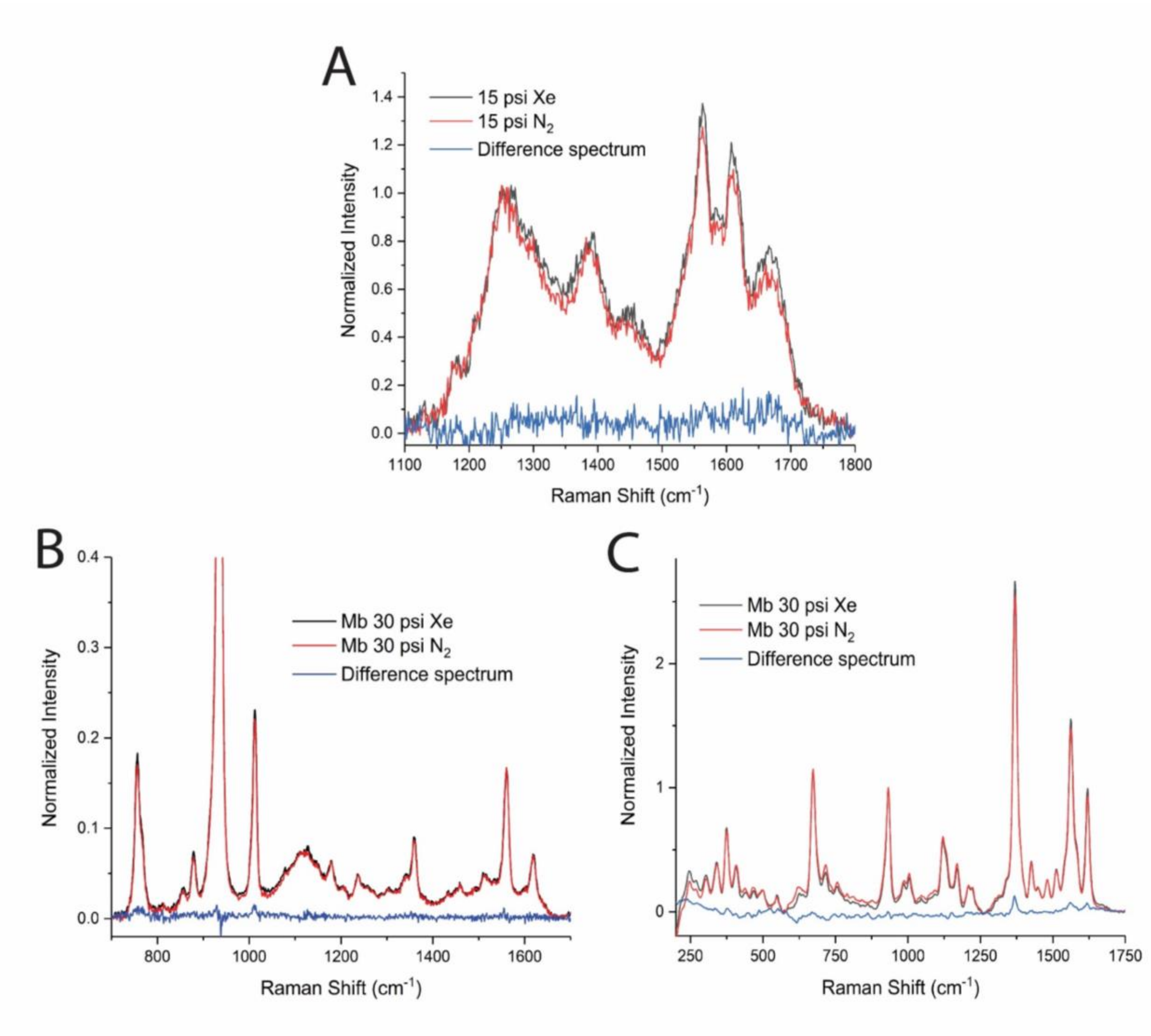

Figure 4.7 Resonance Raman spectra of horse heart myoglobin. (A) 204 nm excitation of 0.3 mg/mL Mb in the presence of 15 psi Xe (black) or 15 psi nitrogen (red). (B)) 229 nm excitation of 0.5 mg/mL Mb in the presence of 30 psi Xe (black) or 30 psi nitrogen (red) an internal standard of ClO_4^- was used to normalized the spectra and is seen at 935 cm^{-1}. (C) 405 nm exitation of 0.5 mg/mL Mb under or 30 psi Xe (black) or 30 psi nitrogen (red) an internal standard of ClO_4^- was used to normalized the spectra and is seen at 935 cm^{-1}. The difference spetra of Xe and nitrogen for each excitation is shown in blue.

Resonance Raman spectra using 229 nm excitation is dominated by contributions from the aromatic side chains. At 229 nm, electronic transitions of tryptophan (Trp), tyrosine (Tyr), phenylalanine (Phe), and histidine (His) are visible.[138, 187, 232] Changes in the sidechain structure and packing can be monitored using dihedral angles, water exposure, and the aromatic ring geometries. Although Xe binds near aromatic amino acids, there were no measurable differences in sidechain packing from the presence of Xe (Figure 4.7B).

Raman spectra of Mb using 405 nm excitation is in resonance with the Soret absorbance band which reports on the heme group and its ligands.[233] The primary Xe binding site is located proximal to the heme. Due to Xe's bulky size and location of binding, changes to the heme vibrations due to Xe binding were also monitored. No changes in the heme vibrations were observed (Figure 4.7C).

Although it has been shown that Xe binds to Mb, there were no measurable differences in the Mb vibrations from the presence of Xe. Any changes to Mb from Xe binding are outside the sensitivity of our measurements, further showing how difficult it can be to detect the presence of Xe.

4.4.3 ^{129}Xe NMR

We used ^{129}Xe NMR to gain insight into Xe-protein interactions for development of more sensitive Xe sensors. Binding models using ^{129}Xe NMR have been developed and studied to investigate the different interactions between Xe and proteins in solution.[184, 234-237] The work of Locci, et al. [184] used ^{129}Xe NMR to characterize the interactions between Xe and multiple proteins, including horse Mb, hen egg white lysozyme, and horse cytochrome c. Locci, et al., additionally characterized non-specific interactions between Xe and the protein surface. They determined that low concentrations of Xe cause the chemical shift to be upfield of the buffer while the increased concentration of Xe caused downfield shifts. They attributed this phenomenon to non-specific interactions between Xe and the protein surface.

Xe chemical shifts can be fit to a two-site binding model derived by Locci, et al.[184] (Equation 4.3), where δ_{obs} is the observed chemical shift, δ_{out} is the chemical shift of Xe not bound to the protein, δ_{in} is the chemical shift of Xe bound to the protein, and ρ_{bound} is the population fraction of Xe bound to the protein.

$$\delta_{obs} = \delta_{out} + (\delta_{in} - \delta_{out})\rho_{bound}$$

Equation 4.3

In the case of Xe binding to Mb, Xe interactions can be divided into three groups: Xe free in solution (not interacting with the protein), Xe interacting non-specifically with the surface of the protein, and Xe specifically bound to a site or sites within the protein (i.e. the proximal site in myoglobin). Locci, et al., showed that the binding of Xe to Mb could be approximated as a 1:1 complex where Xe exchanges rapidly between a specific binding site (Xe_{in}) and all other environments (Xe_{out}). This is described by the kinetic form:

$$K_{eq} = \frac{[Xe]_{in}}{[Mb][Xe]_{out}}$$

Equation 4.4

4.4.3.1 ^{129}Xe NMR Myoglobin Binding Models

To use the Xe binding models for other proteins that demonstrated affinity for Xe binding, we reproduced the published binding models for Xe-Mb interactions. Since Xe is in fast chemical exchange between its binding environments, it is a measure of the population-weighted chemical shift for Xe in the solution for that specific pressure (Figure 4.8).[184, 237] By collecting ^{129}Xe NMR spectra for samples over a range of Xe pressures we were able to fit the data to the binding models. For samples with lower Xe pressures, more scans were needed to achieve the signal-to-noise for reliable chemical shifts.

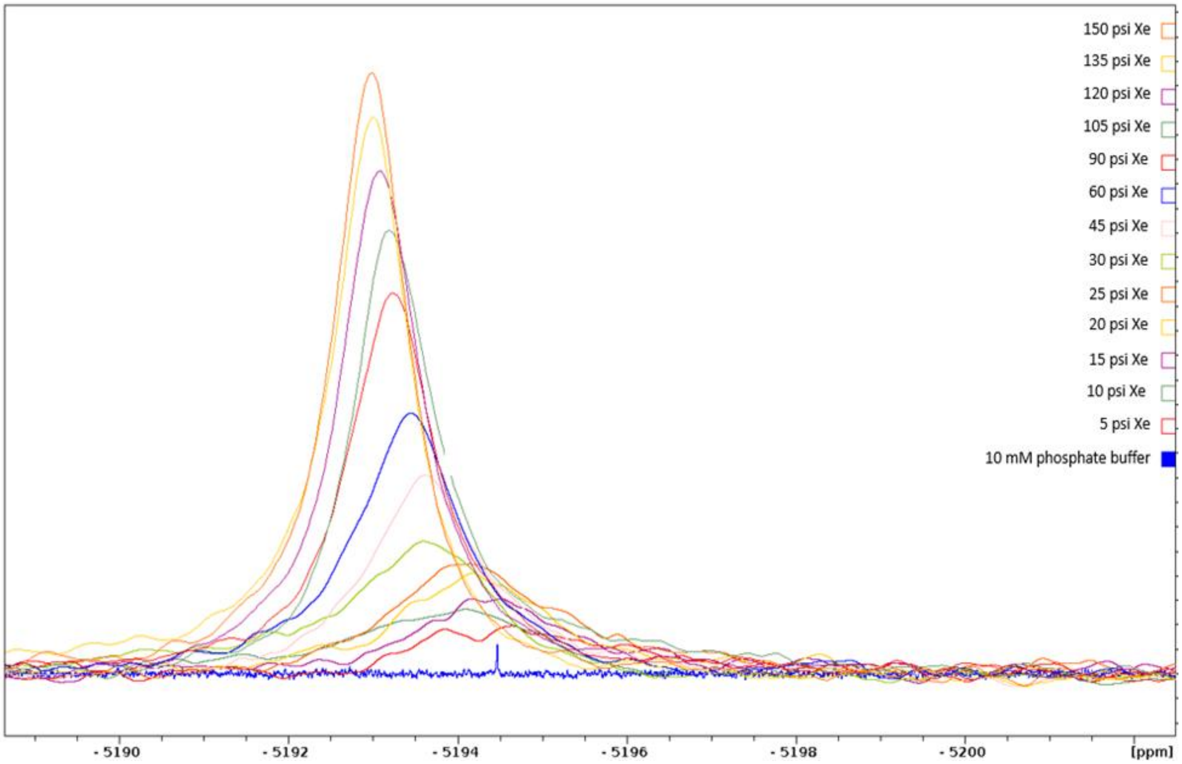

Figure 4.8 Xe chemical shift and linewidth dependence on Xe pressure in a 0.8 mM myoglobin in 80% H_2O/20% D_2O solution. 150 psi Xe in 10 mM phosphate buffer in 80% H_2O/20% D_2O shown for reference.

With one set of NMR spectra at a concentration of 0.8 mM Mb we varied the Xe pressure. As a result of the varied pressure, there are three parameters which change: δ_{in}, δ_{out}, and K_{eq}. Using a second set of NMR spectra taken at a concentration of 1.2 mM Mb and similar Xe pressures, we fit the data to the binding model to look at Xe-Mb binding affinity. The slope of the observed chemical shift values was used to determine the binding affinity, which agreed well with the literature value. We confirmed Xe binding to Mb and our ability to use ^{129}Xe NMR to study Xe-protein interactions.

4.4.3.2 ^{129}Xe NMR Serine Proteases

We attempted to model Xe-serine protease interactions for sensor development using ^{129}Xe NMR. Serine proteases (SPs) are a class of enzymes that cleave peptide bonds in proteins. SPs contain an active site with a catalytic triad consisting of serine, histidine, and aspartic acid residues. This catalytic triad is located in a hydrophobic pocket that is near the protein surface.[238] Xe has been shown to act as a serine protease inhibitor by binding near the catalytic triad and the primary specificity pocket.[180, 239]

^{129}Xe chemical shifts of 25 mM elastase were measured under 60, 90, 120, and 150 psi Xe gas and are reported in Appendix B. The measured chemical shift of Xe increases linearly with Xe pressure. At neutral pH, 25 µM elastase was the most concentrated solution possible. Increasing the pH to 11 made it possible to achieve a more concentrated elastase solution of 72 µM elastase.

The linear trend in the Xe chemical shift values for elastase differed from the change in Xe chemical shift values previously measured in Mb (Figure 4.9). Occupancy for Xe binding to elastase crystals has been shown to be ~0.64 at 4 atm Xe pressure and ~0.78 at 8 atm Xe pressure.[240] Even if it is assumed that there is full Xe occupancy under solution conditions, only one Xe atom binds to each elastase molecule. The maximum concentration of Xe specifically bound to the protein would then be 25 µM or 72 µM. With a Xe pressure of 15 psi (4.4 mM Xe in solution) 72 µM is ~2% of the Xe present in solution specifically bound to protein.

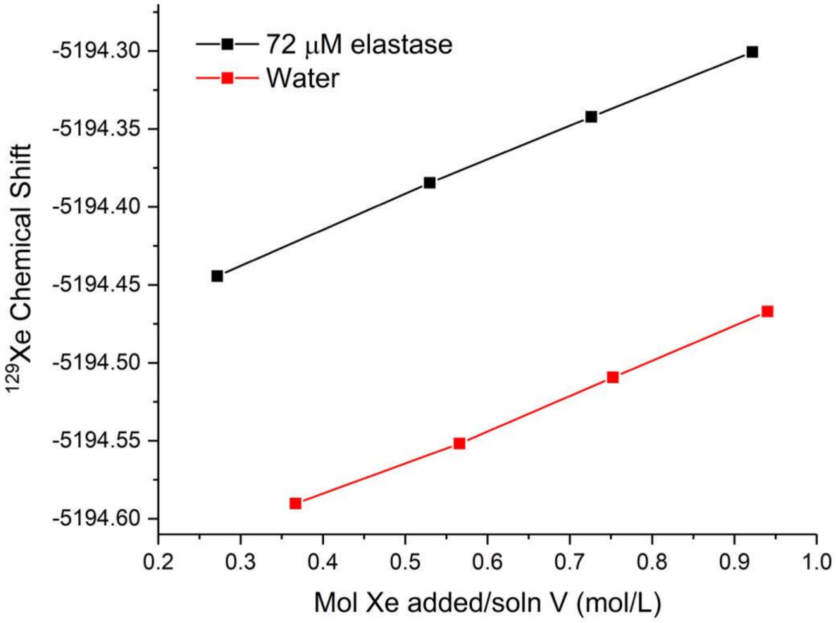

Figure 4.9. Xe chemical shift values for 72 μM elastase in water/D$_2$O (black) compared to water/D$_2$O (red) for varying amounts of Xe. The moles of Xe were calculated from the difference in sample mass with and without Xe. Similar slopes between Xe in water and Xe in elastase indicates binding models are unreliable for determining Xe binding affinity with these data.

Using the Xe binding model from Equation 4.3 it can be shown that the Xe bound to the protein alters the observed chemical shift through the population fraction of Xe bound, ρ_{bound} . Therefore, since the protein bound Xe fraction is very small compared to the fraction of Xe not bound to the protein, the observed chemical shift is dominated by the chemical shift of Xe in the solvent.

To accurately determine the binding affinity between Xe and elastase, the Xe and protein concentrations would need to be on the same order of magnitude, as they previously were between Xe and Mb. Solubility limits of elastase make it impossible to increase the elastase concentration to what is needed. The other strategy for measuring Xe binding affinity would be to decrease the concentration of Xe. However, this would require Xe pressure well below atmospheric pressure. Amounts of Xe that low would be difficult to measure Using ^{129}Xe NMR.

We then switched studies to the serine protease trypsin which has a much larger solubility in aqueous solutions than elastase in an attempt to elucidate Xe-trypsin interactions. Trypsin is known to cleave after lysine and arginine residues; however, the cleavage is not specific to any protein, causing trypsin to cleave other trypsin molecules. One trypsin molecule cleaving a second trypsin molecule is referred to as autolysis. Trypsin autolysis is very fast and depends on protein concentration, occurring within minutes to hours.[241] As the protein concentration increases so does the rate of autolysis.

Solutions of 6-8 mM trypsin at pH 7 were used to monitor Xe binding. In order to monitor chemical shifts from Xe binding, trypsin solutions needed to be highly concentrated (>4 mM trypsin). Initial measurements of the neutral pH trypsin solution showed the Xe chemical shifts were time dependent due to autolysis (Figure 4.10). Further investigation into trypsin's autolysis in the presence of Xe suggested the presence of elevated Xe pressures may lower the autolysis that occurs in the trypsin solution. This would support previous claims that Xe inhibits serine protease activity, but more investigation would be needed.[180, 242] New studies also have suggested Xe binding can increase protein stability.[243]

The inherently low solubility of serine proteases makes them difficult to monitor using ^{129}Xe NMR. Although trypsin is soluble in the concentrations needed for Xe monitoring, its autolysis leads to Xe chemical shifts that are variable with time making them unreliable. We were not able to use ^{129}Xe NMR to gain further insights into Xe-protein interactions for Xe detection.

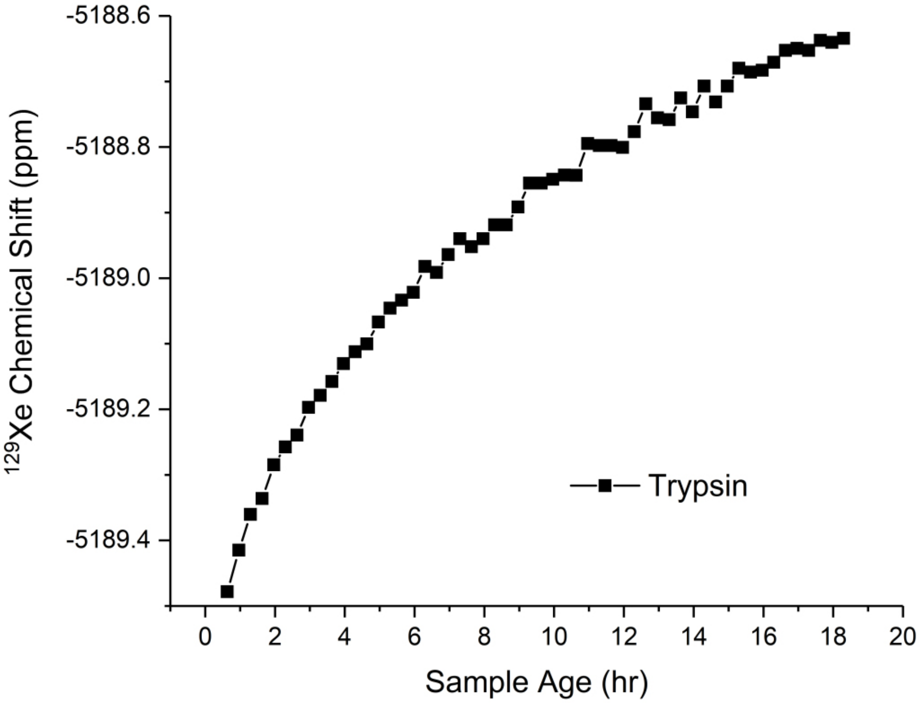

Figure 4.10^{129}Xe chemical shift values of trypsin solutions over time. A neutral pH trypsin solution was within trypsin's optimal pH for activity. The neutral pH solution showed changes in the Xe chemical shift overtime due to autolysis.

4.4.4 EtOH and pNIPAM Xe Monitoring

As expected, Xe-protein binding interactions are difficult to monitor as there is little to no change in protein structure caused by the presence of Xe. While the mechanism behind Xe binding is not well known, it is known that Xe binding cavities in proteins are primarily hydrophobic in nature and contain a significant amount of aromatic amino acids. Our pNIPAM CCAs can be modified to be more hydrophobic and are sensitive to the presence of additional hydrophobic groups, such as Xe. We investigated the use of our pNIPAM CCAs containing PS nanoparticles for monitoring the presence of Xe. Polystyrene CCAs were chosen due to their sharp diffraction bands and high diffraction intensity that enable monitoring of small changes in the wavelength. The addition of hydrophobic polystyrene also creates a more favorable Xe binding environment.

Initial measurements using pNIPAM CCAs in pure water did not show any differences in the LCST between samples with Xe and those with N_2. This was not unexpected as Xe's solubility decreases with elevated temperature.[244] Since the presence of Xe is difficult to monitor, our aim was to work close to pNIPAm's LCST which has been shown to increase pNIPAm's sensitivity to changes in pNIPAM's environment, such as analyte binding.[245] Based on our previous studies using pNIPAM CCAs in solutions containing ethanol, we equilibrated our pNIPAM CCAs with polystyrene nanoparticles in 0.18 mol fraction EtOH. The 0.18 mol fraction EtOH lowered pNIPAM's LCST and enabled more sensitive monitoring at room temperatures and obvious shifts in the diffraction band. Xe also has an increased solubility in ethanol by almost an order of magnitude.[246-247] Working with ethanol as a cosolvent is a promising direction for Xe detection.

Initial trends in the data suggest the presence of Xe lowers the pNIPAM LCST when a water-ethanol mixture is used as the mobile phase. The LCST of samples containing 0.18 mol fraction ethanol showed a decrease in the LCST of ~0.5 ˚C from the presence of 40 psi Xe (Figure 4.11). Current limitations with temperature control for CCA reflectance measurements put the ~0.5 ˚C shift from Xe on the edge of our limit of detection, however the presence of 40 psi N_2 did not show significant shifts in the LCST leading to the belief that LCST shift is from Xe-pNIPAM interactions.

Although 0.20 mol fraction of ethanol is not ideal for use in our current pNIPAM sensors, we investigated the effects of Xe on the LCST from the increased ethanol concentration. If Xe's solubility in EtOH-water mixtures is a linear relationship at low concentrations of EtOH, the larger mol fraction of EtOH should increase Xe's concentration in solution. If Xe binds to the polymer, causing a shift in the LCST, an increased concentration of Xe in solution should result in larger LCST shifts from Xe-pNIPAM interactions. We saw a similar trend with 0.2 mol fraction of EtOH as we did with 0.18 mol fraction EtOH where solutions containing Xe had lower LCSTs than solutions containing nitrogen. The difference in the LCST between samples with nitrogen and samples with Xe was ~0.7 ˚C, supporting our conclusion that the shift in LCST is from the presence of Xe however further investigation is needed.

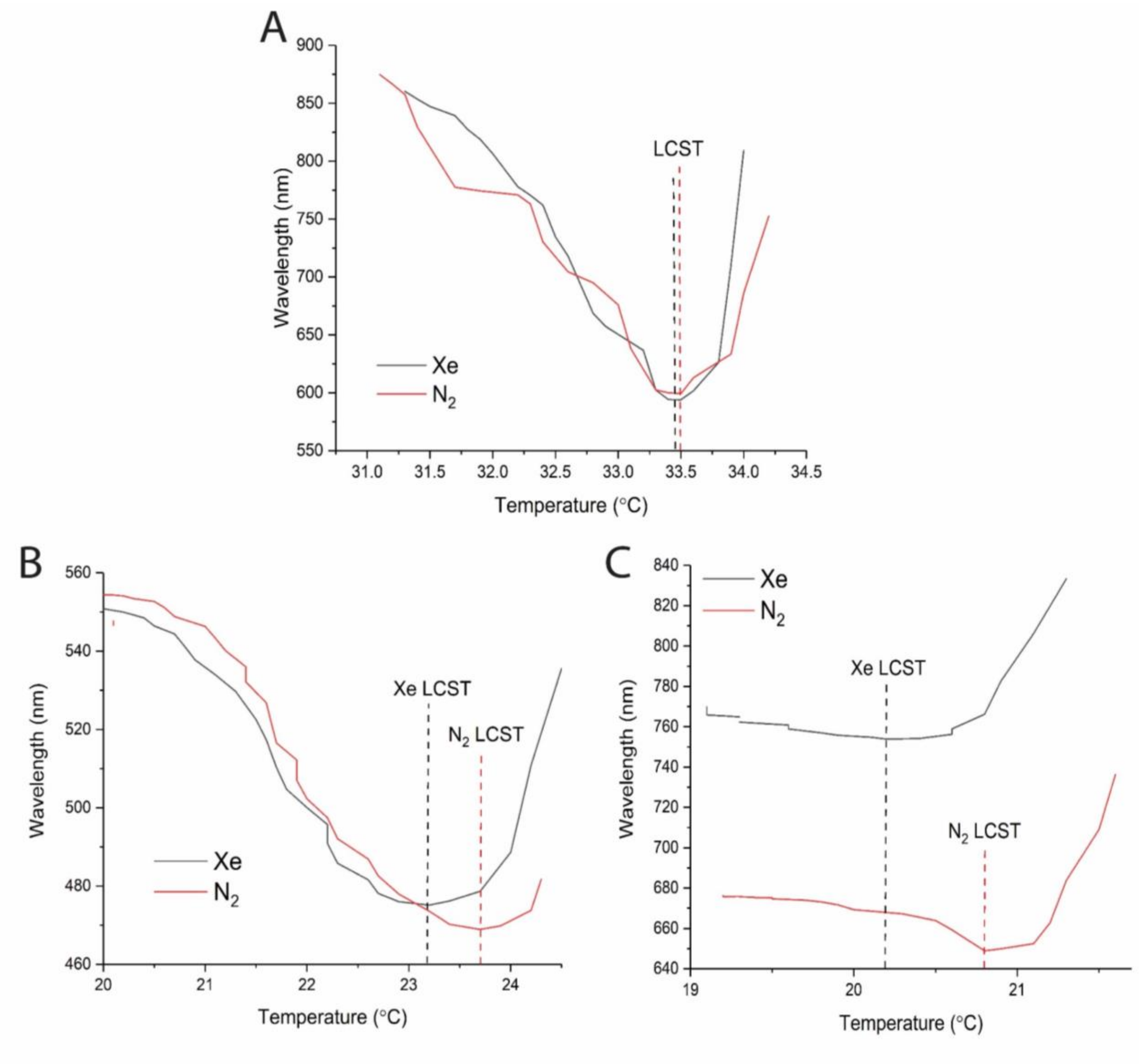

Figure 4.11 Examples of pNIPAM CCA LCST as determined by reflectance bands in the presence of 40 psi N_2 (red) or Xe (black). (A) pNIPAM LCSTs were measured in pure water and showed no significant difference in LCST. (B) pNIPAM LCSTs were measure in 0.18 mol fraction EtOH/water mixture showing a possible shift of ~0.5 ˚C. (C) pNIPAM LCSTs were measure in 0.20 mol fraction EtOH/water mixture showing a possible shift of ~0.7 ˚C. The switch between N_2 and Xe gas was made by gently degassing the sample followed by repressurizing

4.5 Conclusions and Future Directions

We investigated the use of pNIPAM hydrogels containing crystalline colloidal arrays for development of portable sensors. The thermoresponsive polymer pNIPAM has an LCST that is altered by changes to the pNIPAM environment including changes in solvent, the addition of comonomers, or the presence of hydrophobic groups within the polymer network. We monitored decreases in pNIPAM's LCST from the addition of low concentrations of the comonomers hydroxyphenyl acrylamide (HPA). The addition of 1-5 % w/v HPA decreased the observable LCST by 1 ˚C due to the changes in the pNIPAM sensing environment. Addition of the cosolvent ethanol showed contributions of co-nonsolvency within the pNIPAM hydrogel leading to LCSTs that were significantly lowered at 24 ˚C for 0.18 mol fraction ethanol and 21 ˚C for 0.2 mol fraction ethanol.

Xe is a hydrophobic atom that plays a large role in the medical field and environmental monitoring of human activity. Development of a portable sensor for the presence of Xe would enable more widespread detection. Our data suggests that using a pNIPAM CCA mobile phase of 0.18 mol fraction ethanol in water, there is a shift in the pNIPAM CCA LCST of ~0.5 ˚C. While further investigation into this trend is needed, we believe pNIPAM CCAs can be adapted for use as portable sensors for the presence of other hydrophobic compounds.

Future investigations will focus more on the fabrication of pNIPAM hydrogels containing comonomers and how the hydrophobicity/hydrophilicity affects use of the pNIPAM LCST for analyte detection. We will also look at the addition of 2D photonic crystals (2DPC) instead of CCAs for monitoring hydrogel volume due to issues with CCA incorporation within the polymer network when fabricating modified pNIPAM CCAs. pNIPAM hydrogels containing 2DPCs have shown successful addition of hydrophobic comonomers such as tertbutyl alcohol without observable phase separation.[200] The use of a 2DPC will decrease changes in the pNIPAM environment from the presence of the CCA nanoparticles. 2DPCs can also be added to hydrogel networks after polymerization[82], enabling a two-step fabrication process and better incorporation of comonomers for sensor development.

4.6 Acknowledgements

Funding for this work was provided by the Defense Threat Reduction Agency award number HDTRA1-18-1-0017 and the University of Pittsburgh. Collaborative efforts and discussions were made with FLIR Detection Inc. and the Baker group at the University of Washington. ^{129}Xe NMR data was collected and analyzed with the assistance of Damodaran Krishnan Archary from the University of Pittsburgh's NMR facility along with the use of a 10 mm NMR probe from an anonymous benefactor. The authors thank Dr. Sunil Saxena from the University of Pittsburgh for additional insights into ^{129}Xe spectroscopy and NMR dynamics processes.

5.0 Summary of Results and Future Directions

5.1 Summary of Results

In this work, we studied photonic crystal hydrogels and their adaptability as sensing materials. Our work highlights the adaptability of our photonic crystal hydrogel sensors for biomolecular sensing and their use as sensing motifs for a wide range of applications. Our investigations focused on how small modifications to stimuli responsive hydrogels can be used to easily monitor the presence of varying analytes. Chapter 1 briefly discusses photonic crystal diffraction and hydrogel behavior for the development of photonic crystal hydrogel sensors.

In Chapter 2, we investigate the use of photonic crystal hydrogels containing oxyamine recognition groups for the detection of lactate. By converting lactate to pyruvate, we were able to use oxime ligation to attach pyruvate within the hydrogel network. We successfully monitored lactate indirectly through its enzymatic conversion to pyruvate. Our work is the first demonstration of an enzyme coupled photonic crystal hydrogel sensor for indirect detection of analytes. We were able to detect lactate concentrations of 0.24 mM in buffer solutions and < 4 mM in serum solutions.

Chapter 3 discusses 2DPC hydrogels that contain DNA aptamers as crosslinks for analyte detection. We successfully detected the protein thrombin at concentrations below 500 μM within 2 h using our DNA hydrogels. Fabrication of these DNA aptamer hydrogels was previously used for small molecule detection. Our work showed DNA aptamer hydrogels are highly sensitive and easily adaptable for different targets by modifying the DNA aptamer used.

Work discussed in Chapter 4 begins our investigations into pNIPAM's LCST for sensor development. Sensitivity of pNIPAM's LCST to small changes in the polymer's environment can lead to large volume changes making LCST monitoring a promising direction for sensor development. Our work is the first to look at how pNIPAM CCAs can be modified to better sense hydrophobic analytes using shifts in pNIPAM's LCST. We determined pNIPAM is so sensitive to its environment, the material of the CCA can impact fabrication and the addition of comonomers.

The development of hydrogels as responsive materials, particularly for sensing, requires characterization of the hydrogel's fabrication and behavior. Complex hydrogel swelling responses can make adapting sensors for different targets and environments a complex and time-consuming process. We have demonstrated how small modifications to our hydrogel sensors can be made to detect diverse analytes. Our findings include the addition of the LDH enzyme to detect lactate instead of pyruvate and using a different DNA aptamer sequence to change from detecting the small molecule adenosine to the large protein thrombin. Our sensors are easily fabricated and retain sensitivity in complex samples such as serum solutions.

5.2 Future Directions

5.2.1 Mitigating 2DPC Hydrogel Swelling Response to NAD During Enzymatic Reactions

Our research into oxyamine functionalized 2DPC hydrogels showed use for indirect monitoring of lactate. Lactate detection in this work relied on lactate's conversion to pyruvate using the enzyme lactate dehydrogenase. Like many other enzymatic processes, LDH's production of pyruvate requires the cofactor nicotinamide adenine dinucleotide (NAD). In Chapter 2, we investigated interferences in lactate detection from NAD attachment to our 2DPC hydrogels during sensing. The presence of NAD during sensing can increase the limit of detection (LoD) by over 200 x's, limiting analyte detection.

Removal of NAD from solution before attachment to the hydrogel will significantly lower detection limits, however NAD removal can be a complex process[248] that may impact detection of other small molecules within the solution. Modification of NAD using alginic acid has been shown to cause precipitation of NAD under acidic conditions.[102-103] We hypothesize the use of NAD^+ modified with alginic acid would enable us to precipitate out NAD during lactate detection. We use LDH denaturation to avoid the conversion of pyruvate back to lactate during hydrogel attachment. During denaturation, we lower the solution pH to < 2 which is also reported to lead to precipitation of the alginic acid modified NAD, eliminating additional attachment to our sensor.

While the use of modified NAD moieties is helpful for NAD removal in buffer solutions, NAD is also present in biological fluids such as serum. If the concentration of our desired analyte is significantly low, detection may be difficult from attachment of the unmodified NAD in the solution. NAD imprinted polymer networks have been created using acrylamide-acrylamidophenylboronic acid copolymers.[249-250] We believe the addition of an NAD imprinted hydrogel after the enzymatic production of pyruvate can be used to trap and remove NAD present in complex solutions without causing a negative impact to sensing.

We believe both the use of modified NAD moieties and NAD imprinted hydrogels are promising methods for removal of sensing interferences from the presence of NAD. Studies investigating their use may lead to lower sensor LoDs and allowing detection of analytes that have typically have concentrations <100 μM in biological fluids such as phenylalanine using its enzymatic conversion by phenylalanine dehydrogenase.

5.2.2 DNA Aptamer Hydrogels: Protein Stability and Sensor Reversibility

Our DNA aptamer hydrogels detected the protein thrombin through thrombin-aptamer interactions with amino acids on the protein surface. Protein-aptamer interactions are highly specific due to the sequence of both the protein and aptamer, along with the protein's folded structure.

Some proteins have active and inactive structures. For thrombin, one of its inactive forms, prothrombin (Figure 5.1), is present in blood until it undergoes activation. During activation, prothrombinase cleaves prothrombin into the active thrombin form and two fragments.[251] Since there are many thrombin binding aptamers[252] that are able to bind to different locations on the thrombin structure[253], we hypothesize that by switching our DNA aptamer sequence to one that only binds to prothrombin, we can differentiate between active thrombin and its inactive form.

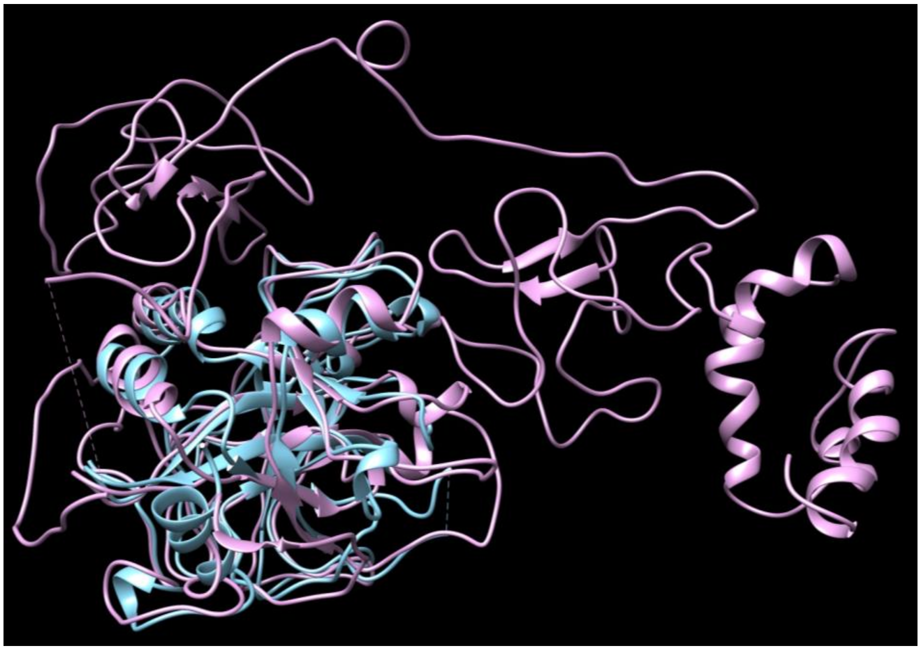

Figure 5.1 Structural alignment comparison of human thrombin (blue) to human prothrombin (pink). PDB ID 3U69 and 6BJR respectively.

If a protein's structure is altered in such a way that the amino acid sequence used for detection is no longer accessible, aptamer-protein binding will not occur. Protein structure can be altered due to degradation or denaturation affecting surface available amino acids.[254]. Denaturation can occur due to changes in the protein's environment such as changes in temperature, pressure, pH, or the presence of certain chemicals.[255] We hypothesize protein denaturation can lead to changes in the DNA aptamer binding site resulting in a lack of sensor response.

We believe further characterization of our 2DPC hydrogel's response to proteins using other DNA aptamer sequences can lead to monitoring protein conformation and activity.

5.2.3 2DPC pNIPAM Hydrogel Sensor Fabrication and Hydrogel Modification

Our pNIPAM hydrogels contain a crystalline colloidal array (CCA) which is used to monitor hydrogel volume changes through shifts in the CCA's diffraction. However, CCA fabrication is highly sensitive to solution conditions. High ionic strength solutions inhibit nanoparticle self-assembly, impacting our ability to increase polymer solubility using charged monomers or organic solvents.

Two-dimensional photonic crystals (2DPCs) are a single layer of hexagonally ordered nanoparticles instead of multilayered structures. The use of 2DPCs decouples the photonic crystal self-assembly from the monomer solution composition while still monitoring hydrogel volume changes. We hypothesize replacing our CCAs with 2DPCs will enable addition of hydroxyphenyl acrylate (HPA) to our pNIPAM hydrogels to increase detection of caffeine.

Switching from pNIPAM CCAs to 2DPC pNIPAM hydrogels will allow us to fabricate hydrogels of different compositions more easily. Development of other pNIPAM co-polymers will also expand detectable analytes based on the formation of different analyte-co-polymer complexes.

We believe pNIPAM hydrogels show promise for sensor development based on the sensitivity of their LCST and further investigation should be performed.

Appendix A Supporting Information for Chapter 3

Appendix A.1 Determination of Thrombin Concentration

The concentration of thrombin stock solution was determined using a Pierce Rapid Gold BCA protein assay kit. The manufacturer's protocol was followed using a BSA standard. Samples were analyzed in 96-well plates in a SpectraMax M2 plate reader with absorbance at 480 nm.

Appendix A.2 Calculating the Dissociation Constant (K_D) of the Thrombin-Binding Aptamer

$$fraction_{bound} = \frac{[aptamer \cdot thrombin]}{[free\ aptamer] + [aptamer \cdot thrombin]}$$

$$fraction_{bound} = \frac{1}{\frac{[free\ aptamer]}{[aptamer \cdot thrombin]} + 1}$$

$$K_D = \frac{[free\ aptamer][free\ thrombin]}{[aptamer \cdot thrombin]}, fraction_{bound} = \frac{1}{\frac{K_D}{[free\ thrombin]} + 1}$$

$$fraction_{bound} = \frac{[free\ thrombin]}{K_D + [free\ thrombin]}$$

Thus, when K_D = [free thrombin], $fraction_{bound}$ = ½. Assuming $fraction_{bound}$ is proportional to the 2DPC hydrogel particle spacing, and [free thrombin] = the concentration of thrombin in solution, K_D can be estimated as the thrombin concentration at half the maximum 2DPC hydrogel particle spacing.

Appendix A.3 Linear fit Data for Calibration Curve in Thrombin-Binding Buffer

Appendix Table 1 Linear fit data for the calibration curve in thrombin-binding buffer

Adjusted R-squared	Slope	Y-intercept
0.9836	60.95 ± 3.93	-111.74 ± 11.10

Linear fits were generated with a weighted least squares method using the software OriginLab.

Appendix A.4 Linear Fit Data for Calibration Curve in Alternate Buffer

Appendix Table 2 Linear fit data for the calibration curve in alternate buffer

Adjusted R-squared	Slope	Y-intercept
0.9663	16.88 ± 1.81	-38.47 ± 5.44

Linear fits were generated with a weighted least squares method using the software OriginLab.

Appendix A.5 Linear Fit Data for Calibration Curve in Diluted Serum Buffer

Appendix Table 3 Linear fit data for the calibration curve in adiluted serum buffer

Adjusted R-squared	Slope	Y-intercept
0.9563	84.03 ± 10.29	-184.27 ± 27.98

Linear fits were generated with a weighted least squares method using the software OriginLab.

Appendix B Supporting Information for Chapter 4

Appendix B.1 Fitting of 204 nm UVRR Spectra for Protein Structure Determination

Spectral fitting of Mb at 204 nm is based off fitting by Cai et al.[138] and can be found in Appendix Figure 1. Bands at ~1252, ~1300, ~1330, and ~1387 cm^{-1} were assigned to the amide III_3 ($AmIII_3$), amide III_2 ($AmIII_2$), amide III_1 ($AmIII_1$), and $C_\alpha H$ stretching bands respectively.[138, 231] Previous work in the Asher group showed that there is a sinusoidal correlation between the $AmIII_3$ frequency and the peptide backbone Ramachandran ψ angle.[229-230, 256] Additionally, the presence or absence of the 1387 cm^{-1} $C_\alpha H$ bending band is a secondary indicator of the protein's structure. This vibration is coupled with the amide N-H bending vibration when the two groups are in physical proximity to one another. Therefore, in an α-helical conformation, such as that adopted by Mb, the band will be present.[229]

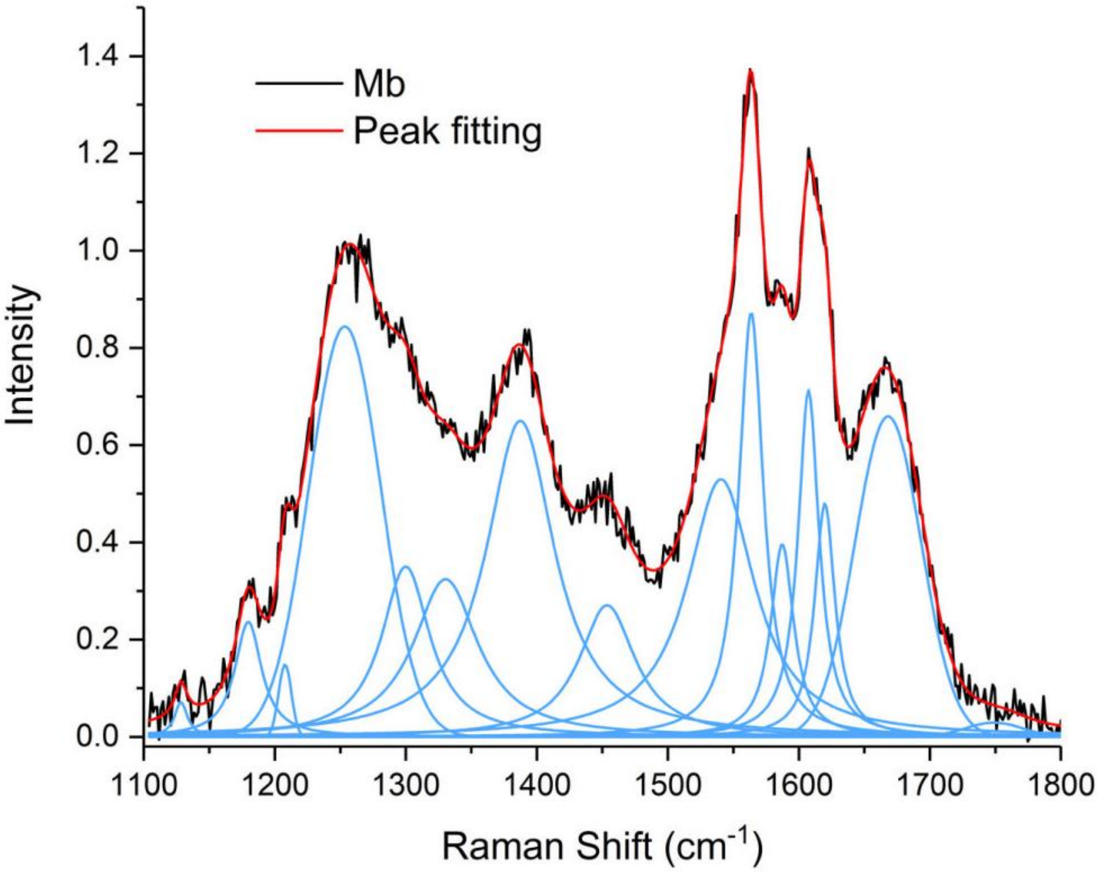

Appendix Figure 1 Resonance Raman spectrum of horse heart myoglobin at 204 nm excitation (black). Modeled bands are in blue and sum to the modeled peak fitting (red) which overlaps heavily with experimental data.

An AmIII$_3$ frequency of ~1260 cm^{-1} is indicative of an α-helical structure.[230] In our spectra, the AmIII$_3$ bands are downshifted slightly from this value to 1252 cm^{-1} as the bands in our data are broad, ~60 cm^{-1}. Therefore, these UVRR results generally agree with the crystal structure data and we concluded that Mb has a distribution of Ramachandran ψ angles that contain the α-helical geometry.

The 1 cm^{-1} between the AmIII$_3$ bands of the air atmosphere and xenon atmosphere Mb UVRR spectra is within the ~5 cm^{-1} precision of our spectrometer.[191] We concluded that there is no difference between the two bands and, therefore, little to no difference in the secondary structures of the Mb with and without Xe bound. This is confirmed by comparing the crystal structures of Mb with and without Xe bound (Appendix Figure 2). There is very little difference between the two aligned crystal structures, indicating that there is little to no change in the secondary structure of Mb upon Xe binding.

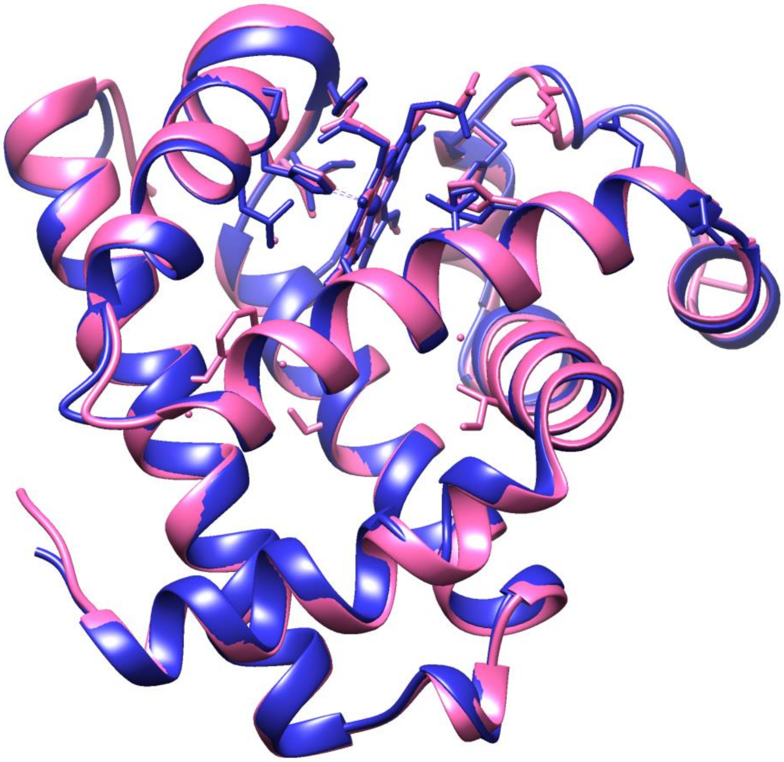

Appendix Figure 2 Crystal structures of myoglobbin with Xe bound (PDB 1J52-pink) and without Xe bound (PDB 1VXA- blue)

The sharp band at 1563 cm^{-1} was assigned to an O_2 stretching vibration.[231] This band overlaps with the amide II (AmII) band, which appears as a shoulder on the low wavenumber side of the O_2 stretching band.[138, 231] When the band is modeled as a linear sum of two Lorentzian bands, the AmII band can be resolved. We can then assign a band at 1537 cm^{-1} to the AmII band.

The band at 1668 cm^{-1} is assigned to the amide I (AmI) band.[231] This band predominantly involves C=O stretching of the amide carbonyl. It is sensitive to the hydrogen bonding and dielectric environment of these carbonyls.[257-260] An AmI band frequency of 1660 cm^{-1} is indicative of backbone-backbone hydrogen bonding, and an AmI band frequency of 1680 cm^{-1} is indicative of backbone-water hydrogen bonding. With an AmI band frequency of 1668 cm^{-1} and a broad linewidth, we can conclude that there is a distribution of hydrogen bonding environments within the Mb structure, but most of these environments are made up of backbone-backbone hydrogen bonds. This agrees with the overall α-helical structure of Mb. We assigned the 1451 cm^{-1} band to the Arg sidechain. It arises from an overtone of the Arg side chain guanidinium CN3 out-of-plane bending vibration.[138, 261]

Finally, the bands at 1178, 1205, 1587, 1605, and 1617 cm^{-1} are assigned to the Y9a/F9a, Y7a/F7a, F8b, Y8b/F8a, and Y8a vibrations, respectively.[138, 186, 262] These are aromatic amino acid vibrational bands, and they are sensitive to their local environment. Additionally, the Asher group showed that their Raman cross sections are correlated with changes to solvation.[187, 263] The signal-to-noise ratio (S/N) of these spectra does not allow us to assign any specific features when the difference between Mb with and without Xe is analyzed.

Appendix B.2 Resonance Raman Band Assignment for Myoglobin

Appendix Table 4 Summary of 204 nm excitation UVRR spectroscopic peaks monitored for myoglobin

Frequency (cm^{-1})	Peak Assignment	Reference
1178	Y9a/F9a	138, 186, 262
1205	Y7a/F7a	138, 186, 262
1252	$AmIII_3$	231
1300	$AmIII_2$	231
1332	$AmIII_1$	231
1387	$C_\alpha H$ Bend	138, 231
1451	Arg CN_3 Bend	138, 261
1537	AmII	231
1563	O_2 Stretch	231
1587	F8b	138, 186, 262
1605	Y8b/F8a	138, 186, 262
1617	Y8a	138, 186, 262
1668	AmI	231

Appendix Table 5 Summary of 229 nm excitation UVRR spectroscopic peaks monitored for myoglobin

Frequency (cm^{-1})	Peak Assignment	Reference
760	W18	187, 264
881	W17	264
935	ClO_4^-	
1014	W16	187, 264
1179	Y9a	187, 264
1238	W10	264
1360	W7	187, 264
1564	W3	187, 264
1625	Y8a	187, 264

Appendix Table 6 Summary of 405 nm excitation RR spectroscopic peaks monitored for myoglobin

Frequency (cm^{-1})	Peak Assignment	Reference
931	ν_{46}	233
1121	ν_5	233
1169	ν_{30}	233
1369	ν_4	233
1426	ν_{28}	233
1562	ν_2	233
1620	$\nu(C_a=C_b)$	233

Appendix B.1 ^{129}Xe NMR Chemical Shifts of Proteins

Appendix Table 7^{129}Xe chemical shift values for myoglobin in 80% H_2O/20% D_2O

Myoglobin Concentration (mM)	**Xe Pressure (psi)**	**Solution pH**	**^{129}Xe Chemical Shift (ppm)**
0.8	5	~7	-5194.6
	10	~7	-5194.1
	15	~7	-5194.5
	20	~7	-5194.2
	25	~7	-5194.1
	30	~7	-5193.8
	45	~7	-5193.6
	60	~7	-5193.5
	90	~7	-5193.3
	105	~7	-5193.2
	120	~7	-5193.1
	135	~7	-5193.0
	150	~7	-5192.9
1.2	15	~7	-5194.0
	30	~7	-5193.2
	60	~7	-5192.9
	150	~7	-5191.8

Appendix Table 8 ^{129}Xe chemical shift values for elastate in 80% H_2O/20% D_2O

Elastase Concentration (mM)	Xe Pressure (psi)	Solution pH	^{129}Xe Chemical Shift (ppm)
25	60	5.5	-5194.1
	90	5.5	-5194.0
	120	5.5	-5193.9
	150	5.5	-5193.8
72	15	11	-5194.5
	30	11	-5194.4
	45	11	-5194.3
	60	11	-5194.2

References

1.Cai, Z.; Smith, N. L.; Zhang, J.-T.; Asher, S. A., Two-Dimensional Photonic Crystal Chemical and Biomolecular Sensors. *Analytical Chemistry* **2015,** *87* (10), 5013-5025.

2.Dandan Men Dilong Liu Yue, L., Visualized optical sensors based on two/three-dimensional photonic crystals for biochemicals. *Science bulletin (Beijing)* **2016,** *61* (17), 1358-1371.

3.Haleem, A.; Javaid, M.; Singh, R. P.; Suman, R.; Rab, S., Biosensors applications in medical field: A brief review. *Sensors International* **2021,** *2*, 100100.

4.Purohit, B.; Vernekar, P. R.; Shetti, N. P.; Chandra, P., Biosensor nanoengineering: Design, operation, and implementation for biomolecular analysis. *Sensors International* **2020,** *1*, 100040.

5.Hirsch, I. B., Introduction: History of Glucose Monitoring. In *Role of Continuous Glucose Monitoring in Diabetes Treatment*, American Diabetes Association: Arlington, VA, 2018.

6.Tonyushkina, K.; Nichols, J. H., Glucose meters: a review of technical challenges to obtaining accurate results. *J Diabetes Sci Technol* **2009,** *3* (4), 971-80.

7.Oliver, N. S.; Toumazou, C.; Cass, A. E. G.; Johnston, D. G., Glucose sensors: a review of current and emerging technology. *Diabetic Medicine* **2009,** *26* (3), 197-210.

8.Rasmi, Y.; Li, X.; Khan, J.; Ozer, T.; Choi, J. R., Emerging point-of-care biosensors for rapid diagnosis of COVID-19: current progress, challenges, and future prospects. *Analytical and Bioanalytical Chemistry* **2021,** *413* (16), 4137-4159.

9.Chu, H.; Liu, C.; Liu, J.; Yang, J.; Li, Y.; Zhang, X., Recent advances and challenges of biosensing in point-of-care molecular diagnosis. *Sens Actuators B Chem* **2021,** *348*, 130708.

10.Rooney, K. D.; Schilling, U. M., Point-of-care testing in the overcrowded emergency department – can it make a difference? *Critical Care* **2014,** *18* (6), 692.

11.Heidt, B.; Siqueira, W. F.; Eersels, K.; Diliën, H.; van Grinsven, B.; Fujiwara, R. T.; Cleij, T. J., Point of care diagnostics in resource-limited settings: A review of the present and future of PoC in its most needed environment. *Biosensors* **2020,** *10* (10), 133.

12.Coombs, N. C.; Campbell, D. G.; Caringi, J., A qualitative study of rural healthcare providers' views of social, cultural, and programmatic barriers to healthcare access. *BMC Health Services Research* **2022,** *22* (1), 438.

13.Salmond, S.; Dorsen, C., Time to Reflect and Take Action on Health Disparities and Health Inequities. *Orthop Nurs* **2022,** *41* (2), 64-85.

14.Holtz, J. H.; Asher, S. A., Polymerized colloidal crystal hydrogel films as intelligent chemical sensing materials. *Nature* **1997,** *389* (6653), 829-832.

15.Holtz, J. H.; Holtz, J. S. W.; Munro, C. H.; Asher, S. A., Intelligent Polymerized Crystalline Colloidal Arrays: Novel Chemical Sensor Materials. *Analytical Chemistry* **1998,** *70* (4), 780-791.

16.Lee, K.; Asher, S. A., Photonic Crystal Chemical Sensors: pH and Ionic Strength. *Journal of the American Chemical Society* **2000,** *122* (39), 9534-9537.

17.Cai, S.; Suo, Z., Mechanics and chemical thermodynamics of phase transition in temperature-sensitive hydrogels. *Journal of the Mechanics and Physics of Solids* **2011,** *59* (11), 2259-2278.

18.Jiang, L.; Wen, L., 2 - Photonic sensitive switchable materials☆. In *Biophotonics for Medical Applications*, Meglinski, I., Ed. Woodhead Publishing: 2015; pp 25-51.

19.Xing, Y.; Zeng, B.; Yang, W., Light responsive hydrogels for controlled drug delivery. *Front Bioeng Biotechnol* **2022,** *10*, 1075670.

20.Roy, D.; Cambre, J. N.; Sumerlin, B. S., Future perspectives and recent advances in stimuli-responsive materials. *Progress in Polymer Science* **2010,** *35* (1), 278-301.

21.El-Husseiny, H. M.; Mady, E. A.; Hamabe, L.; Abugomaa, A.; Shimada, K.; Yoshida, T.; Tanaka, T.; Yokoi, A.; Elbadawy, M.; Tanaka, R., Smart/stimuli-responsive hydrogels: Cutting-edge platforms for tissue engineering and other biomedical applications. *Materials Today Bio* **2022,** *13*, 100186.

22.Heskins, M.; Guillet, J. E., Solution Properties of Poly(N-isopropylacrylamide). *Journal of Macromolecular Science: Part A - Chemistry* **1968,** *2* (8), 1441-1455.

23.Fujishige, S.; Kubota, K.; Ando, I., Phase transition of aqueous solutions of poly(N-isopropylacrylamide) and poly(N-isopropylmethacrylamide). *The Journal of Physical Chemistry* **1989,** *93* (8), 3311-3313.

24.Flory, P. J., *Principles of polymer chemistry*. Cornell University Press: Ithaca,, 1953; p 672 p.

25.Hirokawa, Y.; Tanaka, T., Volume phase transition in a nonionic gel. *The Journal of Chemical Physics* **1984,** *81* (12), 6379-6380.

26.Sheehan, C. J.; Bisio, A. L., Polymer/Solvent Interaction Parameters. *Rubber Chemistry and Technology* **1966,** *39* (1), 149-192.

27.Katsumoto, Y.; Tanaka, T.; Sato, H.; Ozaki, Y., Conformational Change of Poly(N-isopropylacrylamide) during the Coil−Globule Transition Investigated by Attenuated Total Reflection/Infrared Spectroscopy and Density Functional Theory Calculation. *The Journal of Physical Chemistry A* **2002,** *106* (14), 3429-3435.

28.Bischofberger, I.; Calzolari, D. C. E.; De Los Rios, P.; Jelezarov, I.; Trappe, V., Hydrophobic hydration of poly-N-isopropyl acrylamide: a matter of the mean energetic state of water. *Scientific reports* **2014,** *4*, 4377-4377.

29.Futscher, M. H.; Philipp, M.; Müller-Buschbaum, P.; Schulte, A., The Role of Backbone Hydration of Poly(N-isopropyl acrylamide) Across the Volume Phase Transition Compared to its Monomer. *Scientific Reports* **2017,** *7* (1), 17012.

30.Tanaka, T.; Fillmore, D.; Sun, S.-T.; Nishio, I.; Swislow, G.; Shah, A., Phase Transitions in Ionic Gels. *Physical Review Letters* **1980,** *45* (20), 1636-1639.

31.Reese, C. E.; Guerrero, C. D.; Weissman, J. M.; Lee, K.; Asher, S. A., Synthesis of Highly Charged, Monodisperse Polystyrene Colloidal Particles for the Fabrication of Photonic Crystals. *Journal of Colloid and Interface Science* **2000,** *232* (1), 76-80.

32.Hulst, H. C. v. d., *Light scattering by small particles*. Wiley: New York, 1957.

33.Joannopoulos, J. D., *Photonic crystals : molding the flow of light*. 2nd ed.; Princeton University Press: Princeton, 2008.

34.Vigneron, J. P.; Simonis, P., Natural photonic crystals. *Physica B: Condensed Matter* **2012,** *407* (20), 4032-4036.

35.Lin, S.-Y.; Chow, E.; Hietala, V.; Villeneuve, P. R.; Joannopoulos, J. D., Experimental Demonstration of Guiding and Bending of Electromagnetic Waves in a Photonic Crystal. *Science* **1998,** *282* (5387), 274-276.

36.Butt, M. A.; Khonina, S. N.; Kazanskiy, N. L., Recent advances in photonic crystal optical devices: A review. *Optics & Laser Technology* **2021,** *142*, 107265.

37.Hou, J.; Li, M.; Song, Y., Recent advances in colloidal photonic crystal sensors: Materials, structures and analysis methods. *Nano Today* **2018,** *22*, 132-144.

38.Lee, H. S.; Shim, T. S.; Hwang, H.; Yang, S.-M.; Kim, S.-H., Colloidal Photonic Crystals toward Structural Color Palettes for Security Materials. *Chemistry of Materials* **2013,** *25* (13), 2684-2690.

39.Li, Q.; Jonas, U.; Zhao, X. S.; Kappl, M., The forces at work in colloidal self-assembly: a review on fundamental interactions between colloidal particles. *Asia-Pacific Journal of Chemical Engineering* **2008,** *3* (3), 255-268.

40.Manoharan, V. N., Colloidal matter: Packing, geometry, and entropy. *Science* **2015,** *349* (6251), 1253751.

41.Hachisu, S.; Kobayashi, Y.; Kose, A., Phase separation in monodisperse latexes. *Journal of Colloid and Interface Science* **1973,** *42* (2), 342-348.

42.Monovoukas, Y.; Gast, A. P., The experimental phase diagram of charged colloidal suspensions. *Journal of Colloid and Interface Science* **1989,** *128* (2), 533-548.

43.Lubensky, T. C., Soft condensed matter physics. *Solid State Communications* **1997,** *102* (2), 187-197.

44.Smith, N. L.; Coukouma, A.; Dubnik, S.; Asher, S. A., Debye ring diffraction elucidation of 2D photonic crystal self-assembly and ordering at the air–water interface. *Physical Chemistry Chemical Physics* **2017,** *19* (47), 31813-31822.

45.Bragg, W. L., The diffraction of short electromagnetic Waves by a Crystal. *Scientia (Milano)* **1929,** *23* (45), 153.

46.Míguez, H.; López, C.; Meseguer, F.; Blanco, A.; Vázquez, L.; Mayoral, R.; Ocaña, M.; Fornés, V.; Mifsud, A., Photonic crystal properties of packed submicrometric SiO2 spheres. *Applied Physics Letters* **1997,** *71* (9), 1148-1150.

47.Kittel, C., *Introduction to solid state physics*. 8th ed. ed.; Wiley: Hoboken, NJ, 2005.

48.Tikhonov, A.; Kornienko, N.; Zhang, J.-T.; Wang, L.; Asher, S. A., Reflectivity enhanced two-dimensional dielectric particle array monolayer diffraction. *Journal of Nanophotonics* **2012,** *6* (1), 063509-063509.

49.Rundquist, P. A.; Photinos, P.; Jagannathan, S.; Asher, S. A., Dynamical Bragg diffraction from crystalline colloidal arrays. *The Journal of Chemical Physics* **1989,** *91* (8), 4932-4941.

50.Sinitskii, A. S.; Knot'ko, A. V.; Tretyakov, Y. D., Silica photonic crystals: synthesis and optical properties. *Solid State Ionics* **2004,** *172* (1), 477-479.

51.Ameen, S.; Caruso, G., *Lactic Acid in the Food Industry*. 1 ed.; Springer Cham: 2017.

52.Bellomo, R., Bench-to-bedside review: lactate and the kidney. *Crit Care* **2002,** *6* (4), 322-6.

53.Jeppesen, J. B.; Mortensen, C.; Bendtsen, F.; Møller, S., Lactate metabolism in chronic liver disease. *Scandinavian Journal of Clinical and Laboratory Investigation* **2013,** *73* (4), 293-299.

54.Balla, E.; Daniilidis, V.; Karlioti, G.; Kalamas, T.; Stefanidou, M.; Bikiaris, N. D.; Vlachopoulos, A.; Koumentakou, I.; Bikiaris, D. N., Poly(lactic Acid): A Versatile Biobased Polymer for the Future with Multifunctional Properties—From Monomer Synthesis, Polymerization Techniques and Molecular Weight Increase to PLA Applications. *Polymers* **2021,** *13* (11), 1822.

55.Taib, N.-A. A. B.; Rahman, M. R.; Huda, D.; Kuok, K. K.; Hamdan, S.; Bakri, M. K. B.; Julaihi, M. R. M. B.; Khan, A., A review on poly lactic acid (PLA) as a biodegradable polymer. *Polymer Bulletin* **2023,** *80* (2), 1179-1213.

56.Trzeciak, S.; Dellinger, R. P.; Chansky, M. E.; Arnold, R. C.; Schorr, C.; Milcarek, B.; Hollenberg, S. M.; Parrillo, J. E., Serum lactate as a predictor of mortality in patients with infection. *Intensive Care Medicine* **2007,** *33* (6), 970-977.

57.Iscra, F.; Gullo, A.; Biolo, G., Bench-to-bedside review: lactate and the lung. *Crit Care* **2002,** *6* (4), 327-9.

58.Bleiberg, B.; Steinberg, J. J.; Katz, S. D.; Wexler, J.; LeJemtel, T., Determination of plasma lactic acid concentration and specific activity using high-performance liquid chromatography. *J Chromatogr* **1991,** *568* (2), 301-8.

59.Zamanova, M. K.; Glotova, V. N.; Izhenbina, T. N.; Krutas, D. S.; Novikov, V. T., Simultaneous HPLC-UV Determination of Lactic Acid, Glycolic Acid, Glycolide, Lactide and Ethyl Acetate in Monomers for Producing Biodegradable Polymers. *Procedia Chemistry* **2014,** *10*, 244-251.

60.Brandt, R. B.; Siegel, S. A.; Waters, M. G.; Bloch, M. H., Spectrophotometric assay for d-(−)-lactate in plasma. *Anal Biochem* **1980,** *102* (1), 39-46.

61.McLellan, A. C.; Phillips, S. A.; Thornalley, P. J., Fluorimetric assay of d-lactate. *Anal Biochem* **1992,** *206* (1), 12-16.

62.Jones Owen, V. M.; Lechocki, S., A modified gas chromatographic method for lactate analysis. *Clinical Biochemistry* **1974,** *7* (1), 97-101.

63.Bonaventura, J. M.; Sharpe, K.; Knight, E.; Fuller, K. L.; Tanner, R. K.; Gore, C. J., Reliability and accuracy of six hand-held blood lactate analysers. *J Sports Sci Med* **2015,** *14* (1), 203-14.

64.Xu, L.; Zhou, Z.; Fan, M.; Fang, X., Advances in wearable flexible electrochemical sensors for sweat monitoring: A mini-review. *International Journal of Electrochemical Science* **2023,** *18* (1), 13-19.

65.Xue, Q.; Yeung, E. S., Indirect fluorescence determination of lactate and pyruvate in single erythrocytes by capillary electrophoresis. *J Chromatogr A* **1994,** *661* (1-2), 287-95.

66.Pundir, C. S.; Narwal, V.; Batra, B., Determination of lactic acid with special emphasis on biosensing methods: A review. *Biosensors and Bioelectronics* **2016,** *86*, 777-790.

67.Rattu, G.; Khansili, N.; Maurya, V. K.; Krishna, P. M., Lactate detection sensors for food, clinical and biological applications: a review. *Environmental Chemistry Letters* **2021,** *19* (2), 1135-1152.

68.Shen, Y.; Liu, C.; He, H.; Zhang, M.; Wang, H.; Ji, K.; Wei, L.; Mao, X.; Sun, R.; Zhou, F., Recent Advances in Wearable Biosensors for Non-Invasive Detection of Human Lactate. *Biosensors* **2022,** *12* (12), 1164.

69.Karpova, E. V.; Laptev, A. I.; Andreev, E. A.; Karyakina, E. E.; Karyakin, A. A., Relationship Between Sweat and Blood Lactate Levels During Exhaustive Physical Exercise. *ChemElectroChem* **2020,** *7* (1), 191-194.

70.Okawara, H.; Sawada, T.; Nakashima, D.; Maeda, Y.; Minoji, S.; Morisue, T.; Katsumata, Y.; Matsumoto, M.; Nakamura, M.; Nagura, T., Realtime Monitoring of Local Sweat Rate Kinetics during Constant-Load Exercise Using Perspiration-Meter with Airflow Compensation System. *Sensors (Basel)* **2022,** *22* (15).

71.Rabost-Garcia, G.; Colmena, V.; Aguilar-Torán, J.; Vieyra Galí, J.; Punter-Villagrasa, J.; Casals-Terré, J.; Miribel-Catala, P.; Muñoz, X.; Cadefau, J.; Padullés, J.; Brotons Cuixart, D., Non-Invasive Multiparametric Approach To Determine Sweat-Blood Lactate Bioequivalence. *ACS Sens* **2023,** *8* (4), 1536-1541.

72.Maeda, Y.; Okawara, H.; Sawada, T.; Nakashima, D.; Nagahara, J.; Fujitsuka, H.; Ikeda, K.; Hoshino, S.; Kobari, Y.; Katsumata, Y.; Nakamura, M.; Nagura, T., Implications of the Onset of Sweating on the Sweat Lactate Threshold. *Sensors (Basel)* **2023,** *23* (7).

73.Martin, G. S.; Mannino, D. M.; Eaton, S.; Moss, M., The epidemiology of sepsis in the United States from 1979 through 2000. *N Engl J Med* **2003,** *348* (16), 1546-54.

74.Dombrovskiy, V. Y.; Martin, A. A.; Sunderram, J.; Paz, H. L., Rapid increase in hospitalization and mortality rates for severe sepsis in the United States: a trend analysis from 1993 to 2003. *Crit Care Med* **2007,** *35* (5), 1244-50.

75.Dellinger, R. P.; Levy, M. M.; Rhodes, A.; Annane, D.; Gerlach, H.; Opal, S. M.; Sevransky, J. E.; Sprung, C. L.; Douglas, I. S.; Jaeschke, R.; Osborn, T. M.; Nunnally, M. E.; Townsend, S. R.; Reinhart, K.; Kleinpell, R. M.; Angus, D. C.; Deutschman, C. S.; Machado, F. R.; Rubenfeld, G. D.; Webb, S. A.; Beale, R. J.; Vincent, J. L.; Moreno, R., Surviving sepsis campaign: international guidelines for management of severe sepsis and septic shock: 2012. *Crit Care Med* **2013,** *41* (2), 580-637.

76.Chen, H.; Zhao, C.; Wei, Y.; Jin, J., Early lactate measurement is associated with better outcomes in septic patients with an elevated serum lactate level. *Critical Care* **2019,** *23* (1), 351.

77.Liu, V.; Morehouse, J. W.; Soule, J.; Whippy, A.; Escobar, G. J., Fluid volume, lactate values, and mortality in sepsis patients with intermediate lactate values. *Ann Am Thorac Soc* **2013,** *10* (5), 466-73.

78.Lee, S. M.; An, W. S., New clinical criteria for septic shock: serum lactate level as new emerging vital sign. *Journal of Thoracic Disease* **2016,** *8* (7), 1388-1390.

79.Vincent, J.-L.; Quintairos e Silva, A.; Couto, L.; Taccone, F. S., The value of blood lactate kinetics in critically ill patients: a systematic review. *Critical Care* **2016,** *20* (1), 257.

80.Han, X.; Edelson, D. P.; Snyder, A.; Pettit, N.; Sokol, S.; Barc, C.; Howell, M. D.; Churpek, M. M., Implications of Centers for Medicare & Medicaid Services Severe Sepsis and Septic Shock

Early Management Bundle and Initial Lactate Measurement on the Management of Sepsis. *Chest* **2018,** *154* (2), 302-308.

81.Cai, Z.; Kwak, D. H.; Punihaole, D.; Hong, Z.; Velankar, S. S.; Liu, X.; Asher, S. A., A photonic crystal protein hydrogel sensor for Candida albicans. *Angewandte Chemie International Edition* **2015,** *54* (44), 13036-13040.

82.Smith, N. L.; Coukouma, A. E.; Wilson, D. C.; Ho, B.; Gray, V.; Asher, S. A., Stimuli-Responsive Pure Protein Organogel Sensors and Biocatalytic Materials. *ACS Applied Materials & Interfaces* **2020,** *12* (1), 238-249.

83.Jang, K.; Westbay, J. H.; Asher, S. A., DNA-Crosslinked 2D Photonic Crystal Hydrogels for Detection of Adenosine Actuated by an Adenosine-Binding Aptamer. *ACS Sensors* **2022,** *7* (6), 1648-1656.

84.Jang, K.; Horne, W. S.; Asher, S. A., Human Serum Phenylpyruvate Quantification Using Responsive 2D Photonic Crystal Hydrogels via Chemoselective Oxime Ligation: Progress toward Developing Phenylalanine-Sensing Elements. *ACS Applied Materials & Interfaces* **2020,** *12* (35), 39612-39619.

85.Gray, L. R.; Tompkins, S. C.; Taylor, E. B., Regulation of pyruvate metabolism and human disease. *Cell Mol Life Sci* **2014,** *71* (14), 2577-604.

86.Zhang, F.; Cao, L.; Yang, W., Preparation of Monodisperse and Anion-Charged Polystyrene Microspheres Stabilized with Polymerizable Sodium Styrene Sulfonate by Dispersion Polymerization. *Macromolecular Chemistry and Physics* **2010,** *211* (7), 744-751.

87.Zhang, J. T.; Wang, L.; Lamont, D. N.; Velankar, S. S.; Asher, S. A., Fabrication of large-area two-dimensional colloidal crystals. *Angew Chem Int Ed Engl* **2012,** *51* (25), 6117-20.

88.Javed, M. H.; Azimuddin, S. M. I.; Hussain, A. N.; Ahmed, A.; Ishaq, M., Purification and characterization of lactate dehydrogenase from Varanus liver. *Experimental & Molecular Medicine* **1997,** *29* (1), 25-30.

89.Wendeler, M.; Grinberg, L.; Wang, X.; Dawson, P. E.; Baca, M., Enhanced Catalysis of Oxime-Based Bioconjugations by Substituted Anilines. *Bioconjug Chem* **2014,** *25* (1), 93-101.

90.Foucher, C. D.; Tubben, R. E., Lactic Acidosis. In *StatPearls*, StatPearls Publishing
Copyright © 2023, StatPearls Publishing LLC.: Treasure Island (FL) ineligible companies. Disclosure: Robert Tubben declares no relevant financial relationships with ineligible companies., 2023.

91.Belenky, P.; Bogan, K. L.; Brenner, C., NAD+ metabolism in health and disease. *Trends in Biochemical Sciences* **2007,** *32* (1), 12-19.

92.Osterman, A., Biogenesis and Homeostasis of Nicotinamide Adenine Dinucleotide Cofactor. *EcoSal Plus* **2009,** *3* (2).

93.Sorci, L.; Kurnasov, O.; Rodionov, D. A.; Osterman, A. L., 7.08 - Genomics and Enzymology of NAD Biosynthesis. In *Comprehensive Natural Products II*, Liu, H.-W.; Mander, L., Eds. Elsevier: Oxford, 2010; pp 213-257.

94.Ulrich, S.; Boturyn, D.; Marra, A.; Renaudet, O.; Dumy, P., Oxime Ligation: A Chemoselective Click-Type Reaction for Accessing Multifunctional Biomolecular Constructs. *Chemistry – A European Journal* **2014,** *20* (1), 34-41.

95.Moyle, P. M.; Muir, T. W., Method for the Synthesis of Mono-ADP-ribose Conjugated Peptides. *Journal of the American Chemical Society* **2010,** *132* (45), 15878-15880.

96.Liu, C.; Yu, X., ADP-ribosyltransferases and poly ADP-ribosylation. *Curr Protein Pept Sci* **2015,** *16* (6), 491-501.

97.Morgan, R. K.; Cohen, M. S., Detecting Protein ADP-Ribosylation Using a Clickable Aminooxy Probe. *Methods Mol Biol* **2017,** *1608*, 71-77.

98.Lowry, O. H.; Passonneau, J. V.; Rock, M. K., The Stability of Pyridine Nucleotides. *Journal of Biological Chemistry* **1961,** *236* (10), 2756-2759.

99.Oppenheimer, N. J.; Kaplan, N. O., Structure of the primary acid rearrangement product of reduced nicotinamide adenine dinucleotide (NADH). *Biochemistry* **1974,** *13* (23), 4675-4685.

100.Metzler, D. E., Vitamins and Coenzymes. In *Encyclopedia of Physical Science and Technology (Third Edition)*, Meyers, R. A., Ed. Academic Press: New York, 2003; pp 509-528.

101.Braidy, N.; Villalva, M. D.; Grant, R., NADomics: Measuring NAD+ and Related Metabolites Using Liquid Chromatography Mass Spectrometry. *Life* **2021,** *11* (6), 512.

102.Aizawa, M.; Coughlin, R. W.; Charles, M., Electrochemical characterization of immobilized NAD+. *Biochimica et Biophysica Acta (BBA) - Bioenergetics* **1976,** *440* (1), 233-240.

103.Coughlin, R. W.; Aizawa, M.; Charles, M., Preparation and properties of soluble–insoluble nicotinamide coenzymes. *Biotechnology and Bioengineering* **1976,** *18* (2), 199-208.

104.Wang, Y.; Li, C.; Pielak, G. J., Effects of Proteins on Protein Diffusion. *Journal of the American Chemical Society* **2010,** *132* (27), 9392-9397.

105.Abriata, L. A.; Spiga, E.; Peraro, M. D., Molecular Effects of Concentrated Solutes on Protein Hydration, Dynamics, and Electrostatics. *Biophys J* **2016,** *111* (4), 743-755.

106.Goodwin, M. L.; Harris, J. E.; Hernández, A.; Gladden, L. B., Blood lactate measurements and analysis during exercise: a guide for clinicians. *J Diabetes Sci Technol* **2007,** *1* (4), 558-69.

107.Li, Q.; Liu, S.; Mbola, N. M.; Shea, K. J.; Meng, Z.; Dong, X.; Xue, M., Responsive hydrogel-based three-dimensional photonic crystal sensor for lactic acid detection. *Analytical and Bioanalytical Chemistry* **2022,** *414* (26), 7695-7704.

108.Mabey, D.; Peeling, R. W.; Ustianowski, A.; Perkins, M. D., Diagnostics for the developing world. *Nature Reviews Microbiology* **2004,** *2* (3), 231-240.

109.Organization, W. H., *Global status report on noncommunicable diseases 2014*. World Health Organization: 2014.

110.Gowri, A.; Kumar, N. A.; Anand, B. S., Recent advances in nanomaterials based biosensors for point of care (PoC) diagnosis of COVID-19–a minireview. *TrAC Trends in Analytical Chemistry* **2021,** *137*, 116205.

111.Altug, H.; Oh, S.-H.; Maier, S. A.; Homola, J., Advances and applications of nanophotonic biosensors. *Nature nanotechnology* **2022,** *17* (1), 5-16.

112.Chadha, U.; Bhardwaj, P.; Agarwal, R.; Rawat, P.; Agarwal, R.; Gupta, I.; Panjwani, M.; Singh, S.; Ahuja, C.; Selvaraj, S. K., Recent progress and growth in biosensors technology: A critical review. *Journal of Industrial and Engineering Chemistry* **2022**.

113.Peeling, R. W.; Heymann, D. L.; Teo, Y.-Y.; Garcia, P. J., Diagnostics for COVID-19: moving from pandemic response to control. *The Lancet* **2022,** *399* (10326), 757-768.

114.Akgönüllü, S.; Kılıç, S.; Esen, C.; Denizli, A., Molecularly Imprinted Polymer-Based Sensors for Protein Detection. *Polymers* **2023,** *15* (3), 629.

115.Kang, Y.; Aye, L.; Ngo, T. D.; Zhou, J., Performance evaluation of low-cost air quality sensors: A review. *Science of The Total Environment* **2022,** *818*, 151769.

116.Kimble, K. W.; Walker, J. P.; Finegold, D. N.; Asher, S. A., Progress toward the development of a point-of-care photonic crystal ammonia sensor. *Analytical and bioanalytical chemistry* **2006,** *385*, 678-685.

117.Dincer, C.; Bruch, R.; Costa-Rama, E.; Fernández-Abedul, M. T.; Merkoçi, A.; Manz, A.; Urban, G. A.; Güder, F., Disposable sensors in diagnostics, food, and environmental monitoring. *Advanced Materials* **2019,** *31* (30), 1806739.

118.Das, A. J.; Wahi, A.; Kothari, I.; Raskar, R., Ultra-portable, wireless smartphone spectrometer for rapid, non-destructive testing of fruit ripeness. *Scientific reports* **2016,** *6* (1), 1-8.

119.Kalimuthu, K.; Arivalagan, J.; Mohan, M.; Christyraj, J. R. S. S.; Arockiaraj, J.; Muthusamy, R.; Ju, H.-J., Point of care diagnosis of plant virus: Current trends and prospects. *Molecular and Cellular Probes* **2022,** *61*, 101779.

120.Baldi, P.; La Porta, N., Molecular approaches for low-cost point-of-care pathogen detection in agriculture and forestry. *Frontiers in Plant Science* **2020,** *11*, 570862.

121.Frickmann, H.; Podbielski, A.; Kreikemeyer, B., Resistant gram-negative bacteria and diagnostic point-of-care options for the field setting during military operations. *BioMed Research International* **2018,** *2018*.

122.Walker, J. P.; Asher, S. A., Acetylcholinesterase-based organophosphate nerve agent sensing photonic crystal. *Analytical chemistry* **2005,** *77* (6), 1596-1600.

123.Sharma, A.; Tok, A. I. Y.; Alagappan, P.; Liedberg, B., Point of care testing of sports biomarkers: Potential applications, recent advances and future outlook. *TrAC Trends in Analytical Chemistry* **2021,** *142*, 116327.

124.Castelli, F. A.; Rosati, G.; Moguet, C.; Fuentes, C.; Marrugo-Ramírez, J.; Lefebvre, T.; Volland, H.; Merkoçi, A.; Simon, S.; Fenaille, F., Metabolomics for personalized medicine: the input of analytical chemistry from biomarker discovery to point-of-care tests. *Analytical and Bioanalytical Chemistry* **2022,** *414* (2), 759-789.

125.Ellington, A. D.; Szostak, J. W., In vitro selection of RNA molecules that bind specific ligands. *Nature* **1990,** *346* (6287), 818-822.

126.Tuerk, C.; Gold, L., Systematic evolution of ligands by exponential enrichment: RNA ligands to bacteriophage T4 DNA polymerase. *Science* **1990,** *249* (4968), 505-510.

127.Li, J.; Mo, L.; Lu, C.-H.; Fu, T.; Yang, H.-H.; Tan, W., Functional nucleic acid-based hydrogels for bioanalytical and biomedical applications. *Chemical Society Reviews* **2016,** *45* (5), 1410-1431.

128.Ye, B.-F.; Zhao, Y.-J.; Cheng, Y.; Li, T.-T.; Xie, Z.-Y.; Zhao, X.-W.; Gu, Z.-Z., Colorimetric photonic hydrogel aptasensor for the screening of heavy metal ions. *Nanoscale* **2012,** *4* (19), 5998-6003.

129.Yin, B.-C.; Ye, B.-C.; Wang, H.; Zhu, Z.; Tan, W., Colorimetric logic gates based on aptamer-crosslinked hydrogels. *Chemical Communications* **2012,** *48* (9), 1248-1250.

130.Shen, P.; Jang, K.; Cai, Z.; Zhang, Y.; Asher, S. A., Aptamer-functionalized 2D photonic crystal hydrogels for detection of adenosine. *Microchimica Acta* **2022,** *189* (11), 1-10.

131.Nutiu, R.; Li, Y., Structure-Switching Signaling Aptamers. *Journal of the American Chemical Society* **2003,** *125* (16), 4771-4778.

132.Kong, L.; Xu, J.; Xu, Y.; Xiang, Y.; Yuan, R.; Chai, Y., A universal and label-free aptasensor for fluorescent detection of ATP and thrombin based on SYBR Green Idye. *Biosensors and Bioelectronics* **2013,** *42*, 193-197.

133.Lv, Z.; Liu, J.; Zhou, Y.; Guan, Z.; Yang, S.; Li, C.; Chen, A., Highly sensitive fluorescent detection of small molecules, ions, and proteins using a universal label-free aptasensor. *Chemical Communications* **2013,** *49* (48), 5465-5467.

134.Liu, Z.; Yuan, R.; Chai, Y.; Zhuo, Y.; Hong, C.; Yang, X.; Su, H.; Qian, X., Highly sensitive, reusable electrochemical aptasensor for adenosine. *Electrochimica Acta* **2009,** *54* (26), 6207-6211.

135.Zhang, K.; Zhu, X.; Wang, J.; Xu, L.; Li, G., Strategy to Fabricate an Electrochemical Aptasensor: Application to the Assay of Adenosine Deaminase Activity. *Analytical Chemistry* **2010,** *82* (8), 3207-3211.

136.Xu, X.; Goponenko, A. V.; Asher, S. A., Polymerized polyHEMA photonic crystals: pH and ethanol sensor materials. *Journal of the American Chemical Society* **2008,** *130* (10), 3113-3119.

137.Lee, K.; Asher, S. A., Photonic crystal chemical sensors: pH and ionic strength. *Journal of the American Chemical Society* **2000,** *122* (39), 9534-9537.

138.Cai, Z.; Zhang, J.-T.; Xue, F.; Hong, Z.; Punihaole, D.; Asher, S. A., 2D Photonic Crystal Protein Hydrogel Coulometer for Sensing Serum Albumin Ligand Binding. *Analytical Chemistry* **2014,** *86* (10), 4840-4847.

139.Jang, K.; Westbay, J. H.; Asher, S. A., DNA-Crosslinked 2D Photonic Crystal Hydrogels for Detection of Adenosine Actuated by an Adenosine-Binding Aptamer. *ACS sensors* **2022**.

140.Shen, P.; Li, M.; Li, R.; Han, B.; Ma, H.; Hou, X.; Zhang, Y.; Wang, J.-J., Aptamer-functionalized smart photonic hydrogels: application for the detection of thrombin in human serum. *NPG Asia Materials* **2022,** *14* (1), 1-12.

141.Di Cera, E., Thrombin. *Molecular aspects of medicine* **2008,** *29* (4), 203-254.

142.Bock, L. C.; Griffin, L. C.; Latham, J. A.; Vermaas, E. H.; Toole, J. J., Selection of single-stranded DNA molecules that bind and inhibit human thrombin. *Nature* **1992,** *355* (6360), 564-566.

143.Zhang, F.; Cao, L.; Yang, W., Preparation of Monodisperse and Anion-Charged Polystyrene Microspheres Stabilized with Polymerizable Sodium Styrene Sulfonate by Dispersion Polymerization. *Macromolecular Chemistry and Physics* **2010,** *211* (7), 744-751.

144.Zhang, J. T.; Wang, L.; Lamont, D. N.; Velankar, S. S.; Asher, S. A., Fabrication of large-area two-dimensional colloidal crystals. *Angewandte Chemie* **2012,** *124* (25), 6221-6224.

145.Zhang, J.-T.; Chao, X.; Liu, X.; Asher, S. A., Two-dimensional array Debye ring diffraction protein recognition sensing. *Chemical Communications* **2013,** *49* (56), 6337-6339.

146.Rehman, F. N.; Audeh, M.; Abrams, E. S.; Hammond, P. W.; Kenney, M.; Boles, T. C., Immobilization of acrylamide-modified oligonucleotides by co-polymerization. *Nucleic Acids Res* **1999,** *27* (2), 649-655.

147.Flory, P., *Principles of Polymer Chemistry*. Ithaca, NY, 1953.

148.García, P. S.; Ciavatta, V. T.; Fidler, J. A.; Woodbury, A.; Levy, J. H.; Tyor, W. R., Concentration-dependent dual role of thrombin in protection of cultured rat cortical neurons. *Neurochemical research* **2015,** *40*, 2220-2229.

149.Owczarzy, R.; You, Y.; Moreira, B. G.; Manthey, J. A.; Huang, L.; Behlke, M. A.; Walder, J. A., Effects of sodium ions on DNA duplex oligomers: improved predictions of melting temperatures. *Biochemistry* **2004,** *43* (12), 3537-3554.

150.Owczarzy, R.; Moreira, B. G.; You, Y.; Behlke, M. A.; Walder, J. A., Predicting stability of DNA duplexes in solutions containing magnesium and monovalent cations. *Biochemistry* **2008,** *47* (19), 5336-5353.

151.Yang, H.; Liu, H.; Kang, H.; Tan, W., Engineering target-responsive hydrogels based on aptamer− target interactions. *Journal of the American Chemical Society* **2008,** *130* (20), 6320-6321.

152.Wang, X.; Wang, X., Aptamer-functionalized hydrogel diffraction gratings for the human thrombin detection. *Chemical Communications* **2013,** *49* (53), 5957-5959.

153.Cho, E. J.; Lee, J.-W.; Ellington, A. D., Applications of Aptamers as Sensors. *Annual Review of Analytical Chemistry* **2009,** *2* (1), 241-264.

154.Nagatoishi, S.; Isono, N.; Tsumoto, K.; Sugimoto, N., Loop residues of thrombin-binding DNA aptamer impact G-quadruplex stability and thrombin binding. *Biochimie* **2011,** *93* (8), 1231-1238.

155.Longsworth, L. G., Temperature Dependence of Diffusion in Aqueous Solutions. *The Journal of Physical Chemistry* **1954,** *58* (9), 770-773.

156.Edidin, M.; Petit, V. A., The effect of temperature on the lateral diffusion of plasma membrane proteins. *Ciba Found Symp* **1977,** (52), 155-74.

157.Nawrocki, G.; Wang, P. H.; Yu, I.; Sugita, Y.; Feig, M., Slow-Down in Diffusion in Crowded Protein Solutions Correlates with Transient Cluster Formation. *J Phys Chem B* **2017,** *121* (49), 11072-11084.

158.In *Clinical Methods: The History, Physical, and Laboratory Examinations*, Walker, H. K.; Hall, W. D.; Hurst, J. W., Eds. Butterworths
Copyright © 1990, Butterworth Publishers, a division of Reed Publishing.: Boston, 1990.

159.Chi, Z.; Chen, X. G.; Holtz, J. S. W.; Asher, S. A., UV Resonance Raman-Selective Amide Vibrational Enhancement: Quantitative Methodology for Determining Protein Secondary Structure. *Biochemistry* **1998,** *37* (9), 2854-2864.

160.Xu, X.; Goponenko, A. V.; Asher, S. A., Polymerized PolyHEMA Photonic Crystals: pH and Ethanol Sensor Materials. *Journal of the American Chemical Society* **2008,** *130* (10), 3113-3119.

161.Weissman, J. M.; Sunkara, H. B.; Tse, A. S.; Asher, S. A., Thermally Switchable Periodicities and Diffraction from Mesoscopically Ordered Materials. *Science* **1996,** *274* (5289), 959-60.

162.Alexeev, V. L.; Sharma, A. C.; Goponenko, A. V.; Das, S.; Lednev, I. K.; Wilcox, C. S.; Finegold, D. N.; Asher, S. A., High Ionic Strength Glucose-Sensing Photonic Crystal. *Analytical Chemistry* **2003,** *75* (10), 2316-2323.

163.Goponenko, A. V.; Asher, S. A., Modeling of Stimulated Hydrogel Volume Changes in Photonic Crystal Pb2+ Sensing Materials. *Journal of the American Chemical Society* **2005,** *127* (30), 10753-10759.

164.Sharma, A. C.; Jana, T.; Kesavamoorthy, R.; Shi, L.; Virji, M. A.; Finegold, D. N.; Asher, S. A., A General Photonic Crystal Sensing Motif: Creatinine in Bodily Fluids. *Journal of the American Chemical Society* **2004,** *126* (9), 2971-2977.

165.Cao, M.; Wang, Y.; Hu, X.; Gong, H.; Li, R.; Cox, H.; Zhang, J.; Waigh, T. A.; Xu, H.; Lu, J. R., Reversible Thermoresponsive Peptide–PNIPAM Hydrogels for Controlled Drug Delivery. *Biomacromolecules* **2019,** *20* (9), 3601-3610.

166.Xu, X.; Liu, Y.; Fu, W.; Yao, M.; Ding, Z.; Xuan, J.; Li, D.; Wang, S.; Xia, Y.; Cao, M., Poly(N-isopropylacrylamide)-Based Thermoresponsive Composite Hydrogels for Biomedical Applications. *Polymers* **2020,** *12* (3), 580.

167.Rana, M. M.; De la Hoz Siegler, H., Tuning the Properties of PNIPAm-Based Hydrogel Scaffolds for Cartilage Tissue Engineering. *Polymers* **2021,** *13* (18), 3154.

168.Lanzalaco, S.; Armelin, E., Poly(N-isopropylacrylamide) and Copolymers: A Review on Recent Progresses in Biomedical Applications. *Gels* **2017,** *3* (4).

169.Yamauchi, H.; Maeda, Y., LCST and UCST Behavior of Poly(N-isopropylacrylamide) in DMSO/Water Mixed Solvents Studied by IR and Micro-Raman Spectroscopy. *The Journal of Physical Chemistry B* **2007,** *111* (45), 12964-12968.

170.Sun, B.; Lin, Y.; Wu, P.; Siesler, H. W., A FTIR and 2D-IR Spectroscopic Study on the Microdynamics Phase Separation Mechanism of the Poly(N-isopropylacrylamide) Aqueous Solution. *Macromolecules* **2008,** *41* (4), 1512-1520.

171.Burba, C. M.; Carter, S. M.; Meyer, K. J.; Rice, C. V., Salt Effects on Poly(N-isopropylacrylamide) Phase Transition Thermodynamics from NMR Spectroscopy. *The Journal of Physical Chemistry B* **2008,** *112* (34), 10399-10404.

172.Islam, M. R.; Ahiabu, A.; Li, X.; Serpe, M. J., Poly (N-isopropylacrylamide) Microgel-Based Optical Devices for Sensing and Biosensing. *Sensors* **2014,** *14* (5), 8984-8995.

173.Choe, A.; Yeom, J.; Shanker, R.; Kim, M. P.; Kang, S.; Ko, H., Stretchable and wearable colorimetric patches based on thermoresponsive plasmonic microgels embedded in a hydrogel film. *NPG Asia Materials* **2018,** *10* (9), 912-922.

174.Atwood, D. A., *Radionuclides in the Environment*. John Wiley & Sons, Incorporated: New York, 2010.

175.Wotawa, G.; Becker, A.; Kalinowski, M.; Saey, P.; Tuma, M.; Zähringer, M., Computation and Analysis of the Global Distribution of the Radioxenon Isotope 133Xe based on Emissions from Nuclear Power Plants and Radioisotope Production Facilities and its Relevance for the Verification of the Nuclear-Test-Ban Treaty. *Pure and Applied Geophysics* **2010,** *167* (4), 541-557.

176.Kalinowski, M. B.; Axelsson, A.; Bean, M.; Blanchard, X.; Bowyer, T. W.; Brachet, G.; Hebel, S.; McIntyre, J. I.; Peters, J.; Pistner, C.; Raith, M.; Ringbom, A.; Saey, P. R. J.; Schlosser, C.; Stocki, T. J.; Taffary, T.; Kurt Ungar, R., Discrimination of Nuclear Explosions against Civilian Sources Based on Atmospheric Xenon Isotopic Activity Ratios. *Pure and applied geophysics* **2010,** *167* (4), 517-539.

177.Achim, P.; Generoso, S.; Morin, M.; Gross, P.; Le Petit, G.; Moulin, C., Characterization of Xe-133 global atmospheric background: Implications for the International Monitoring System of the Comprehensive Nuclear-Test-Ban Treaty. *Journal of Geophysical Research: Atmospheres* **2016,** *121* (9), 4951-4966.

178.Schiltz, M.; Fourme, R.; Broutin, I.; Prangé, T., The catalytic site of serine proteinases as a specific binding cavity for xenon. *Structure* **1995,** *3* (3), 309-316.

179.Dickinson, R.; Peterson, B. K.; Banks, P.; Simillis, C.; Martin, J. C.; Valenzuela, C. A.; Maze, M.; Franks, N. P., Competitive inhibition at the glycine site of the N-methyl-D-aspartate receptor by the anesthetics xenon and isoflurane: evidence from molecular modeling and electrophysiology. *Anesthesiology* **2007,** *107* (5), 756-67.

180.David, H. N.; Haelewyn, B.; Risso, J.-J.; Colloc'h, N.; Abraini, J. H., Xenon is an Inhibitor of Tissue-Plasminogen Activator: Adverse and Beneficial Effects in a Rat Model of Thromboembolic Stroke. *Journal of Cerebral Blood Flow & Metabolism* **2010,** *30* (4), 718-728.

181.Sauguet, L.; Fourati, Z.; Prangé, T.; Delarue, M.; Colloc'h, N., Structural Basis for Xenon Inhibition in a Cationic Pentameric Ligand-Gated Ion Channel. *PLoS One* **2016,** *11* (2), e0149795.

182.Tilton, R. F.; Kuntz, I. D.; Petsko, G. A., Cavities in proteins: structure of a metmyoglobin xenon complex solved to 1.9 .ANG. *Biochemistry* **1984,** *23* (13), 2849-2857.

183.Tilton, R. F.; Singh, U. C.; Kuntz, I. D.; Kollman, P. A., Protein-ligand dynamics: A 96 picosecond simulation of a myoglobin-xenon complex. *Journal of Molecular Biology* **1988,** *199* (1), 195-211.

184.Locci, E.; Dehouck, Y.; Casu, M.; Saba, G.; Lai, A.; Luhmer, M.; Reisse, J.; Bartik, K., Probing Proteins in Solution by 129Xe NMR Spectroscopy. *Journal of Magnetic Resonance* **2001,** *150* (2), 167-174.

185.Rubin, S. M.; Lee, S.-Y.; Ruiz, E. J.; Pines, A.; Wemmer, D. E., Detection and Characterization of Xenon-binding Sites in Proteins by 129Xe NMR Spectroscopy. *Journal of Molecular Biology* **2002,** *322* (2), 425-440.

186.Asher, S. A.; Ludwig, M.; Johnson, C. R., UV Resonance Raman excitation profiles of the aromatic amino acids. *Journal of the American Chemical Society* **1986,** *108* (12), 3186-3197.

187.Chi, Z.; Asher, S. A., UV Raman Determination of the Environment and Solvent Exposure of Tyr and Trp Residues. *The Journal of Physical Chemistry B* **1998,** *102* (47), 9595-9602.

188.Spence, M. M.; Rubin, S. M.; Dimitrov, I. E.; Ruiz, E. J.; Wemmer, D. E.; Pines, A.; Yao, S. Q.; Tian, F.; Schultz, P. G., Functionalized xenon as a biosensor. *Proceedings of the National Academy of Sciences* **2001,** *98* (19), 10654.

189.Hufziger, K. T.; Bykov, S. V.; Asher, S. A., Raman Hyperspectral Imaging Spectrometer Utilizing Crystalline Colloidal Array Photonic Crystal Diffraction. *Applied Spectroscopy* **2014,** *68* (11), 1219-1223.

190.Hufziger, K. T.; Bykov, S. V.; Asher, S. A., Ultraviolet Raman Wide-Field Hyperspectral Imaging Spectrometer for Standoff Trace Explosive Detection. *Applied Spectroscopy* **2017,** *71* (2), 173-185.

191.Bykov, S. L., Igor; Ianoul, Anatoli; Mikhonin, Aleksandr; Munro, Calum; Asher, Sanford A. , Steady-State and Transient Ultraviolet Resonance Raman Spectrometer for the 193–270 nm Spectral Region. *Applied Spectroscopy* **2005,** *59* (12), 1541-1552.

192.Harris, R. K.; Becker, E. D.; Cabral de Menezes, S. M.; Goodfellow, R.; Granger, P., NMR nomenclature. Nuclear spin properties and conventions for chemical shifts(IUPAC Recommendations 2001). *Pure and Applied Chemistry* **2001,** *73* (11), 1795-1818.

193.Harris, R. K.; Becker, E. D.; Cabral de Menezes, S. M.; Granger, P.; Hoffman, R. E.; Zilm, K. W., Further conventions for NMR shielding and chemical shifts (IUPAC Recommendations 2008). *Pure and Applied Chemistry* **2008,** *80* (1), 59-84.

194.Trypsin from bovine pancreas Type 1 Sigma-Aldrich: 2016.

195.J61874 Elastase, porcine pancreas. https://www.alfa.com/en/catalog/J61874/.

196.Pace, C. N.; Vajdos, F.; Fee, L.; Grimsley, G.; Gray, T., How to measure and predict the molar absorption coefficient of a protein. *Protein Science* **1995,** *4* (11), 2411-2423.

197.Takeoka, Y.; Watanabe, M., Tuning Structural Color Changes of Porous Thermosensitive Gels through Quantitative Adjustment of the Cross-Linker in Pre-gel Solutions. *Langmuir* **2003,** *19* (22), 9104-9106.

198.Rey, M.; Hou, X.; Tang, J. S. J.; Vogel, N., Interfacial arrangement and phase transitions of PNiPAm microgels with different crosslinking densities. *Soft Matter* **2017,** *13* (46), 8717-8727.

199.Spry, R. J.; Kosan, D. J., Theoretical Analysis of the Crystalline Colloidal Array Filter. *Applied Spectroscopy* **1986,** *40* (6), 782-784.

200.Zhang, J.-T.; Smith, N.; Asher, S. A., Two-Dimensional Photonic Crystal Surfactant Detection. *Analytical Chemistry* **2012,** *84* (15), 6416-6420.

201.Costa, M. C. M.; Silva, S. M. C.; Antunes, F. E., Adjusting the low critical solution temperature of poly(N-isopropyl acrylamide) solutions by salts, ionic surfactants and solvents: A rheological study. *Journal of Molecular Liquids* **2015,** *210*, 113-118.

202.Singh, R.; Deshmukh, S. A.; Kamath, G.; Sankaranarayanan, S. K. R. S.; Balasubramanian, G., Controlling the aqueous solubility of PNIPAM with hydrophobic molecular units. *Computational Materials Science* **2017,** *126*, 191-203.

203.Khalil, R. M., Complexation of Paracetamol with Xanthine Derivatives. *Egyptian Journal of Pharmaceutical Sciences* **1992,** *33*, 757-769.

204.Saha, A.; Mukherjee, A. K., Absorption spectrometric study of charge transfer complex formation between 4-acetamidophenol (paracetamol) and a series of quinones including Vitamin K3. *Spectrochimica Acta Part A: Molecular and Biomolecular Spectroscopy* **2004,** *60* (8), 1731-1737.

205.Okore, V. C.; Osuji, A. C., Thermodynamic considerations of the interaction between caffeine and paracetamol in aqueous solutions. *Boll Chim Farm* **2001,** *140* (5), 345-50.

206.Kolehmainen, E., Caffeine as a Gelator. *Gels* **2016,** *2* (1).

207.Asquith, R. S.; Rivett, D. E., The Photolysis of Tyrosine and its Possible Relationship to the Yellowing of Wool. *Textile Research Journal* **1969,** *39* (7), 633-637.

208.Nascimento, G. E. D.; Soares Oliveira, M. A.; da Rocha Santana, R. M.; Ribeiro, B. G.; Silva Sales, D. C.; Rodríguez-Díaz, J. M.; Napoleão, D. C.; da Motta Sobrinho, M. A.; Duarte, M., Investigation of paracetamol degradation using LED and UV-C photo-reactors. *Water Sci Technol* **2020,** *81* (12), 2545-2558.

209.Kamenjicki, M.; Lednev, I. K.; Mikhonin, A.; Kesavamoorthy, R.; Asher, S. A., Photochemically Controlled Photonic Crystals. *Advanced Functional Materials* **2003,** *13* (10), 774-780.

210.Hatton, B.; Mishchenko, L.; Davis, S.; Sandhage, K. H.; Aizenberg, J., Assembly of large-area, highly ordered, crack-free inverse opal films. *Proc Natl Acad Sci U S A* **2010,** *107* (23), 10354-9.

211.Sakai, M.; Kim, H.; Arai, Y.; Teratani, T.; Kawai, Y.; Kuwahara, Y.; Abe, K.; Kuwana, Y.; Ikeda, K.; Yamada, K.; Takeoka, Y., Monodisperse Silica Nanoparticle–Carbon Black Composite Microspheres as Photonic Pigments. *ACS Applied Nano Materials* **2020,** *3* (7), 7047-7056.

212.Hartlen, K. D.; Athanasopoulos, A. P.; Kitaev, V., Facile preparation of highly monodisperse small silica spheres (15 to >200 nm) suitable for colloidal templating and formation of ordered arrays. *Langmuir* **2008,** *24* (5), 1714-20.

213.Yokoi, T.; Wakabayashi, J.; Otsuka, Y.; Fan, W.; Iwama, M.; Watanabe, R.; Aramaki, K.; Shimojima, A.; Tatsumi, T.; Okubo, T., Mechanism of Formation of Uniform-Sized Silica Nanospheres Catalyzed by Basic Amino Acids. *Chemistry of Materials* **2009,** *21* (15), 3719-3729.

214.Lofgreen, J. E.; Ozin, G. A., Controlling morphology and porosity to improve performance of molecularly imprinted sol–gel silica. *Chemical Society Reviews* **2014,** *43* (3), 911-933.

215.Han, Y.; Lu, Z.; Teng, Z.; Liang, J.; Guo, Z.; Wang, D.; Han, M. Y.; Yang, W., Unraveling the Growth Mechanism of Silica Particles in the Stöber Method: In Situ Seeded Growth Model. *Langmuir* **2017,** *33* (23), 5879-5890.

216.Bischofberger, I.; Calzolari, D. C. E.; Trappe, V., Co-nonsolvency of PNiPAM at the transition between solvation mechanisms. *Soft Matter* **2014,** *10* (41), 8288-8295.

217.Xue, N.; Qiu, X.-P.; Aseyev, V.; Winnik, F. M., Nonequilibrium Liquid–Liquid Phase Separation of Poly(N-isopropylacrylamide) in Water/Methanol Mixtures. *Macromolecules* **2017,** *50* (11), 4446-4453.

218.Nothdurft, K.; Müller, D. H.; Brands, T.; Bardow, A.; Richtering, W., Enrichment of methanol inside pNIPAM gels in the cononsolvency-induced collapse. *Physical Chemistry Chemical Physics* **2019,** *21* (41), 22811-22818.

219.Yong, H.; Merlitz, H.; Fery, A.; Sommer, J.-U., Polymer Brushes and Gels in Competing Solvents: The Role of Different Interactions and Quantitative Predictions for Poly(N-isopropylacrylamide) in Alcohol–Water Mixtures. *Macromolecules* **2020,** *53* (7), 2323-2335.

220.Costa, R. O. R.; Freitas, R. F. S., Phase behavior of poly(N-isopropylacrylamide) in binary aqueous solutions. *Polymer* **2002,** *43* (22), 5879-5885.

221.Osaka, N.; Shibayama, M., Pressure Effects on Cononsolvency Behavior of Poly(N-isopropylacrylamide) in Water/DMSO Mixed Solvents. *Macromolecules* **2012,** *45* (4), 2171-2174.

222.Liu, L.; Wang, T.; Liu, C.; Lin, K.; Liu, G.; Zhang, G., Specific Anion Effect in Water–Nonaqueous Solvent Mixtures: Interplay of the Interactions between Anion, Solvent, and Polymer. *The Journal of Physical Chemistry B* **2013,** *117* (37), 10936-10943.

223.Prangé, T.; Schiltz, M.; Pernot, L.; Colloc'h, N.; Longhi, S.; Bourguet, W.; Fourme, R., Exploring hydrophobic sites in proteins with xenon or krypton. *Proteins: Structure, Function, and Bioinformatics* **1998,** *30* (1), 61-73.

224.Roose, B. W.; Zemerov, S. D.; Dmochowski, I. J., Xenon-Protein Interactions: Characterization by X-Ray Crystallography and Hyper-CEST NMR. *Methods Enzymol* **2018,** *602*, 249-272.

225.Bartik, K.; Luhmer, M.; Dutasta, J.-P.; Collet, A.; Reisse, J., 129Xe and 1H NMR Study of the Reversible Trapping of Xenon by Cryptophane-A in Organic Solution. *Journal of the American Chemical Society* **1998,** *120* (4), 784-791.

226.Menge, H.; Kühn, H.; Blümich, B.; Blümler, P.; Schneider, H., A comparison of 2H and 129Xe NMR as a probe of the effect of crosslinking in rubbery materials. *Macromolecular Materials and Engineering* **2000,** *282* (1), 1-4.

227.Locci, E.; Roose, P.; Bartik, K.; Luhmer, M., Probing polymer colloids by 129Xe NMR. *Journal of Colloid and Interface Science* **2009,** *330* (2), 344-351.

228.Bolhuis, P. G.; Frenkel, D.; Mau, S.-C.; Huse, D. A., Entropy difference between crystal phases. *Nature* **1997,** *388* (6639), 235-236.

229.Asher, S. A.; Ianoul, A.; Mix, G.; Boyden, M. N.; Karnoup, A.; Diem, M.; Schweitzer-Stenner, R., Dihedral ψ Angle Dependence of the Amide III Vibration: A Uniquely Sensitive UV Resonance Raman Secondary Structural Probe. *Journal of the American Chemical Society* **2001,** *123* (47), 11775-11781.

230.Mikhonin, A. V.; Bykov, S. V.; Myshakina, N. S.; Asher, S. A., Peptide Secondary Structure Folding Reaction Coordinate: Correlation between UV Raman Amide III Frequency, Ψ Ramachandran Angle, and Hydrogen Bonding. *The Journal of Physical Chemistry B* **2006,** *110* (4), 1928-1943.

231.Oladepo, S. A.; Xiong, K.; Hong, Z.; Asher, S. A.; Handen, J.; Lednev, I. K., UV Resonance Raman Investigations of Peptide and Protein Structure and Dynamics. *Chemical Reviews* **2012,** *112* (5), 2604-2628.

232.Chi, Z.; Asher, S. A., UV Resonance Raman Determination of Protein Acid Denaturation: Selective Unfolding of Helical Segments of Horse Myoglobin. *Biochemistry* **1998,** *37* (9), 2865-2872.

233.Hu, S.; Smith, K. M.; Spiro, T. G., Assignment of Protoheme Resonance Raman Spectrum by Heme Labeling in Myoglobin. *Journal of the American Chemical Society* **1996,** *118* (50), 12638-12646.

234.Bartik, K.; Luhmer, M.; Heyes, S. J.; Ottinger, R.; Reisse, J., Probing Molecular Cavities in α-Cyclodextrin Solutions by Xenon NMR. *Journal of Magnetic Resonance, Series B* **1995,** *109* (2), 164-168.

235.Rubin, S. M.; Spence, M. M.; Goodson, B. M.; Wemmer, D. E.; Pines, A., Evidence of nonspecific surface interactions between laser-polarized xenon and myoglobin in solution. *Proceedings of the National Academy of Sciences* **2000,** *97* (17), 9472.

236.Rubin, S. M.; Spence, M. M.; Pines, A.; Wemmer, D. E., Characterization of the Effects of Nonspecific Xenon–Protein Interactions on 129Xe Chemical Shifts in Aqueous Solution: Further Development of Xenon as a Biomolecular Probe. *Journal of Magnetic Resonance* **2001,** *152* (1), 79-86.

237.Corda, M.; Era, B.; Fais, A.; Casu, M., Structural investigation of pig metmyoglobin by 129Xe NMR spectroscopy. *Biochimica et Biophysica Acta (BBA) - General Subjects* **2004,** *1674* (2), 182-192.

238.Sumi, H.; Ulstrup, J., Dynamics of protein conformational fluctuation in enzyme catalysis with special attention to proton transfers in serine proteinases. *Biochim Biophys Acta* **1988,** *955* (1), 26-42.

239.Abraini, J. H. Pharmaceutical composition comprising at least one thrombolytic agent (A) and at least one gas (B) selected from the group consisting of nitrous oxide, argon, xenon, helium, neon. US 8,435,569 B2, 2013.

240.Schiltz, M.; Prangé, T.; Fourme, R., On the preparation and X-ray data collection of isomorphous xenon derivatives. *Journal of Applied Crystallography* **1994,** *27* (6), 950-960.

241.Vestling, M. M.; Murphy, C. M.; Fenselau, C., Recognition of trypsin autolysis products by high-performance liquid chromatography and mass spectrometry. *Analytical Chemistry* **1990,** *62* (21), 2391-2394.

242.David, H. N.; Haelewyn, B.; Risso, J.-J.; Abraini, J. H., Modulation by the noble gas argon of the catalytic and thrombolytic efficiency of tissue plasminogen activator. *Naunyn-Schmiedeberg's Archives of Pharmacology* **2013,** *386* (1), 91-95.

243.Wiebelhaus, N.; Singh, N.; Zhang, P.; Craig, S. L.; Beratan, D. N.; Fitzgerald, M. C., Discovery of the Xenon-Protein Interactome Using Large-Scale Measurements of Protein Folding and Stability. *J Am Chem Soc* **2022,** *144* (9), 3925-3938.

244.Crovetto, R.; Fernández-Prini, R.; Japas, M. L., Solubilities of inert gases and methane in H2O and in D2O in the temperature range of 300 to 600 K. *The Journal of Chemical Physics* **1982,** *76* (2), 1077-1086.

245.Jung, S.; MacConaghy, K. I.; Kaar, J. L.; Stoykovich, M. P., Enhanced Optical Sensitivity in Thermoresponsive Photonic Crystal Hydrogels by Operating Near the Phase Transition. *ACS Applied Materials & Interfaces* **2017,** *9* (33), 27927-27935.

246.Segebarth, N.; Aïtjeddig, L.; Locci, E.; Bartik, K.; Luhmer, M., Novel Method for the Measurement of Xenon Gas Solubility Using 129Xe NMR Spectroscopy. *The Journal of Physical Chemistry A* **2006,** *110* (37), 10770-10776.

247.Linnemann, M.; Nikolaychuk, P. A.; Muñoz-Muñoz, Y. M.; Baumhögger, E.; Vrabec, J., Henry’s Law Constant of Noble Gases in Water, Methanol, Ethanol, and Isopropanol by Experiment and Molecular Simulation. *Journal of Chemical & Engineering Data* **2020,** *65* (3), 1180-1188.

248.Lu, W.; Wang, L.; Chen, L.; Hui, S.; Rabinowitz, J. D., Extraction and Quantitation of Nicotinamide Adenine Dinucleotide Redox Cofactors. *Antioxid Redox Signal* **2018,** *28* (3), 167-179.

249.Raitman, O. A.; Chegel, V. I.; Kharitonov, A. B.; Zayats, M.; Katz, E.; Willner, I., Analysis of NAD(P)+ and NAD(P)H cofactors by means of imprinted polymers associated with Au surfaces:: A surface plasmon resonance study. *Analytica Chimica Acta* **2004,** *504* (1), 101-111.

250.Pogorelova, S. P.; Zayats, M.; Bourenko, T.; Kharitonov, A. B.; Lioubashevski, O.; Katz, E.; Willner, I., Analysis of NAD(P)+/NAD(P)H Cofactors by Imprinted Polymer Membranes Associated with Ion-Sensitive Field-Effect Transistor Devices and Au−Quartz Crystals. *Analytical Chemistry* **2003,** *75* (3), 509-517.

251.Owen, W. G.; Esmon, C. T.; Jackson, C. M., The conversion of prothrombin to thrombin. I. Characterization of the reaction products formed during the activation of bovine prothrombin. *J Biol Chem* **1974,** *249* (2), 594-605.

252.Bock, L. C.; Griffin, L. C.; Latham, J. A.; Vermaas, E. H.; Toole, J. J., Selection of single-stranded DNA molecules that bind and inhibit human thrombin. *Nature* **1992,** *355* (6360), 564-6.

253.Troisi, R.; Balasco, N.; Autiero, I.; Vitagliano, L.; Sica, F., Exosite Binding in Thrombin: A Global Structural/Dynamic Overview of Complexes with Aptamers and Other Ligands. *Int J Mol Sci* **2021,** *22* (19).

254.Tanford, C., Protein Denaturation. In *Advances in Protein Chemistry*, Anfinsen, C. B.; Anson, M. L.; Edsall, J. T.; Richards, F. M., Eds. Academic Press: 1968; Vol. 23, pp 121-282.

255.Damodaran, S., Protein: Denaturation. In *Handbook of Food Science, Technology, and Engineering - 4 Volume Set*, Hui, Y. H.; Sherkat, F., Eds. CRC Press: United States, 2005; pp 132-145.

256.Asher, S. A.; Mikhonin, A. V.; Bykov, S., UV Raman Demonstrates that α-Helical Polyalanine Peptides Melt to Polyproline II Conformations. *Journal of the American Chemical Society* **2004,** *126* (27), 8433-8440.

257.Punihaole, D.; Jakubek, R. S.; Dahlburg, E. M.; Hong, Z.; Myshakina, N. S.; Geib, S.; Asher, S. A., UV Resonance Raman Investigation of the Aqueous Solvation Dependence of Primary Amide Vibrations. *The Journal of Physical Chemistry B* **2015,** *119* (10), 3931-3939.

258.Punihaole, D.; Jakubek, R. S.; Workman, R. J.; Asher, S. A., Interaction Enthalpy of Side Chain and Backbone Amides in Polyglutamine Solution Monomers and Fibrils. *J Phys Chem Lett* **2018,** *9* (8), 1944-1950.

259.Myshakina, N. S.; Ahmed, Z.; Asher, S. A., Dependence of Amide Vibrations on Hydrogen Bonding. *The Journal of Physical Chemistry B* **2008,** *112* (38), 11873-11877.

260.Wang, Y.; Purrello, R.; Georgiou, S.; Spiro, T. G., UVRR spectroscopy of the peptide bond. 2. Carbonyl H-bond effects on the ground- and excited-state structures of N-methylacetamide. *Journal of the American Chemical Society* **1991,** *113* (17), 6368-6377.

261.Hong, Z.; Wert, J.; Asher, S. A., UV Resonance Raman and DFT Studies of Arginine Side Chains in Peptides: Insights into Arginine Hydration. *The Journal of Physical Chemistry B* **2013,** *117* (24), 7145-7156.

262.Ludwig, M.; Asher, S. A., Ultraviolet resonance Raman excitation profiles of tyrosine: dependence of Raman cross sections on excited-state intermediates. *Journal of the American Chemical Society* **1988,** *110* (4), 1005-1011.

263.Xu, M.; Ermolenkov, V. V.; Uversky, V. N.; Lednev, I. K., Hen egg white lysozyme fibrillation: a deep-UV resonance Raman spectroscopic study. *J Biophotonics* **2008,** *1* (3), 215-29.

264.Cho, N.; Song, S.; Asher, S. A., UV Resonance Raman and Excited-State Relaxation Rate Studies of Hemoglobin. *Biochemistry* **1994,** *33* (19), 5932-5941.